In presenting the dissertation as a partial fulfillment of the requirements for an advanced degree from the Georgia Institute of Technology, I agree that the Library of the Institute shall make it available for inspection and circulation in accordance with its regulations governing materials of this type. I agree that permission to copy from, or to publish from, this dissertation may be granted by the professor under whose direction it was written, or, in his absence, by the Dean of the Graduate Division when such copying or publication is solely for scholarly purposes and does not involve potential financial gain. It is understood that any copying from, or publication of, this dissertation which involves potential financial gain will not be allowed without written permission.

7/25/68

FLUID SLOSH DAMPERS

A THESIS

Presented to

The Faculty of the Graduate Division

by

Bashir Ahmad Sayar

In Partial Fulfillment

of the Requirement for the Degree

Doctor of Philosophy

in the School of Mechanical Engineering

Georgia Institute of Technology

September, 1971

FLUID SLOSH DAMPERS

Approved:

Co-chairman

Co-chairman

Date Approved Aug 16, 1971

ACKNOWLEDGEMENTS

The author expresses sincere appreciation to his thesis advisor, Dr. Joseph R. Baumgarten, for his constant encouragement and his valuable suggestions during the progress of this research. The author also wishes to express gratitude to his co-advisor, Dr. Ward O. Winer, for his helpfulness and concern; Dr. Prateen V. Desai, whose comments and suggestions were always valuable; Dr. Harold L. Johnson and Dr. Wilton W. King, who served as members of the advisory committee, for their valuable critiques and corrections.

The author also thanks EDC/AID (Educational Development Center through Agency for International Developments) for providing financial support in the course of completion of this investigation.

This thesis is dedicated to Shafica, the author's wife, whose love, patience, and hard work made the completion of this project possible.

TABLE OF CONTENTS

Page

ACKNOWLEDGMENTS ii

LIST OF TABLES v

LIST OF ILLUSTRATIONS vi

GLOSSARY OF ABBREVIATIONS ix

SUMMARY xiii

Chapter

I. INTRODUCTION 1

Main System
Auxiliary System

II. EVALUATION OF A PENDULUM MODEL (FORCED VIBRATION) 8

The Pendulum Analogy
Stability Boundaries
Force Output of the Pendulum

III. MODIFICATION OF THE PENDULUM MODEL (FORCED VIBRATION). . . 25

Modified Pendulum
Force Output of the Modified Pendulum
Stability Boundaries

IV. APPLICATION AS VIBRATION DAMPER (FREE VIBRATION) 37

General Equations of Motion
Parametric Presentation

V. LINEAR FLUID (PENDULUM) MOTION 44

Equations of Motion
Digital Computer Program and Analysis
Comparison to Experiments and Analysis of "Beat"

VI. NONLINEAR FLUID (PENDULUM) MOTION 81

Equations of Motion
Digital Computer Program
Theoretical and Experimental Analysis

TABLE OF CONTENTS (Concluded)

Page

VII. EXPERIMENTATION 95

Forced Vibration (Single Degree of Freedom)
Free Vibration (Two Degrees of Freedom)
Viscous Damping and Viscosities

VIII. CONCLUSIONS AND REMARKS 123

Forced Vibration
Free Vibration
Recommendations

APPENDICES 129

A. PENDULUM ANALOGY 130

B. EXPERIMENTAL STABILITY BOUNDARIES 133

C. EXPERIMENTAL FORCE-FREQUENCY PLOTS 141

D. PROGRAM AND OUTPUT ROOTS OF THE CHARACTERISTIC EQUATION OF THE LINEAR SYSTEM 151

E. SAMPLE DESIGN CALCULATION 156

F. PROGRAM AND SAMPLE OUTPUT OF THE NONLINEAR FLUID MOTION 160

BIBLIOGRAPHY 166

Literature Cited
Other References

VITA 170

LIST OF TABLES

Table		Page
1.	Coefficients of Cubic Spring	30
2.	Design Specifications and Damping of Coupled System $\Omega = 0.70$	64
3.	Design Specifications and Damping of Coupled System $\Omega = 0.95$	66
4.	Design Specifications and Damping of Coupled System $\Omega = 1.20$	68
5.	Instrumentation and Equipment List	98
6.	Kinematic Viscosities of Aqueous Glycerin and the Corresponding Specific Weights	122

LIST OF ILLUSTRATIONS

Figure		Page
1.	Pendulum Analogy	10
2.	Stability Boundaries	14
3.	Force Output of a Constrained Pendulum	16
4.	Force Output for Small and Large Pendulum Oscillations	19
5.	Comparison of Pendulum and Fluid Force Response	22
6.	Large Amplitude Fluid Motion	23
7.	Fluid Rotation	24
8.	Modified Pendulum	26
9.	Coefficients of the Cubic Spring	29
10.	Force Response of the Modified Pendulum Compared to the Experiments	31
11.	Force Response of the Modified Pendulum, Present Experiment and Abramson's [11] Experiments	32
12.	Stability Boundaries of Modified Pendulum	35
13.	Two Degree Freedom System Coupled	39
14.	Logarithmic Decrements of the Main System For $\zeta_p = 0.02$	53
15.	Logarithmic Decrements of the Main System For $\zeta_p = 0.04$	54
16.	Logarithmic Decrements of the Main System For $\zeta_p = 0.06$	55
17.	Logarithmic Decrements of the Main System For $\zeta_p = 0.08$	56
18.	Logarithmic Decrements of the Main System For $\zeta_p = 0.10$	57
19.	Logarithmic Decrements of the Main System For $\zeta_p = 0.20$	58
20.	Logarithmic Decrements of the Main System For $\zeta_p = 0.30$	59
21.	Logarithmic Decrements of the Main System For $\zeta_p = 0.40$	60

LIST OF ILLUSTRATIONS (Continued)

Figure		Page
22.	The Effect of Mass Ratio on Critical Tuning Frequency Ratio	61
23.	The Effect of Mass Ratio and Viscous Damping on the Damping of the Main System	62
24.	Influence of the Viscous Damping on the Damping of the Main System (Ω = 0.70)	63
25.	Influence of the Viscous Damping on the Damping of the Main System (Ω = 0.95)	65
26.	Influence of the Viscous Damping on the Damping of the Main System (Ω = 1.2)	67
27.	Effect of small Structural Damping on the Critical tuning Frequency Ratio (Ω_p)	69
28.	Effect of Small Structural Damping on the Logarithmic Decrements of Motion	70
29.	Beat Phenomena	75
30.	Ideal Response (if beat does not exist)	78
31.	Theoretical and Experimental Response of the Main System for Large Initial Displacements (ζ_p = 0.0129)	87
32.	Theoretical and Experimental Response of the Main System for Large Initial Displacements (ζ_p = 0.1095)	88
33.	Theoretical and Experimental Response of the Main System for Large Initial Displacements (ζ_p = 0.2040)	89
34.	Experimental Response of the Main System for Large ϵ, $\Omega < \Omega_p$	91
35.	Experimental Response of the Main System for Large ϵ, $\Omega > \Omega_p$	92
36.	Nonlinear Response for Plain and Modified Pendulum	94
37.	Experimental Setup for Forced Vibration	96
38.	Load Cell Bridge Circuit and External Connections	100
39.	Load Cell Calibration Curve	101

LIST OF ILLUSTRATIONS (Concluded)

Figure		Page
40.	Displacement Transducer Circuit and External Connections	103
41.	Displacement Transducer Calibration Curve	104
42.	Variation of Natural Frequency as a Function of Fluid Height	106
43.	Experimental Setup for Free Vibration	109
44.	Displacement Transducer Calibration Curve for Free Vibration	110
45.	Response of the Main System at, and on Either Side of the Critical Tuning Frequency	111
46.	Disappearance of Beat with Increase in the Viscous Damping at Critical Tuning Frequency	112
47.	Response of the Main System Before and After the Application of the Slosh Damper	113
48.	Experimental Setup for Measuring Viscous Damping	117
49.	Viscous Damping for Fluid Sloshing in Spherical Containers	118
50.	Viscous Damping for Fluid Sloshing in Spherical Containers	119
51.	Specific Gravity of Aqueous Glycerin	120
52.	Dynamic Viscosities of Aqueous Glycerin	121
53.	Ratio of Pendulum or Sloshing Mass to Total Liquid Mass in Partially Filled Containers	131
54.	Ratio of Pendulum or Sloshing Mass to Total Liquid Mass in Completely Filled Containers	131
55.	Pendulum Arm-Length Ratio	132
56.	Stationary or Non-Sloshing Mass Ratio	132
57-63.	Stability Boundaries	134
64-72.	Force-Frequency Plots	142

GLOSSARY OF ABBREVIATIONS

$\|a\|$	dimensionless amplitude factor
a_i	real part of the roots of the characteristic equation
A	$\epsilon^{1/3} \|a\|$
b_i	imaginary part of the roots of the characteristic equation
C_p	coefficient of viscous damping of the fluid (pendulum)
C_m	coefficient of the structural damping of the main system
D	container diameter
D_e	dissipative energy of the coupled system
$F=F_H$	fluid slosh force
G	acceleration of gravity
H	fluid height
K	$2\ \delta_p \epsilon^{-2/3}$
K_m	total spring stiffness of the main system
L_p	pendulum arm length
L_o	hinge point location of pendulum arm
L_s	length of the supporting wires
m	number of cycles
M_f	mass of fluid in partially filled container
M_F	mass of fluid in completely filled container
M_m	mass of the main system
M_o	stationarey mass of the fluid
M_p	Mass of the pendulum

M_s	mass of the support
M_t	mass of the fluid container
M_w	mass of the added weight
M	total mass $(M_o + M_p + M_s + M_t + M_w)$
P_i	locus of the critical tuning frequencies
q_i	generalized coordinates
Q_i	generalized forces
R	gain resistance
S_i	roots of the characteristic equation
t	time
T_e	kinetic energy of the coupled system
T	tension in the pendulum cord
v	$(\Omega_f^2 - 1)/\epsilon^{2/3}$
V	potential energy of the coupled system
V_i	volume of the fluid climbing the container boundary
V_t	velocity of the pendulum
W...	weight M... G
x	displacement of the main system
x_o	excitation displacement
X_o	initial displacement of the main system (also excitation amplitude)
X	x/X_o
Y(I)	list of variables assigned to the coordinates
α	second coordinate of the spherical pendulum
β	coefficient of the cubic spring
γ_s	coordinates of the supporting wires

δ	logarithmic decrement
$\delta_{env.}$	logarithmic decrement of the beat envelop
δ_{pm}	logarithmic decrement of main system after m cycles
δ_p	logarithmic decrement of the pendulum
δ_{pc}	critical value of δ_p
Δ	dummy variable
ϵ	X_o/L_p
ϵ_c	critical value of ϵ
ζ_p	viscous damping factor
ζ_{pc}	critical value of ζ_p at which the main system exhibit maximum damping
ζ_m	structural damping factor
η	coefficient of the cubic term of modified pendulum
θ	planar coordinate of the pendulum
Λ	$1/2\ \epsilon^{2/3}\omega t$
λ	measure of stability in Miles' [14] analysis
μ	mass ratio
υ	kinematic viscosity ($ft^2/sec.$)
ξ	β/W_p ratio of the nonlinear spring constant to the pendulum weight
ρ	fluid density
τ	dimensionless time
φ	pendulum phase angle
Φ	$\omega t - \varphi$
ω	excitation frequency
ω_p	natural frequency of the pendulum
ω_m	natural frequency of the main system

Ω_f frequency ratio (ω/ω_p)

Ω relative tuning frequency of the damper relative to the main system (ω_p/ω_m)

Ω_p frequency ratio Ω at which the damping is maximum, referred to as critical tuning frequency

SUMMARY

Oscillating fluids impart forces on their containers, and if such containers are attached to other moving media, the imparted forces of the sloshing fluids will be transmitted to the moving body and will influence its motion. It is the interest of this program to make use of such forces in damping the amplitudes of the vibratory systems.

The shape of the container is selected to be spherical, the fluid in its first anti-symmetric mode is modeled as a damped pendulum, and the main vibratory system is modeled as a mass-spring-dashpot system. The coupled free motion of the main system and the auxiliary system (fluid) is studied analytically and experimentally. The influence of the variation in each parameter of the coupled system upon the damping of the main system is studied for the linear fluid motion, while for the nonlinear fluid oscillations only the effect of large initial displacements is investigated. The analysis of linear fluid motion indicates the possibility of designing very efficient fluid slosh dampers at or about the critical value of viscous damping when tuned at the critical tuning frequency. Logarithmic decrements of damping are calculated from the analytical and experimental response of the main system and are compared.

To check the validity of the pendulum model in the nonlinear range of fluid motion, the oscillating fluid under forced vibration was analyzed. The pendulum analogy proved to be deficient for the analysis of the nonlinear fluid motion except at a critical fluid height ($H/D = 0.34$); therefore, proper modification was made and close agreements were obtained.

The analysis of nonlinear fluid motion indicated marked improvement in damping of the main system only for very large amplitudes of motion, while for slightly lower displacements no significant improvement was noticed, specially for small mass ratios.

In the course of the theoretical analysis two computer programs were written in Fortran and were processed by UNIVAC 1108 digital computers. One program was to solve the fourth order characteristic equation of the linearized differential equations and the other program was to use Rung-Kutta method and solve the nonlinear differential equations of the coupled system. In many cases theoretical and experimental analyses are compared and conclusions are drawn.

CHAPTER I

INTRODUCTION

Large amplitudes of vibration produce high fluctuating stresses in structures. Under certain conditions these stresses could cause damage, failure or other serious problems to the vibrating member. There are two possibilities to avoid such problems:

1. To redesign the member to withstand such levels of stress cycles.

2. To improve the damping capacity of the system on hand.

The second method seems to be of more practical importance and has been the subject of investigation of many researchers.

The problem under consideration is that of providing additional damping by means of attaching containers partially filled with fluid to the vibrating members. The amount of the additional damping depends upon the proper selection of the parameters involved.

Factors such as initial displacement of the vibrating member, its natural frequency, amplitude of oscillation of the fluid, its natural frequency, fluid height in the container, its viscosity, size and shape of the container determine the influential parameters of the systems. Some of these parameters are entirely independent of the others while others are interrelated. Some of the parameters can be predetermined while some others can be left as variables. For example, due to a special interest the container shape is selected to be spherical, the vibrating member could be a cantilever beam or an equivalent mass-spring-dashpot

and the direction of oscillation of fluid is selected to be normal to the gravity vector.

Three types of forces seem to contribute to the motion of the container and its attachments, namely, the gravity forces, the dissipative forces, and the inertia forces. The dissipative forces are due to structural damping of the vibrating body, viscosity of fluid and breaking waves of the fluid free surface which can result at very large amplitudes and large fluid heights or from the introduction of baffles. The inertia forces are both frequency and amplitude dependent and may also be influced by variation in other parameters. The amplitude of oscillating fluid is sensitive to the initial displacement and natural frequency of the vibrating members as well as the viscosity of the fluid.

For low amplitudes the fluid motion can be explained by a linear theory while the nonlinearity is introduced mainly due to large amplitudes and the curvature of the container [1]*.

Before attacking the coupled motion of the composite it seems essential to study the two subsystems uncoupled.

Main System

Many vibrating structures can be modeled as a linear or nonlinear mass-spring-dashpot, the theory of which can be found in any standard vibration textbook.

Auxiliary System

Dynamic analyses of continous viscous fluid systems, if at all feasible, often lead to enormous mathematical complexities. These

---

*Numbers in brackets correspond to the references listed in the bibliography.

difficulties are further enhanced when the container exhibits a non-simple geometry. Recent progress in space sciences has led to numerous theoretical and experimental investigations of fuel sloshing in space vehicle tanks. Abramson's report [1] covers topics such as lateral oscillation, vertical vibration, pitching, and swirling of fluids in moving containers. He has examined damping of fluid oscillation, representation of the fluid motion as a mechanical model, impact of fluid on the bulkhead of the containers, and results of theoretical and experimental investigations as well as 447 References have been compared and reported. It is noted that considerably more work has been done on lateral sloshing, and that most of of this work employs a linear analysis based on small oscillations. The study of small amplitude lateral sloshing has also been extended to include various container geometeries, such as spherical, spheroidal, cylindrical, conical, toroidal and rectangular.

In a recent mathematical analysis of sloshing in spherical containers Budiansky [2], through the use of integral equations, successfully determined the natural frequencies and different mode shapes of vibratory motion of the fluid. In this analysis small amplitude oscillation is assumed and the fluid viscosity is neglected. Macarty and Stephens [3] compared their experimental results with the theoretical analysis of Budiansky and demonstrated a good agreement between the two. Leonard [4] studied the frequencies and mode shapes of fluid motion in oblate spheroidal containers and his results for the sphere, which is a special case of a spheroid, checked closely with those obtained by other investigators. Stofan [5] studied the slosh forces in addition to the frequencies and mode shapes. He compared his experimental work with the

solutions of Budinasky and demonstrated close agreement. Stephens [6] studied damping of fluid oscillations in oblate spheroidal tanks with and without baffles. He noticed that viscous damping is comparatively larger for small and large fluid heights. He also concluded that the measured damping for tanks without baffles are not amplitude dependent except for relatively low amplitudes.

Sumner and Stofan [7] considered three sizes of spherical containers with fluids of different viscosities and observed that for small oscillations viscous damping increases with increase in viscosity and decreases with increase in tank diameter. The scope of this investigation covers only one particular fluid height (half full). To obtain information for wider range of fluid heights results of a few additional experiments are reported in Chapter VII.

For many practical purposes one might be interested in analysis of fluid motion as a moving mass in a discrete fashion rather than a continuous media. Mechanical model analogy as a mass-spring-dashpot or a pendulum-dashpot can best represent fluid motion for certain practical purposes. The results of some investigations on the subject are reported by Abramson [1] for different shapes of containers.

On the basis of linear theory, Sumner [8] studied sloshing of fluids in oblate spheroidal containers and also investigated a mechanical model (pendulum) to represent the first mode of fluid oscillation. He later determined the pendulum analogy for the case of a spherical container [9]. Results of the latter report [9] are extensively used throughout the present investigation.

Abramson, Chu, and Garza [10] studied fluid sloshing in spherical

containers and compared their results with the theory of Budiansky and other related experimental works. They also compared the force response of the forced vibration for baffled containers to that of the mechanical model.

On the subject of nonlinear fluid motion, relatively little work is available, most of which is devoted to cylindrical and rectangular tanks. No available theoretical work includes the spherical tank geometry. The only experimental work [11] reported in this connection is carried out for a constant fluid height (half full tank). According to this report the fluid motion exhibits an amplitude-frequency response characteristic which is very similar to that of a softening spring. Although the response of a nonlinear pendulum model also exhibits softening characteristics, it is doubtful if the degree of softening is the same as those of the sloshing fluid. On the other hand, Chen [12] in his analysis of cylindrical containers discovered a critical fluid height above which the fluid behaved as hardening and below which as softening. On the basis of the above two reasons it appears reasonable to investigate the fluid response in spherical containers for different fluid heights and compare the results to that of a pendulum model in the nonlinear range. Such an investigation is reported in detail in Chapters II and III. As a result it was found that the fluid behavior in spherical containers always demonstrated softening for all fluid heights. It was also found that the degree of softening of a pendulum model differs from the fluid for various fluid heights except at a critical fluid height for which a pendulum seemed to agree well with the fluid motion in the nonlinear range.

If the fluid (specially in containers with circular cross section) is excited near resonance the oscillating waves depart from the plan of excitation and rotate about the gravity vector.

Berlot [13] compared the result of energy method he used to that of the linear mechanical model for planar motion and found that a conical pendulum model of the same mass and length can duplicate the fluid rotation. He also compared the boundaries of rotary motion of a conical pendulum model to those obtained from experiments of fluid sloshing in cylindrical containers.

Miles [14] has also studied the regions of stabilities of a spherical pendulum forced at the hinge-point and obtained theoretical expressions for the boundary points. In the first two chapters of the present investigation similar experimental boundaries for spherical containers have been obtained and compared with the theoretical analysis of Miles. The agreement is far better than Berlot's [13] comparison to cylindrical containers.

Stephens [15] seems to be the first to investigate the damping effect of moving fluid (cylindrical container) on the attached vibrating member. He analyzed both a four degree of freedom system and a two degree of freedom system (tank translation and fluid motion) and concluded that the damping of the main system (tank and vibrating member) increased with increase in fluid damping.

It was on the basis of this idea that the problem at hand was undertaken and both linear and nonlinear fluid motions were considered. Chen [12] in his analysis disregards viscous damping of fluid and the structural damping of the main vibrating system. He used forced vibration

to exhibit the usefulness of oscillating fluid as a vibration absorber.

In the present analysis the first anti-symmetric mode of fluid sloshing is considered and the transient response of the main system coupled with the oscillating fluid (pendulum model) under free vibration mode is analyzed. The viscous damping of the coupled system is studied mathematically and experimentally. The equations of motion are derived by the use of Lagrange's energy method and digital computer programs were run to solve both the fourth order characteristic equation of linear motion and the response of the nonlinear fluid motion. In the nonlinear case the Runge-Kutta method of numerical integration is used to predict the response of the coupled system.

CHAPTER II

EVALUATION OF A PENDULUM MODEL

(FORCED VIBRATION)

The Pendulum Analogy

Since the dynamics of moving fluid contributes directly to the motion of the main system, it is essential to analyze the fluid system uncoupled and investigate the characteristics of the influential parameters.

Budiansky [2] treats the moving fluid in a spherical tank as a continuous media, he linearizes the equations of motion, assumes special coordinates and uses sophisticated integral equations to solve for the three lowest frequencies of oscillation. Similar work has been done by Moiseev [16] in which he assumes small oscillation, a general shape for the container and by use of Ritz Variational methods determines the frequencies of oscillation. He applies his general theory to containers of different geometries. For the spherical containers using an electronic computer he calculates the fundamental natural frequencies for different fluid heights. No attempt is made to solve the problem of large amplitudes of oscillations for this geometry or to include the effect of viscosity mainly due to the complexity of the boundary curvature which further complicates the mathematical analysis.

Even for small oscillations the solutions are too cumbersome and for many practical purposes simpler analysis is appreciated. One method

of providing simpler analysis is to model the fluid motion as a mass-spring-dashpot or a pendulum-dashpot. Much of this type of work is reported by Abramson [1].

The only mechanical model (Pendulum) for fluid oscillation in spherical containers is in the form of graphs [9] some of which are reproduced and is provided in appendix A for easy reference. The pendulum analogy is constructed according to the following assumptions:

1. Amplitude of oscillation is small.

2. Viscosity of fluid is negligible.

3. The pendulum arm is normal to the fluid free surface and the fluid free surface remains straight while in motion.

4. The sum of the moving mass and the stationary mass equals the total mass of fluid present in the container.

The pendulum model of fluid oscillation, which is adequate for the first antisymmetric mode in the plane of oscillation, can be further generalized by the addition of a dashpot with experimentally determined coefficients to account for the viscous friction of the moving fluid. The physical system and its equivalent mechanical representation are schematically depicted in Figure 1. For the present investigation the model parameters such as M_p, M_o, L_p, and L_o are determined from Sumner's [9] analogy and are used without any modification in the linear analysis (Chapter V). Values of C_p needed to develop this model are calculated from the empirical equations reported in Chapter VII. Further investigations necessary to evaluate the validity of this model in the non-linear range of fluid motion are reported in this chapter as well as in Chapter III.

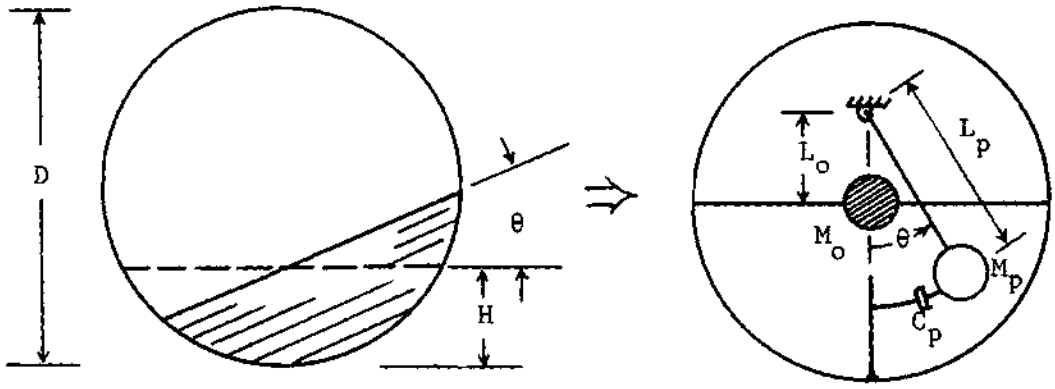

Fluid and Container Equivalent Mechanical Model

Figure 1. Pendulum Analogy

Stability Boundaries

When a spherical container, partially filled with a fluid of relatively low viscosity, is excited with a frequency close to its fundamental natural frequency the oscillation of the fluid departs from the plane of excitation and oscillates in a different plane making a small angle with the plane of excitation. If the frequency or amplitude of oscillation is slightly increased the fluid rotates about a vertical axis passing through the center of the sphere. This fluid rotation is considered unstable [1] and is termed "Swirl." The velocity of rotation in the swirl region sometimes increases to a large value and then decreases to a stop and increases again in the opposite direction. This process repeats itself consecutively. This type of fluid motion has been analyzed both experimentally and mathematically mostly for the case of cylindrical containers [1,13,17,18]. Miles [14] noticed similar type of behavior in the motion of a spherical pendulum excited at the base and mathematically

solved for the boundary points.

Vibration of the main system when coupled with fluid motion can be endangered by the unstable rotation of the fluid if the coupled system is operated at frequencies and amplitudes corresponding to those of the swirl region.

Therefore it is important to recognize these boundaries in order to be able to specify the ranges of operation of fluid slosh dampers for safe performance.

An initial attempt is made to recognize these boundaries experimentally. Furthermore, the validity of the pendulum model is established by comparing the experimental results against those calculated from Miles [14] analysis. Figure 2 shows these stability boundaries.

Miles [14] analyzed a spherical pendulum in general and for the class of differential equations corresponding to those of the spherical pendulum as given by

$$\left[\frac{d^2}{dt^2}+\frac{G}{L_p}\right]\theta - \frac{G}{6L_p}\theta^3 + \tfrac{1}{2}\theta\left[\frac{d^2}{dt^2}+\frac{G}{L_p}\right]\alpha^2 = \epsilon\omega^2\cos\omega t, \quad \text{and} \tag{1}$$

$$\left[\frac{d^2}{dt^2}+\frac{G}{L_p}\right]\alpha - \frac{G}{6L_p}\alpha^3 + \tfrac{1}{2}\alpha\left[\frac{d^2}{dt^2}+\frac{G}{L_p}\right]\theta^2 = 0, \tag{2}$$

he assumed general solutions of the form

$$\theta = \epsilon^{1/3}[f_1(\Lambda)\cos\omega t + f_2(\Lambda)\sin\omega t], \quad \text{and} \tag{3}$$

$$\alpha = \epsilon^{1/3}[f_3(\Lambda)\cos\omega t + f_4(\Lambda)\sin\omega t], \tag{4}$$

where $$\Lambda = \tfrac{1}{2}\epsilon^{2/3}\omega t. \tag{5}$$

To determine the stability of the harmonic motion corresponding to a singular point, say $f_i^{(o)}$, he considered the perturbation solution

$$f_i(\Lambda) = f_i^{(o)} + C_i \exp[(\lambda-k)\Lambda],\ |C_i| \ll 1 . \tag{6}$$

Such a solution tends to the singular point if $\lambda < k$, remains in the neighborhood of the singular point if $\lambda = k$, or departs from this neighborhood if $\lambda > k$. He designated both the singular point and the corresponding harmonic motion as stable if $\lambda \leq k$ or unstable if $\lambda > k$. The spherical pendulum departs from the plane of excitation at these unstable singular points and it is interesting to notice that the corresponding fluid motion also departs from the plane of excitation at such singular points. Therefore, according to the above definition of stability the harmonic planar motion of the fluid can also be considered unstable.

According to Miles calculation the stability boundaries are*:

1. Lower boundaries which also correspond to the points of vertical tangency on an amplitude frequency plot given by

$$a = (4\Omega_f^2)^{1/3}, \text{ and} \tag{7}$$

2. The upper boundaries given by

$$a = -[(4/3)\Omega_f^2]^{1/3}. \tag{8}$$

*In Miles analysis Ω_f^2 is left out of the calculation probably because the stability boundaries are located close to the resonance where $\Omega_f \simeq 1$.

After suitable substitutions equations 9 and 10 will be obtained. The lower boundaries are given by

$$X_o/D = 1.089(L_p/D)\ [1-\Omega^2_f)^{3/2}/\Omega^2_f]\ , \tag{9}$$

and the upper boundaries are given by

$$X_o/D = 1.515\ (L_p/D)\ [(\Omega^2_f-1)^{3/2}/\Omega^2_f]. \tag{10}$$

An experimental setup for forced vibration studies, which is described in Chapter VII was used to determine the slosh force output for various fluid heights. For each fluid height and a fixed excitation amplitude the excitation frequency was varied and the forces were recorded up to the unstable boundary point at which the fluid became unstable. These points (two for each excitation amplitude, one below and one above the resonance) were marked, the force output at the intermediate frequencies being unstable could not be measured. A total of seven fluid heights and five excitation amplitudes for each fluid height were used. The force outputs other than those of the boundaries were not measured for the fifth excitation amplitude. The Force-Frequency plots for the seven fluid heights are included in appendix B.

Agreement between experimental data and those obtained from Miles [14] analysis, is indeed quite satisfactory. A slight disagreement at lower fluid heights and at higher fluid heights is due to viscous damping which is neglected in the analytical calculations. The assumption of small damping in the neighborhood of the half full container is justified for water as the fluid medium, while the viscous damping was relatively higher at lower and higher fluid heights (Chapter VII).

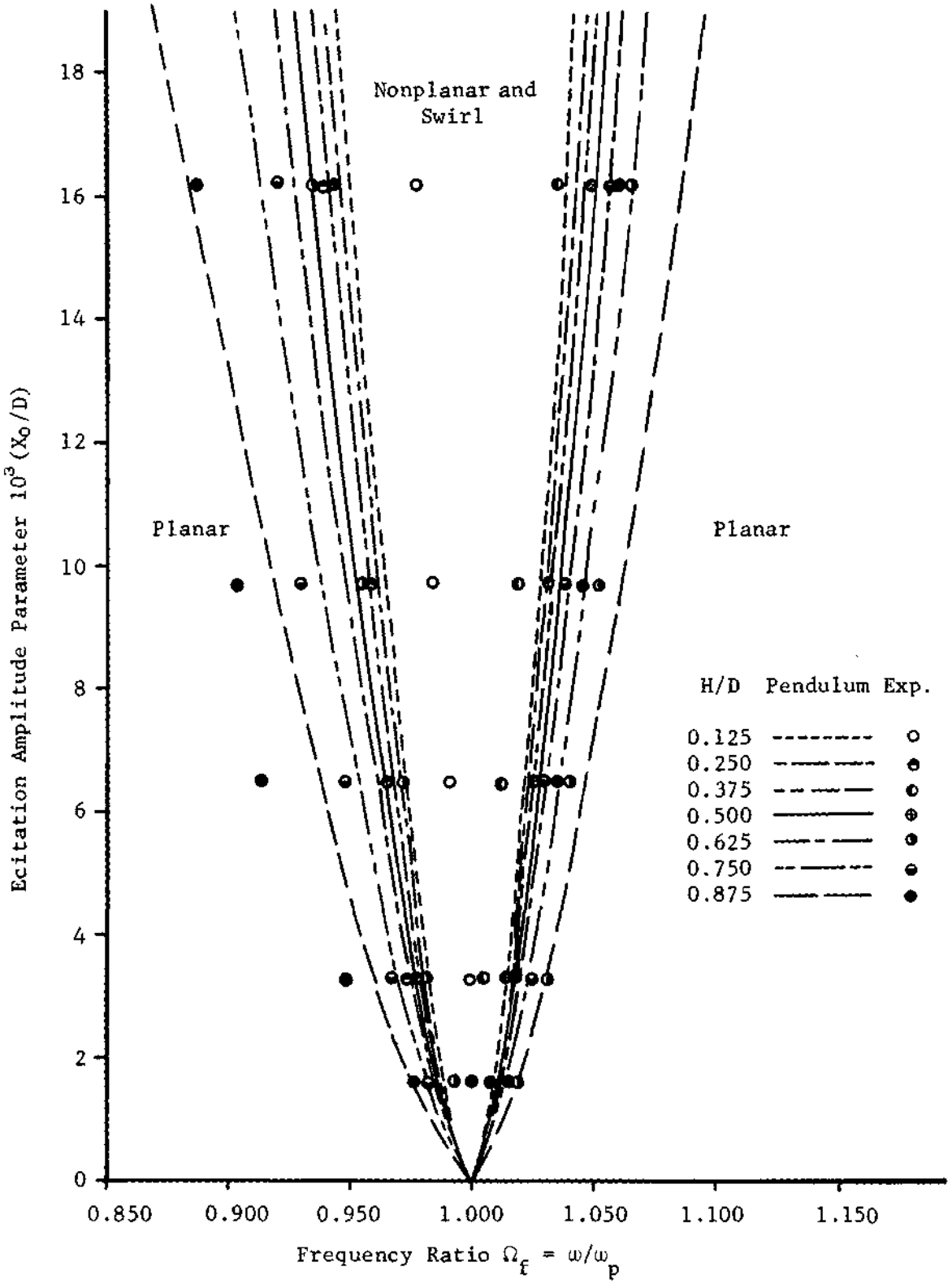

Figure 2. Stability Boundaries

It is worthwhile to indicate that for larger fluid damping, the width of the unstable region becomes narrower and may disappear completely thus indicating that high damping precludes the fluid from becomming dynamically unstable. This fact needs further investigation before a more definitive statement can be made in this regard.

A knowledge of the unstable boundaries allow one or more of the following decisions:

1. Avoid using the coupled system at the range of excitation amplitudes and frequencies which correspond to points between the boundaries. This limitation in turn narrows the range of applicability of such a method of damping which is not desirable.

2. To install splitter plates parallel to the direction of excitation of fluid in the container. This method constrains the fluid motion in the plane of excitation but requires additional fabrications which are not economical and, at times, not desirable.

3. Use high viscous fluids to obtain either a narrow range of instability or none at all.

The decision as to the adaptation of a particular method can be made following further information on fluid response in the entire range of frequency domains. In the present experimentation the method of splitter plate with water as the fluid medium is used and the Force-Frequency plots of appendix C are obtained.

Force Output of the Constrained Pendulum

To use a splitter in the fluid container is equivalent to constraining the spherical pendulum in one plane of motion. Using this method one can supress the fluid rotation and obtain data in the swirl region except

at a narrow band of frequency which corresponds to "Jump" which generally occurs in certain physical systems [19].

Forced vibration measurements as outlined in Chapter VII were made similar to those used for determining the swirl boundaries as explained earlier. Fluid heights and frequency ranges were the same but only four excitation amplitudes were used in the experimentation. To show that an empty container as well as a full container behave as rigid bodies the extremes were also studied. A complete set of Force-Frequency response curves are included in appendix C.

To investigate the validity of the model, the output force of the model can be formulated from Figure 3. Derivation of the pendulum output force is summerized in what follows.

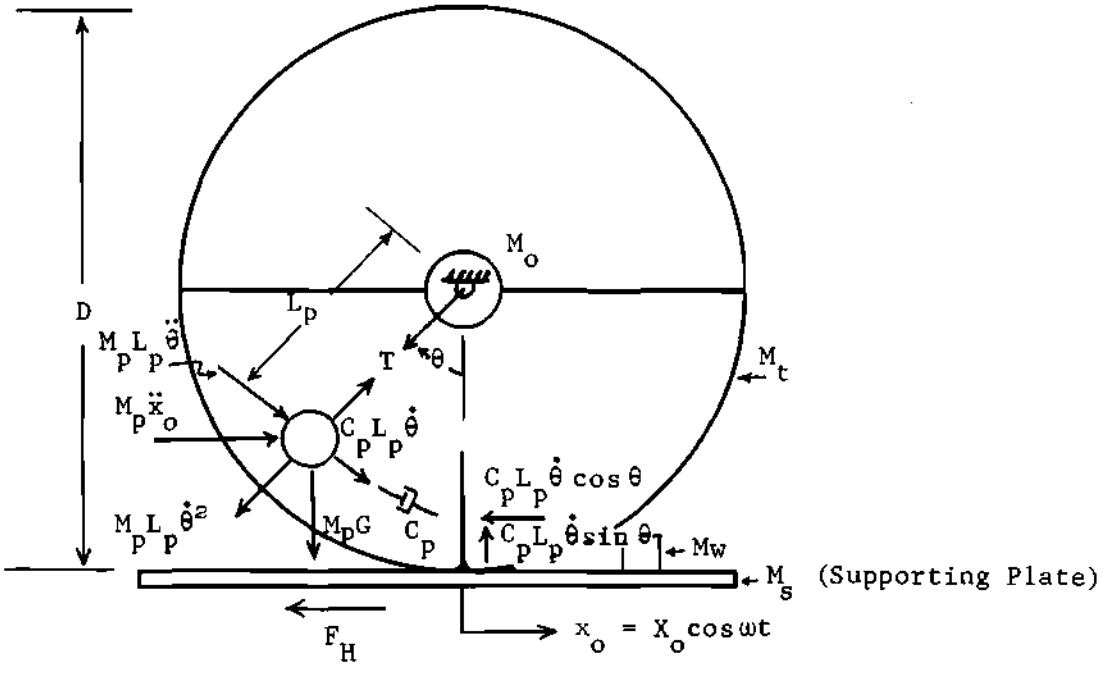

Figure 3. Force Output of Constrained Pendulum

$\sum$ (horizontal forces) = 0

$$F_H = (M_t + M_w + M_s + M_o)\ddot{x}_o - T \sin\theta - C_p L_p \dot{\theta}\cos\theta. \tag{11}$$

$\sum$ (radial Forces Along the Pendulum Cord) = 0

$$T = M_p L_p \dot{\theta}^2 + M_p G\cos\theta - M_p \ddot{x}_o \sin\theta \tag{12}$$

Substituting for T in equation 11 gives

$$F_H = (M_s + M_w + M_t + M_o + M_p \sin\theta^2)\ddot{x}_o - M_p L_p \dot{\theta}^2 \sin\theta - C_p L_p \dot{\theta}\cos\theta - M_p G \sin\theta\cos\theta. \tag{13}$$

$\sum$ (moments About the Pivot) = 0

$$M_p L_p^2 \ddot{\theta} + C_p L_p^2 \dot{\theta} + M_p G L_p \sin\theta + M_p \ddot{x}_o L_p \cos\theta = 0. \tag{14}$$

Solving for $-C_p L_p \dot{\theta}$ from equation 14 and substituting in equation 13, after simplification, the expression for force becomes

$$F_H = M\ddot{x}_o - M_p L_p \dot{\theta}^2 \sin\theta + M_p L_p \ddot{\theta}\cos\theta \tag{15}$$

Dividing equation 14 by $M_p L_p^2$ and simplifying, the equation of motion is obtained as

$$\ddot{\theta} + 2\zeta_p \omega_p \dot{\theta} + \omega_p^2 \sin\theta = \varepsilon\omega^2 \cos\omega t. \tag{16}$$

Approximating sin θ with the two first terms of its series expansion, Duffing's equation will be obtained, the solution of which has beend analyzed by Miles [14], and Stoker [19]. The Duffing equation is

$$\ddot{\theta} + 2\zeta_p \omega_p \dot{\theta} + \omega_p^2 (\theta - \theta^3/6) = \varepsilon\omega^2 \cos\omega t \tag{17}$$

By proper substitution, equation 15 can be written in a more convenient form as

$$|F_H| = W_p \Omega_f^2 \left[(\epsilon/\mu) \cos \omega t + \theta \cos \theta + (A^2-\theta^2) \sin \theta\right]. \tag{18}$$

Equation 18 is an equivalent expression for the slosh force of the fluid containing the inertia term of the container and other attachments.

In the experimental analysis the magnitude of the peak force (maximum with respect to time) was measured. The peak force mathematically is obtained by setting

$$\frac{d|F_H|}{dt} = 0, \text{ for} \tag{19}$$

$$|F_H| = |F_H|_{max} . \tag{20}$$

For the above condition to hold,

$$[\sin^2\Phi]^3 + \frac{2B}{C} [\sin^2\Phi]^2 + \frac{B^2+ D^2}{C^2} [\sin^2\Phi] - \frac{D^2}{C^2} = 0, \tag{21}$$

where

$$B = \left[(\epsilon/\mu A)\cos \varphi - \frac{A^2}{2} (A^2+ 7) + 1\right], \tag{22}$$

$$C = \frac{A^2}{2} (9 + A^2) , \tag{23}$$

$$D = (\epsilon/\mu A)\sin \varphi , \text{ and} \tag{24}$$

$$\Phi = \omega t - \varphi . \tag{25}$$

It is worthy of mentioning that in the derivation of equation 21 it was found necessary to assume sin $\theta \simeq \theta - \theta^3/6$, cos $\theta \simeq 1 - \theta^2/2$ and terms in θ^4 and higher were neglected.

Equation 21 yields one solution when the oscillation is small and gives three solutions when the oscillation is large simply due to the fact that for small oscillation the force output is harmonic (Figure 4-a) and in large oscillation other harmonics are also present (Figure 4-b).

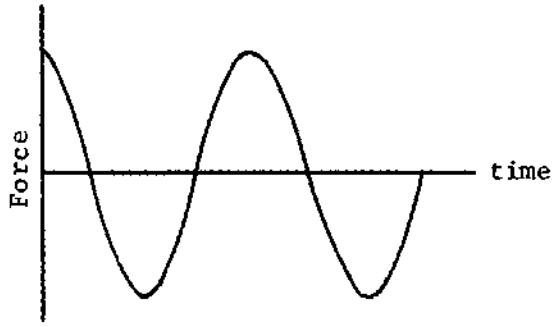

Figure 4-a. Small Oscillation

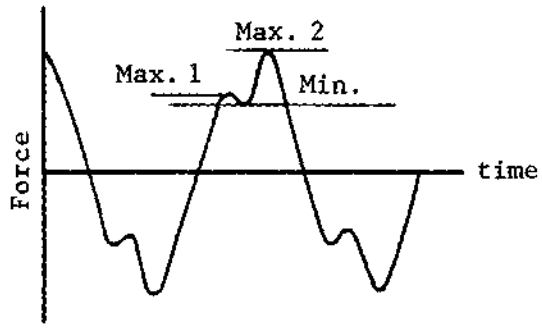

Figure 4-b. Large Oscillation

Figure 4. Force Output for mall and Large Oscillations

The three solutions correspond to points Max. 1, Max. 2 and Min. Since the points Max. 2 were measured from the experimental outputs, the corresponding solutions of equation 21 were used in the mathematical analysis.

According to Miles [14], the solution to Duffing's equation is assumed as

$$\theta = \epsilon^{1/3}|a|\cos|\omega t - \varphi_1| + \epsilon|a_3|\cos|3\omega t - \varphi_3| + 0(\epsilon^{5/3}) \qquad (26)$$

where $|a|$ is a dimensionless amplitude. Substituting solution 26 in equation 17 one obtains

$$\frac{1}{8}|a|^3 + v|a| + \Omega_f^2 \cos\varphi = 0, \quad \text{and} \tag{27}$$

$$K|a| = \Omega_f \sin\varphi, \tag{28}$$

where

$$K = 2\delta_p \epsilon^{-1/3} \tag{29}$$

Using only the first term of the series solution given by equation 26,

$$\theta = \epsilon^{1/3}|a|\cos|\omega t - \varphi|, \tag{30}$$

and eliminating the phase angle from equations 27 and 28 gives

$$\{|a|^2\}^3 + 16v\{|a|^2\}^2 + 64(v^2 + K^2\Omega_f^2)\{|a|^2\} - 64\Omega_f^4 = 0, \tag{31}$$

where

$$v = (\Omega_f^2 - 1)\epsilon^{-2/3}, \quad \text{and} \tag{32}$$

$$A = \epsilon^{1/3}|a|. \tag{33}$$

The peak force was calculated in the following procedure:

1. The frequency ratio Ω_f and excitation amplitude corresponding to the maximum experimental force (in a Force-Frequency plot) were selected.

2. From equation 31 the value of $|a|$ was calculated.

3. For $|F| = |F|_{max.}$, from equation 21, Φ was evaluated.

4. Finally, the value of the force was obtained from equation 18.

The calculated force parameters were compared to the experimental points as shown in Figure 5. The following conclusions can be drawn from the comparison of Figure 5.

1. The pendulum force output and the corresponding experimental force agree well in the linear small oscillation range.

2. In the nonlinear range, the pendulum exhibits stronger softening character than the corresponding mass of fluid below some critical fluid height and weaker softening character above this critical fluid height.

3. The experimental output-force deviates largely from the pendulum output-force for H/D = 7/8.

The variation in the softening character of the fluid could arise from the following fact:

Abramson [1] considers the strong boundary curvature to be a main source of nonlinearity of fluid, simply because the expanding volume for fluid heights less than a radius tends to suppress the motion of the fluid while for fluid heights more than a radius the contracting volume tends to produce breaking waves.

This fact, in the author's opinion, is the main cause of disagreement between the fluid output force and that of the pendulum. As mentioned earlier, the pendulum was constructed on the assumption that the fluid free surface remain normal to the pendulum arm (fluid free surface remain straight), which evidently is not the case for large amplitudes of fluid oscillation. This concept is schematically presented in figure 6.

If the fluid behaves according to the assumption of pendulum analogy [9], it will exert an average force on the container whose horizontal component is shown by F_{H_1}. In this case it equals the horizontal

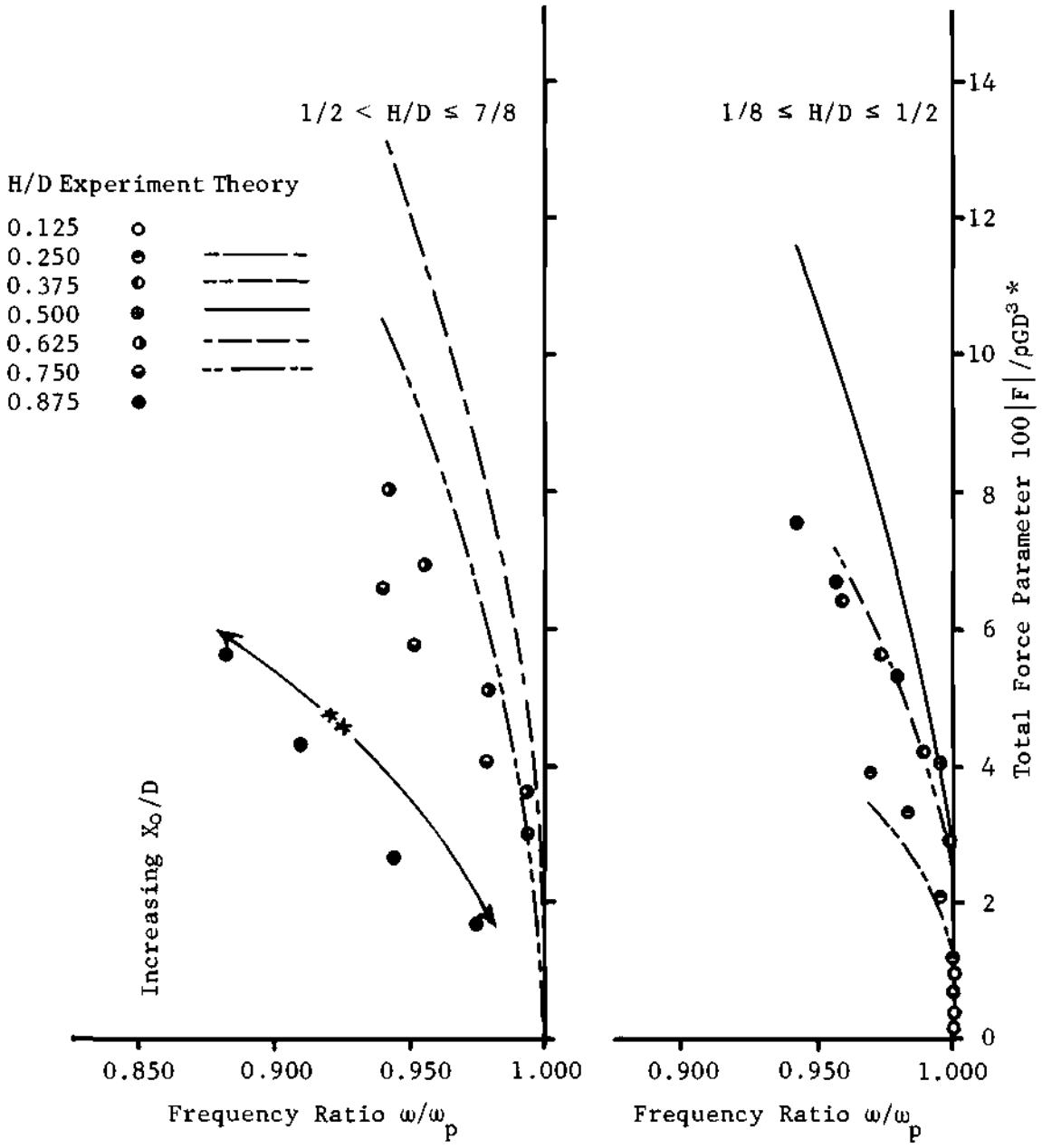

*This parameter corresponds to a maximum value for experimental points and is not necessarily maximum theoretically.

**Comparison is avoided.

Figure 5. Comparison of Pendulum and Fluid Force Response

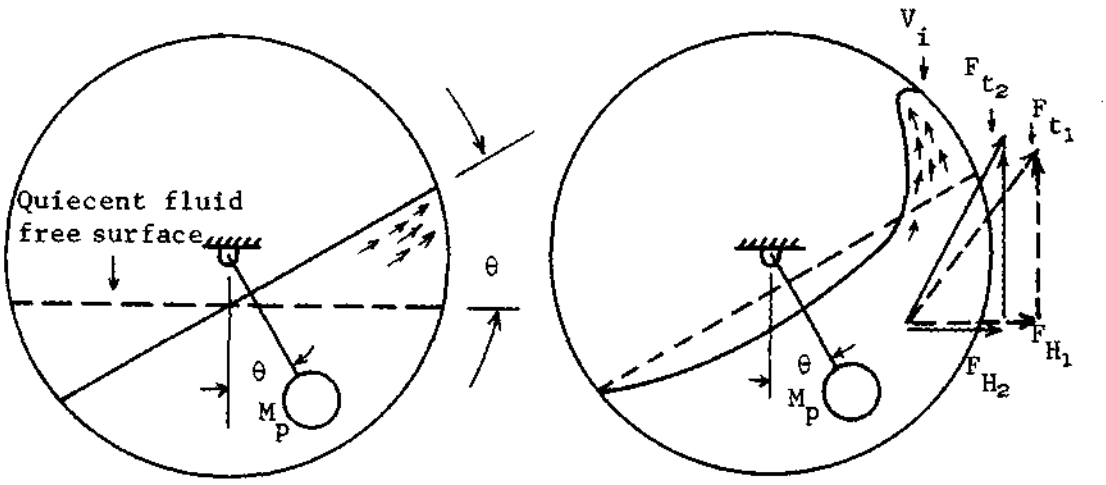

Figure 6. Large Amplitude Fluid Motion

component of the pendulum. But because of the large relative velocity of the fluid particles at the fluid surface, a portion V_i of the fluid climbs the container wall and at the same time because of the contracting volume of container together with the opposition of the fluid particles to the curved container wall the sense of the velocity of these particles change. This in turn causes the momentum of the portion V_i of the fluid to change. This affects the total resultant force and distorts its orientation as well as it reduces its magnitude. The combination of these results in a smaller horizontal component of the average force $F_{H_2} < F_{H_1}$. The component F_{H_2} is sensed by the load cell and recorded, while the component F_{H_1} is calculated from the pendulum. This difference is evident from the comparison of Figure 5. It should be mentioned that an opposite situation exists for lower fluid heights.

For fluid height H/D = 7/8, even for small oscillations, the fluid behaved extremely nonlinearly and in many instances the moving mass of

fluid climbed the container boundaries up to the top and then rotated around the dome and discharged on the opposite side (Figure 7) and, according to the forcing amplitude and frequency sometimes the fluid was particulated. The measured force in no way could be related to the pendulum output unless the pendulum is considered to have a variable mass and to move with very large angle of swing and pass its second singular point [19] and then oscillate about the first singular point again. The comparison of pendulum output and actual fluid motion is, therefore, avoided in this case.

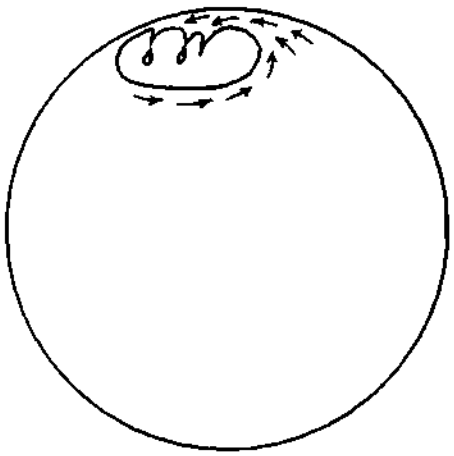

Figure 7. Fluid Rotation.

CHAPTER III

MODIFICATION OF THE PENDULUM MODEL (FORCED VIBRATION)

Modified Pendulum

It seems necessary to modify the pendulum in order to increase its applicability over a wider range of oscillation amplitudes or else to use the pendulum only for small oscillations. As can be seem from Figure 6, it is the difference in the magnitude of the horizontal component of the pendulum force and the actual fluid force ($F_{H_1} - F_{H_2}$) that causes the disagreement and that this difference can be corrected by altering the restoring force of the pendulum by means of attaching a spring ($\beta\theta^n$) in parallel to the dashpot. By proper selection of β and n one can overcome the disagreement and obtain a modified pendulum which models the actual fluid motion for large amplitudes of oscillations.

For n = 1 the order of magnitude of the added spring will be significant even at small oscillations thus influencing the natural frequency of the linear pendulum which should be avoided. n being any number other than three will complicate the equation of motion, but for n = 3 the correction will be in the order of softening of the pendulum and the equation of motion will still be in the form of Duffing's equation, the solution of which is similar to that of the pendulum.

β on the other hand can be determined from the experimental results presented in Appendix C.

Force Output of the Modified Pendulum

Analyzing the modified pendulum as shown in Figure 8, one can write:

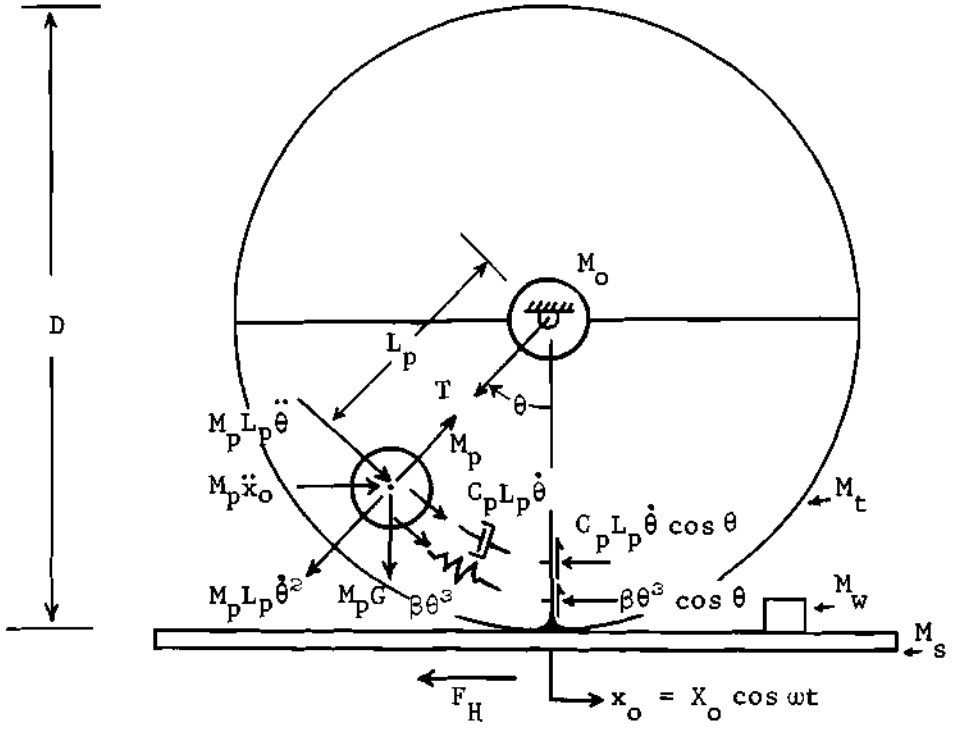

Figure 8. Modified Pendulum

$\sum$ (horizontal forces) = 0

$$F_H = (M_s + M_t + M_w + M_o)\ddot{x}_o - T\sin\theta - C_p L_p \dot{\theta}\cos\theta - \beta\theta^3 \cos\theta \qquad (34)$$

$\sum$ (radial forces along the pendulum card) = 0

$$T = M_p L_p \dot{\theta}^2 + M_p G \cos\theta - M_p \ddot{x}_o \sin\theta \tag{35}$$

$\sum$ (moment about the pivot) = 0

$$M_p L_p^2 \ddot{\theta} + C_p L_p^2 \dot{\theta} + M_p G L_p \sin\theta + M_p \ddot{x}_o L_p \cos\theta + \beta \dot{\theta}^3 L_p \cos\theta = 0 \tag{36}$$

After substitution of equation 35 into equation 36, one obtains

$$F_H = M\ddot{x}_o - M_p L_p \dot{\theta}^2 \sin\theta - M_p G \sin\theta \cos\theta - (C_p L_p \dot{\theta} + \beta\theta^3) \cos\theta. \tag{37}$$

Substituting for $-(C_p L_p \dot{\theta} + \beta\theta^3) \cos\theta$ from equation 36 into equation 37 yields

$$F_H = M\ddot{x}_o - M_p L_p \dot{\theta}^2 \sin\theta + M_p L_p \ddot{\theta} \cos\theta. \tag{38}$$

This equation is the same as equation 15.

Simplifying the equation of motion and approximating $\sin\theta$ with the first two terms of its series expansion yields Duffing's equation as

$$\ddot{\theta} + 2\zeta_p \omega_p \dot{\theta} + \omega_p^2(\theta - \eta\theta^3) = \epsilon\omega^2 \cos\omega t, \tag{39}$$

where

$$\eta = \frac{1}{6} - \beta/W_p. \tag{40}$$

Since the expression for the force remains the same. Equations 18, 19, 20, 21, 22, 23 and 24 are still valid. The equation of motion (equation

39) is different and more general than equation 16. Assuming solution 26 and substituting in equation 39 one obtains

$$\frac{3}{4}\eta|a|^3 + v|a| + \Omega_f^2 \cos\varphi = 0, \text{ and} \tag{41}$$

$$K|a| = \Omega_f \sin\varphi. \tag{42}$$

Eliminating φ from equations 41 and 42 results a cubic equation as

$$\{|a|^2\}^3 + \frac{8v}{3\eta}\{|a|^2\}^2 + \frac{16}{9\eta^2}(v^2 + K^2\Omega_f^2)\{|a|\} - \frac{16\Omega_f^4}{9\eta^2} = 0 \tag{43}$$

Again with the same procedure as in Chapter II, the forces for different values of β/W_p (picked at random) were calculated and compared with the experiment and the value of β/W_p for the best fit was selected as plotted in Figure 9 and presented in Table 1. At the same time the comparison of the modified pendulum with the use of selected β/W_p are made in Figure 10.

All the comparisons between the theory and experiment were based on a single frequency ratio which corresponds to the peak experimental force on a force-frequency plot. To have a better knowledge on the agreement of the model and actual fluid motion over a wide range of frequency ratios the modified pendulum for the half full tank was analyzed and the force parameter for each excitation amplitude corresponding to Abramson's [11] experiment were calculated as the frequency was varied, the results are compared and presented in Figure 11. To check the results of the present experimentation, for the same range of parameters, experiments (as reported in Chapter VII) were run and the force outputs

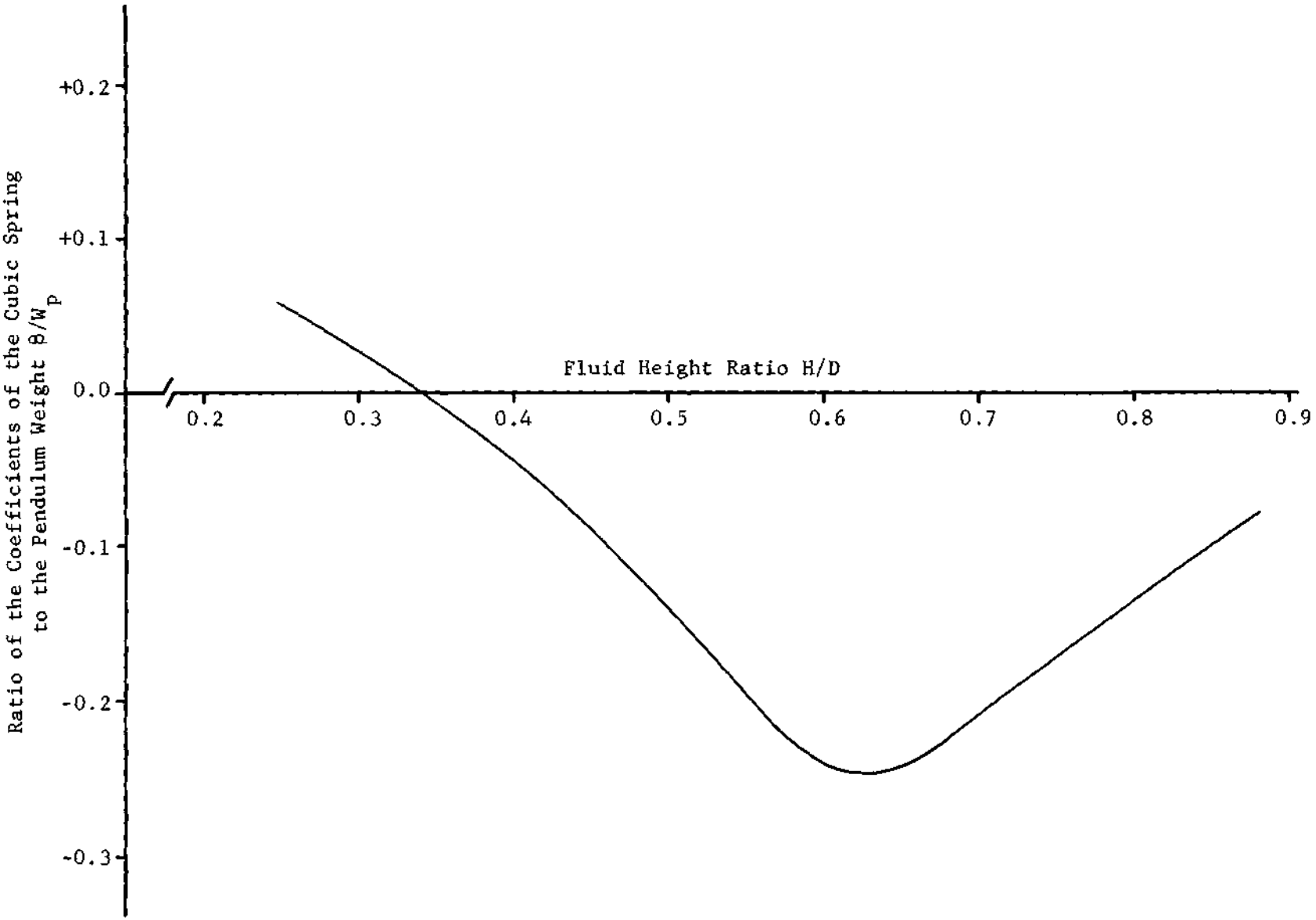

Figure 9. Coefficients of the Cubic Spring

Table 1. Coefficients of the Cubic Spring

H/D	β/W_p	η
0.125	...	...
0.250	+1/18	1/9
0.375	-1/42	8/42
0.500	-1/7	13/42
0.625	-1/4	5/12
0.750	-1/6	1/3
0.875	-1/12	1/4

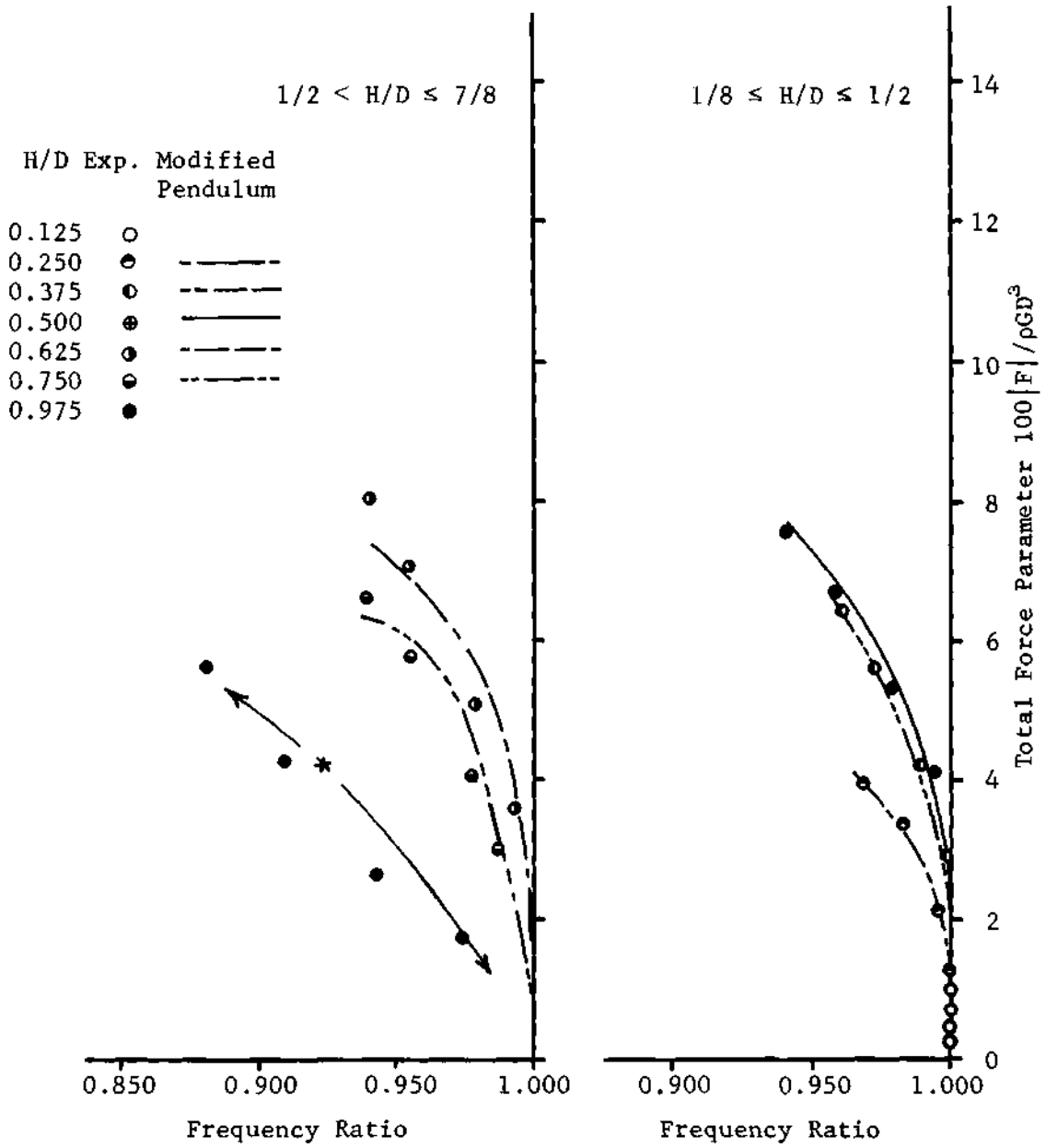

*Comparison is avoided.

Figure 10. Force Response of the Modified Pendulum Compared to the Experiments

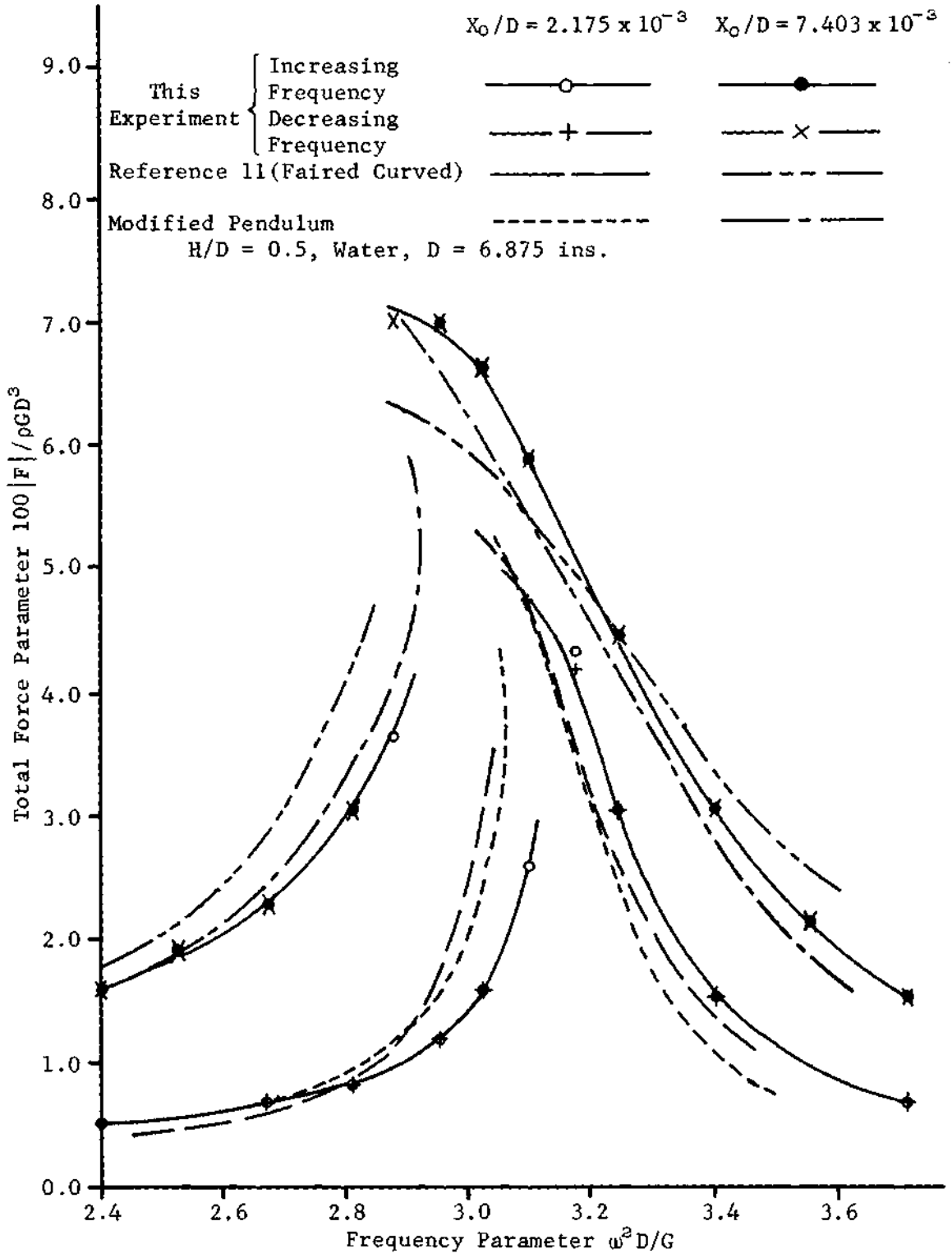

Figure 11. Force Response of the Modified Pendulum, Present Experiment and Abramson's [11] Experiments

were parameterized and plotted on the same figure.

Figure 11 shows good agreement between Abramson's [11] experiment, the present experiment and the modified pendulum.

Before coming to the conclusion of having the best model, it seemed worthwhile to check once again the stability boundaries for the modified pendulum, mainly because the coefficient of the added spring is negative for a wide range of fluid heights and this negative restoring force is a source of instability.

Stability Boundaries

Using Miles [14] perturbation method, the unstable boundaries for the modified pendulum are obtained as follows:

1. Lower boundaries are

$$a = \left(\frac{2\Omega_f^2}{3\eta}\right)^{1/3} \tag{44}$$

2. Upper boundaries are

$$a = -\left(\frac{2\Omega_f^2}{9\eta}\right)^{1/3} \tag{45}$$

After substituting equations 44 and 45 into equation 41 and simplifying, the lower boundaries become

$$X_o/D = \frac{0.4444(L_p/D)}{\sqrt{\eta}}\left[\frac{(1 - \Omega_f^2)^{3/2}}{\Omega_f^2}\right], \tag{46}$$

and the upper boundaries become

$$X_o/D = \frac{0.61972(L_p/D)}{\sqrt{\eta}} \left[\frac{(\Omega_f^2 - 1)^{3/2}}{\Omega_f^2}\right] \tag{47}$$

Once again the results of computations from equations 46 and 47 are compared to the experimental points as shown in Figure 12.

Since the values of β/W_p were small, the unstable region did not grow considerably except for very large fluid heights at which the inclusion of damping which is relatively large at these heights will narrow the unstable region and will result in better agreement. At very low fluid heights the positive values of β/W_p even though small helped the situation and narrowed the unstable region as compared to a planar pendulum.

From the previous analysis it is obvious that the modified pendulum duplicates the fluid dynamics for a wide range of fluid heights, but in order to use sloshing fluid as a means of vibration damping certain facts need to be discussed further.

Sumner's [9] analysis of a linear pendulum model indicates that the magnitude of the stationary mass M_o increases with fluid height, this increase is more rapid for fluid heights above half full and at the same time in this range the magnitude of the sloshing mass M_p is decreasing rapidly. To use fluid heights higher than H/D = 1/2 seems like adding extra weight to the main system which is unacceptable from a design point of view. Therefore the author suggests the use of such a mechanism of damping for the range of fluid heights less or equal to one half. On the other hand, too small a fluid height still has small sloshing mass although the stationary mass is minimum. Therefore the effect of a small

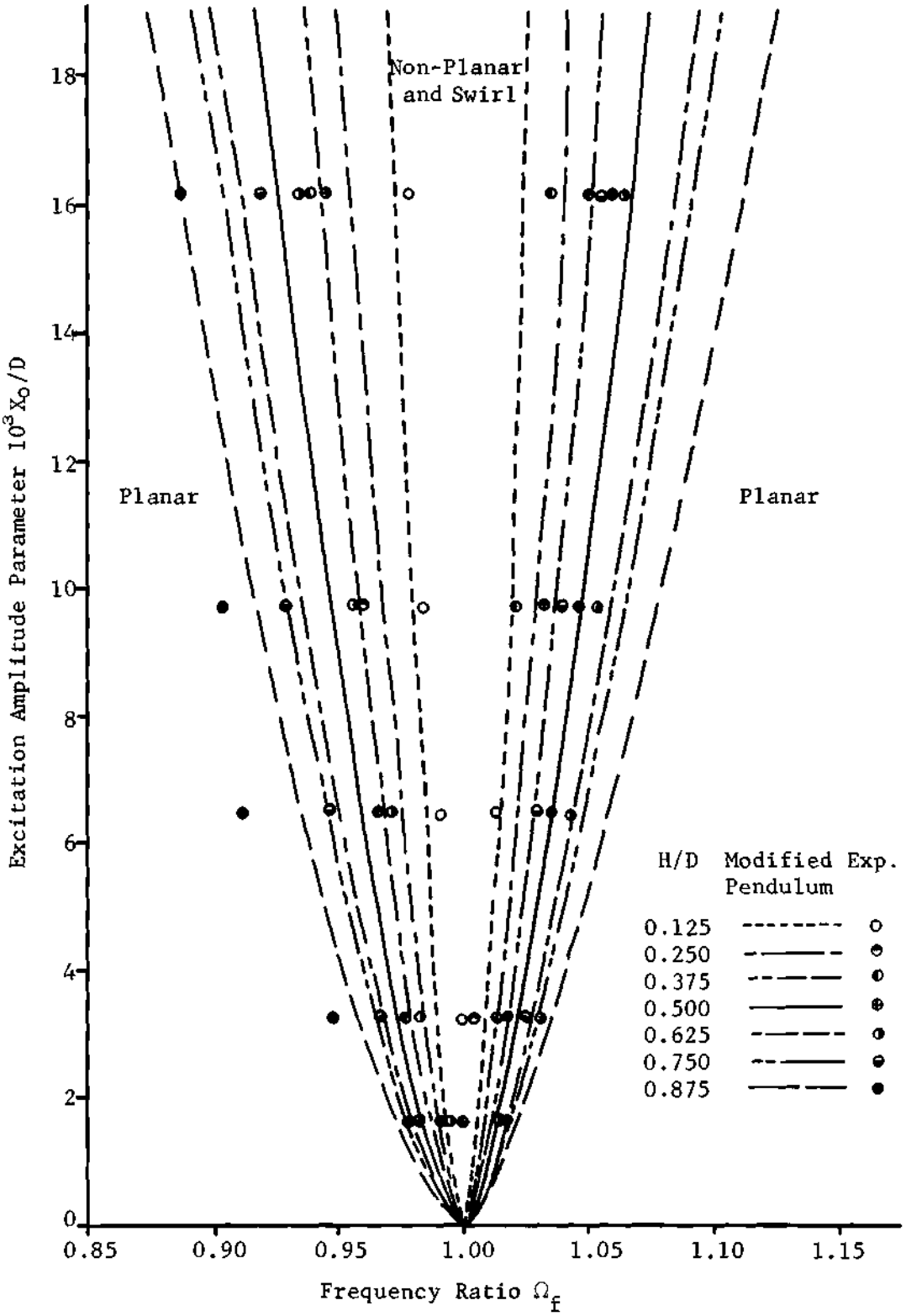

Figure 12. Stability Boundaries of the Modified Pendulum

sloshing mass on the main system would not be noticeable unless the main system has a mass comparative to the sloshing mass, in such a case the use of small fluid heights is suggested mainly because the fluid exhibits very large camping for small heights (Chapter VII).

Figure 9 indicates a critical fluid height (H/D = 0.340) at which the pendulum without any modification duplicates the actual fluid response in linear as well as in nonlinear ranges. The use of this critical height is suggested and if, for any purpose, some other fluid height in this neighborhood is used the modified pendulum should be employed for nonlinear analysis.

CHAPTER IV

APPLICATION AS VIBRATION DAMPER (FREE VIBRATION)

General Equations of Motion

Several methods of damping are used to reduce the amplitude of vibration of elastic members as well as the rigid members. The most effective method used for elastic members is the method of viscoelastic coating which has received considerable attention in recent years. On the other hand for rigid vibrating members a commonly used method is called vibration absorption which is simply a method of attaching an auxiliary mass-spring-dashpot to the main system and designing the parameters such that the two systems are tuned at resonance. The free and forced vibration of such methods have been studied and the range of applicability and their efficiencies have been reported by many researchers. The method of vibration absorption is a very standard method, the analysis of which can be found in any vibration book. Most of the investigators consider the undamped vibration absorber under forced vibration condition which is very effective at a particular frequency but has the disadvantages of producing two other resonance conditions in the vicinity of the tuning frequency. Very little has been done in the case of free vibration of such methods especially when the dashpot is present.

The method under discussion is quite similar to a damped vibration absorber which will be studied under free vibration condition and the efficiency of damping will be predicted from the transient response of

the coupled system. It is simply a method of attaching partially filled fluid containers to the main vibrating members for the purpose of amplitude reduction.

As the modified pendulum was proved to be efficient both for linear as well as for nonlinear fluid motions, it will be used in the derivation of equations of motion.

Referring to Figure 13 one can write the energy expressions as follows:

The kinetic energy of the coupled system is:

$$T_e = \frac{1}{2}(M_s + M_t + M_w + M_o)(L_s\dot{\gamma}_s)^2 + \frac{1}{2}M_p V_t^2 \tag{48}$$

where

$$V_t^2 = (L_s\dot{\gamma}_s)^2 + (L_p\dot{\theta})^2 + 2L_pL_s\dot{\gamma}_s\dot{\theta}\cos\theta. \tag{49}$$

Substituting equation 49 into equation 48 yields

$$T_e = \frac{1}{2}M(L_s\dot{\gamma}_s)^2 + \frac{1}{2}M_p[(L_p\dot{\theta})^2 + 2L_pL_s\dot{\gamma}_s\dot{\theta}\cos\theta]. \tag{50}$$

The potential energy of the coupled system is:

$$V = \frac{1}{2}K_m(L_s\gamma_s)^2 + MGL_s(1 - \cos\gamma_s) + M_pGL_p(1 - \cos\theta) + L_p\beta\int_o^\theta \Delta^3 d\Delta \tag{51}$$

The dissipative energy of the coupled system is:

$$D_e = \frac{1}{2}C_m(L_s\dot{\gamma}_s)^2 + \frac{1}{2}C_p(L_p\dot{\theta})^2 \tag{52}$$

Using Lagrange's Energy Equation

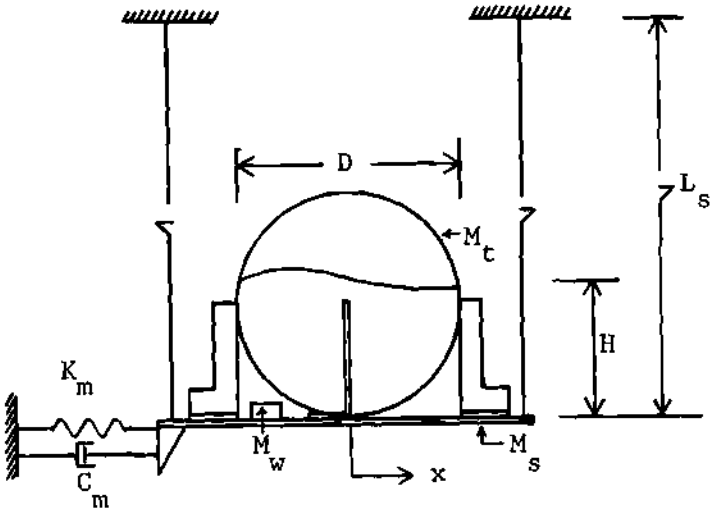

Actual System

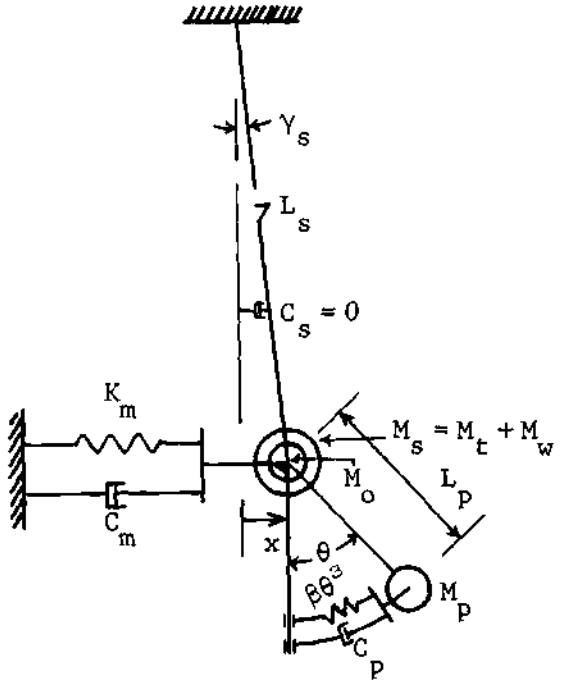

Models Coupled

Figure 13. Two Degree Freedom System Coupled

$$\frac{d}{dt}\left(\frac{\partial T_e}{\partial \dot{q}_i}\right) - \left(\frac{\partial T_e}{\partial q_i}\right) + \left(\frac{\partial V}{\partial q_i}\right) + \left(\frac{\partial D_e}{\partial \dot{q}_i}\right) = Q_i \tag{53}$$

where $q_1 = \gamma_s$ and $q_2 = \theta$.

For free vibration $Q_i = 0$.

Using Lagrange's equation for the γ_s coordinate

$$ML_s\ddot{\gamma}_s + M_pL_pL_s\ddot{\theta}\cos\theta - M_pL_pL_s\dot{\theta}^2\sin\theta + K_mL_s^2\gamma_s + MGL_s\sin\gamma_s + C_mL_s^2\dot{\gamma}_s = 0 \tag{54}$$

Using Lagrange's equation for the θ coordinate

$$M_pL_p^2\ddot{\theta} + M_pL_pL_s\ddot{\gamma}_s\cos\theta + M_pGL_p\sin\theta + C_pL_p^2\dot{\theta} + L_p\beta\theta^3 = 0 \tag{55}$$

Since the lengths of supporting strings are much larger than the amplitude of oscillation of the main mass one can assume

$$L_s\sin\gamma_s = L_s\gamma_s = x \tag{56}$$

Substituting the approximation 56 in equations 54 and 55 and simplifying, the two equations of motion will be obtained as

$$\ddot{x} + \left(\frac{M_p}{M}\right)L_p\ddot{\theta}\cos\theta + \left(\frac{C_m}{M}\right)\dot{x} + \left(\frac{K_m}{M} + \frac{G}{L_s}\right)x - \left(\frac{M_p}{M}\right)L_p\dot{\theta}^2\sin\theta = 0 \tag{57}$$

and

$$\ddot{\theta} + \left(\frac{1}{L_p}\right)\ddot{x}\cos\theta + \left(\frac{C_p}{M_p}\right)\dot{\theta} + \left(\frac{G}{L_p}\right)\sin\theta + \left(\frac{G}{L_p}\right)\left(\frac{\beta}{W_p}\right)\theta^3 = 0. \tag{58}$$

Parametric Presentation

The equations of motion in the form of equations 46 and 47 can be solved for variation in each parameter related to certain properties of

each system such as M_p,L_p, M, C_p, etc., but this process will be tedious and at the same time, the analysis will be too specific. On the other hand, if the equations of motion are converted into dimensionless parameters the analysis will take a more general form and will be of more practical value. For example, instead of finding the effect of variation of M_p and M on the system response separately it will be instructive to investigate the effect of variation of M_p/M as a dimensionless parameter.

In this investigation it is preferable to work with dimensionless parameters and to convert the equations of motion (equations 57 and 58) into another set of equations containing parameters entirely dimensionless.

Letting

$$X = x/X_o, \tag{59}$$

$$\theta = \theta, \tag{60}$$

and

$$\tau = \omega_m t, \tag{61}$$

the original coordinates will be converted into the new set of dimensionless coordinates as follows

$$x = XX_o \tag{62}$$

$$\dot{x} = \frac{dx}{dt} = \frac{dx}{d\tau}\frac{d\tau}{dt} = X_o\omega_m X' \tag{63}$$

$$\ddot{x} = X_o\omega_m^2 X'', \tag{64}$$

where

$$X' = \frac{dX}{d\tau} \text{ and } X'' = \frac{d^2X}{d\tau^2}, \tag{65}$$

also

$$\theta = \theta, \tag{66}$$

$$\dot{\theta} = \frac{d\theta}{dt} = \frac{d\theta}{d\tau}\frac{d\tau}{dt} = \omega_m \theta', \text{ and} \tag{67}$$

$$\ddot{\theta} = \omega_m^2 \theta'', \tag{68}$$

where

$$\theta' = \frac{d\theta}{d\tau} \text{ and } \theta'' = \frac{d^2\theta}{d\tau^2}. \tag{69}$$

Substituting equations 62, 63, 64, 66, 67 and 68 into equations 57 and 58 and dividing the first by $X_o\omega_m^2$ and the second by ω_m^2 the equations of motion will read:

$$X'' + \left(\frac{M_p/M}{X_o/L_p}\right)\theta'' \cos\theta + \left(\frac{C_m/M}{1/\omega_m}\right)X' + \left[\frac{(K_m/M)+(G/L_s)}{\omega_m^2}\right]X - \left(\frac{M_p/M}{X_o/L_p}\right)\theta'^2 \sin\theta = 0 \tag{70}$$

$$\theta'' + \left(\frac{X_o}{L_p}\right)X'' \cos\theta + \left(\frac{C_p}{M_p}\right)\left(\frac{1}{\omega_m}\right)\theta' + \left(\frac{G/L_p}{\omega_m^2}\right)\sin\theta + \left[\frac{(G/L_p)(\beta/w_p)}{\omega_m^2}\right]\theta^3 = 0 \tag{71}$$

Making the following substitutions:

$$X_o/L_p = \epsilon \tag{72}$$

$$M_p/M = \mu \tag{73}$$

$$C_m/M = 2\zeta_m\omega_m \tag{74}$$

Note: Dots on the variables indicate derivative with respect to real time and primes indicate the derivative with respect to dimensionless time.

$$C_p/M_p = 2\zeta_p\omega_p \tag{75}$$

$$G/L_p = \omega_p^2 \tag{76}$$

$$\left(\frac{K_m}{M}+\frac{G}{L_s}\right) = \omega_m^2 \tag{77}$$

$$\omega_p/\omega_m = \Omega \tag{78}$$

the equations of motion 70 and 71 will read

$$X'' + (\mu/\epsilon)\theta''\cos\theta + 2\zeta_m X' + X - (\mu/\epsilon)\,\theta'^2 \sin\theta = 0 \tag{79}$$

$$\theta'' + \epsilon X'' \cos\theta + 2\zeta_p \Omega\theta' + \Omega^2 \sin\theta + \Omega^2 \xi\theta^3 = 0 \tag{80}$$

where

$$\xi = \beta/W_p \tag{81}$$

Equations 79 and 80 are the general equations of motion in parametric form.

CHAPTER V

LINEAR FLUID (PENDULUM) MOTION

Equations of Motion

Most engineering equipment is built on the basis of linear theory mainly because of the mathematical simplicity, practical limitations and ease of manufacturing. It seems advisable that the linear analysis of fluid slosh dampers be discussed in more detail.

The purpose of this investigation is to demonstrate the efficiency of such a device as a damper and to study the influence of design parameters on the response of the main system under free vibration. The measure of damping is selected to be the logarithmic decrement of the decaying response of the main system under the assumption of small oscillations.

The search is aimed towards finding any combination of design parameters which provide the largest logarithmic decrement. The equations of motion are analyzed in parametric form providing a wide range of selection of sphere size, fluid height, fluid viscosity and other physical properties of the auxiliary system (damper) to meet the design criteria.

The analysis covers a survey of all possible combination of parameters which provide best damping and then for the combination of these parameters, experiments are run to check the validity of theoretical analysis.

Considering the general equations of motion 79 and 80 one can assume

small oscillations and write

$$\sin\theta \simeq \theta, \quad \cos\theta \simeq 1, \quad \theta^3 \simeq \text{small}, \quad \theta'^2 \sin\theta \simeq \text{small}$$

Substituting in equations 79 and 80

$$X'' + (\mu/\epsilon)\theta'' + 2\zeta_m X' + X = 0 \tag{82}$$

$$\theta'' + \epsilon X'' + 2\zeta_p \Omega\theta' + \Omega^2\theta = 0 \tag{83}$$

Assuming solutions of the form

$$X = Ae^{sT} \quad \text{and} \quad \theta = Be^{sT} \tag{84}$$

and substituting in equations 82 and 83

$$[(s^2 + 2\zeta_m s + 1)A + ((\mu/\epsilon)s^2)B]e^{sT} = 0 \tag{85}$$

$$[(\epsilon s^2)A + (s^2 + 2\zeta_p \Omega s + \Omega^2)B]e^{sT} = 0 \tag{86}$$

Since $e^{sT} \neq 0$ for all time, for a nontrivial solution the determinant of coefficients must vanish.

$$\begin{vmatrix} (s^2 + 2\zeta_m s + 1) & (\mu/\epsilon)s^2 \\ \epsilon s^2 & (s^2 + 2\zeta_p \Omega s + \Omega^2) \end{vmatrix} = 0 \tag{87}$$

The value of the determinant yields the characteristic equation as

$$(1 - \mu)s^4 + 2(\zeta_p \Omega + \zeta_m)s^3 + (\Omega^2 + 4\zeta_m \zeta_p \Omega + 1)s^2 + 2(\zeta_m \Omega^2 + \zeta_p \Omega)s + \Omega^2 = 0 \tag{88}$$

The solutions of equation 88 are generally pairs of complex conjugates, at least for the range of parameters investigated, and can be written as

$$S_{1,2} = -a_1 \pm ib_1 \tag{89}$$

$$S_{3,4} = -a_2 \pm ib_2 \tag{90}$$

Substituting these solutions in equation 84 and realizing that in linear equations superposition holds one can write

$$X = A_1 e^{S_1 \tau} + A_2 e^{S_2 \tau} + A_3 e^{S_3 \tau} + A_4 e^{S_4 \tau} \tag{91}$$

$$\theta = B_1 e^{S_1 \tau} + B_2 e^{S_2 \tau} + B_3 e^{S_3 \tau} + B_4 e^{S_4 \tau} \tag{92}$$

and

$$X = e^{-a_1 \tau}[C \cos b_1 \tau + D \sin b_1 \tau] + e^{-a_2 \tau}[E \cos b_2 \tau + F \sin b_2 \tau] \tag{93}$$

$$\theta = e^{-a_1 \tau}[H \cos b_1 \tau + I \sin b_1 \tau] + e^{a_2 \tau}[J \cos b_2 \tau + K \sin b_2 \tau] \tag{94}$$

Considering the response of the main system only one can rewrite equation 93 in a different form as

$$X = C' e^{-a_1 \tau} \sin(b_1 \tau + \varphi_1) + E' e^{-a_2 \tau} \sin(b_2 \tau + \varphi_2). \tag{95}$$

It can be seen from equation 95 that the response of the main system is the sum of two decaying harmonic functions and therefore can be analyzed as such. For each component of the response there exists a logarithmic decrement such that

$$\delta_1 = 2\pi\left(\frac{a_1}{b_1}\right) \tag{96}$$

and

$$\delta_2 = 2\pi\left(\frac{a_2}{b_2}\right) \tag{97}$$

It is worthy of mentioning that in the linear analysis the characteristic equation (equation 88) is independent of the initial conditions and that the damping is also independent of initial conditions, this is not true in the nonlinear case which will be discussed later.

The governing parameters of the system are μ, ζ_m, ζ_p and Ω and will be analyzed later.

Digital Computer Program and Analysis

Because of the nature of the complex roots of equation 88, the process of root finding will become tedious unless a digital computer is employed.

A program in Fortran language with the use of a polynomial root finding subroutine was written.* A copy of the computer printout of the main program and a copy of output roots are included in Appendix D.

Using equations 96, 97 and the corresponding roots the values of logarithmic decrements were calculated.

To avoid unnecessary investigations the design parameters were tested in the following regions:

1. The values of the frequency ratio Ω used, range from 0.2 to 1.3, which cover a reasonable range of frequency on either side of the resonance ($\Omega = 1$).

2. Too small a value for mass ratio (μ) is not desirable because

*The subroutine is called ROOTCP and is obtained from a UNIVAC-1108, MATH-PACK.

the mass ratio is directly related to the size ratio of the two uncoupled systems, and that for very small μ the size of the auxiliary system has to be very small compared to the main system, then it is evident that the relative effectiveness of the auxiliary system will be reduced. On the other hand, too large a mass ratio indicates that the auxiliary system should be much larger and too massive compared to the main system which is not desirable either. Another reason for rejection of large mass ratio from design point of view is due to weight penalty which should be kept minimum. Therefore, the range of values covered is from $\mu = 0.1$ to $\mu = 0.5$.

3. Too small a value for viscous damping ζ_p results in a weak coupling condition in which the capacity of dissipation is slight. For this condition, if the mass ratio is considerable the damper is more effective as a vibration absorber. It is in this configuration that Chen [12] used sloshing water as vibration absorber. It should be also noted that if the parameters are not controlled properly for the case of large mass ratio, this condition of fluid sloshing could be very dangerous. This cirtical situation is investigated in more detail in connection with fuel sloshing in tanks of space vehicles [1]. Too large a value of viscous damping is not desirable either, because the fluid (pendulum) will be over damped and will act as a rigid member. Reasonable values of this parameter are considered in the analysis and will be reported later.

4. The parameter ζ_m related to the structural damping of the main system is uncontrollable and is inherent in the system. Since the purpose of this investigation is to provide damping for an undamped main system, the values of ζ_m must be very small or else additional damping

would not be needed. Therefore, for the general theoretical investigations ζ_m is assumed zero and later the effect of small ζ_m is also investigated.

The logarithmic decrements of the two components of motion are calculated from the computer outputs and are plotted in Figures 14 through 21. From a general outlook of the variation of the logarithmic decrements with respect to the frequency ratio one can divide the frequency domain in three regions.

1. For very small frequency ratios ($\Omega < \Omega_p$) one of the components of motion (Eqn. 95) vanishes rapidly and the main system will be described by the remaining component. The component that vanishes rapidly corresponds to the upper curves of Figures 14 through 21 and the dominant component of motion corresponds to the lower curves of Figures 14 through 21.

In this region for the case of linear motion and small amplitudes of oscillations relatively small dissipation (viscous friction) exists. The overall damping, therefore, remains relatively small.

2. For large frequency ratios ($\Omega > \Omega_p$) similar situation exists. In this region the main system behaves like the lower curves of Figures 14 through 21 and the other component of motion (equation 95) exhibiting large damping (upper curves of Figures 14 through 21) diminishes faster. In either case significant amplitudes of fluid motion can not be obtained unless the amplitude of initial displacement is increased, only then due to large amplitude of motion the friction forces increase and therefore the overall damping is expected to be improved. The subject of large amplitudes of fluid motion will be discussed in the next chapter because

of its nonlinear character.

3. For frequency ratios $\Omega = \Omega_p$ as indicated by the intersection of each pair of curves in Figures 14 through 21, both components have the same logarithmic decrements and the coupled system exhibits maximum damping. The relative "tuning" frequency ratios of the damper with respect to the main system (Ω) corresponding to these points of maximum damping are termed critical tuning frequency ratio (Ω_p) throughout the remaining of this program.

It should be noticed that at these frequencies the damper will be quite similar to a tuned-damped vibration absorber. Several other interesting phenomena will be discovered if certain plots are extracted from Figures 14 through 21. The plots may indicate the influence of the parameters upon each other as well as on the overall damping of the main system.

One of such phenomena is the influence of mass ratio upon the critical tuning frequency ratio (Ω_p) of the two systems. Figure 22 indicates an almost linear decrease in critical tuning frequency ratio with increase in the mass ratio. This fact is obvious because for a pendulum with fixed mass and length if the mass of the main system is decreased, the mass ratio will increase (since $\mu = M_p/M$) and at the same time for decreasing mass of the main system, its frequency will increase ($\omega_m \simeq \sqrt{\frac{k_m}{M}}$) and therefore the critical tuning frequency ratio will decrease as a result of increase in the mass ratio.

Two other important facts can be observed from Figure 23 which is also extracted from Figures 14 through 21.

1. The overall damping will not be improved considerably by

increasing the mass ratio. On the other hand, large mass ratios are not desirable from design point of view, therefore by selecting relatively small mass ratios the designer can tune some other sensitive parameters and still obtain considerable damping. For most of the remaining analysis a value of $\mu = 0.1$ which is frequently used in design of vibration absorbers is selected. The value of $\mu = 0.1$ being so small will not contribute much to the weight penalty.

2. The overall damping is very sensitive to the fluid (pendulum) damping, for increasing ζ_p appreciable improvement in damping of the main system can be made. Of course this is true up to a critical value of ζ_p after which the damping of the main system will decrease.

From the previous analysis it was found that the damping of the main system is sensitive to both the frequency ratio and to the viscous damping factor. In order to observe the sensitivity of the overall damping to these two parameters explicit curves are plotted in Figures 24, 25, and 26. The three frequency ratios selected are one at critical tuning and one on either side of the critical tuning.

Figures 24, 25, and 26 exhibit some very important features of the damper.

1. On either side of the critical tuning frequency ratio one component of the motion decays rapidly and the main system behaves like the component with smaller logarithmic decrement, while at the cirtical tuning frequency ratio the two components have equal importance and have the same logarithmic decrement up to the critical value of viscous damping after which one component decays much faster and the main system again behaves like the component with small logarithmic decrement.

2. At the critical tuning frequency, the logarithmic decrements increase linearly with the increase in viscous damping up to a critical value of ζ_p and then decreases. For frequency ratios on either side of the critical tuning the linearity is only up to about half the critical value of ζ_p and then the increase takes a slightly nonlinear form up to the critical value of viscous damping.

3. The critical value of viscous damping differs for different frequency ratios and possibly for different mass ratios.

Unfortunately due to the complex interrelation of parameters to the logarithmic decrement as can be seen from the characteristic equation, explicit values or expressions for the critical viscous damping factor ζ_{pc} could not be obtained, but the values for specific mass ratio and frequency ratio can be obtained from plots like those of Figures 24, 25, and 26. As mentioned earlier it is interesting to study the effect of small structural damping on the general outlook of the previous investigations. For this purpose Figures 27 and 28 are plotted which exhibit two important features.

1. Figure 27 indicates that the critical tuning frequency ratios (Ω_p) decrease if the structural damping is in the order of magnitude of the viscous damping and that for $\zeta_p \gg \zeta_m$ the decrease is considerably small.

2. Figure 28 indicates that the effect of small structural damping upon the logarithmic decrements of motion is simply additive regardless of the magnitude of the viscous damping.

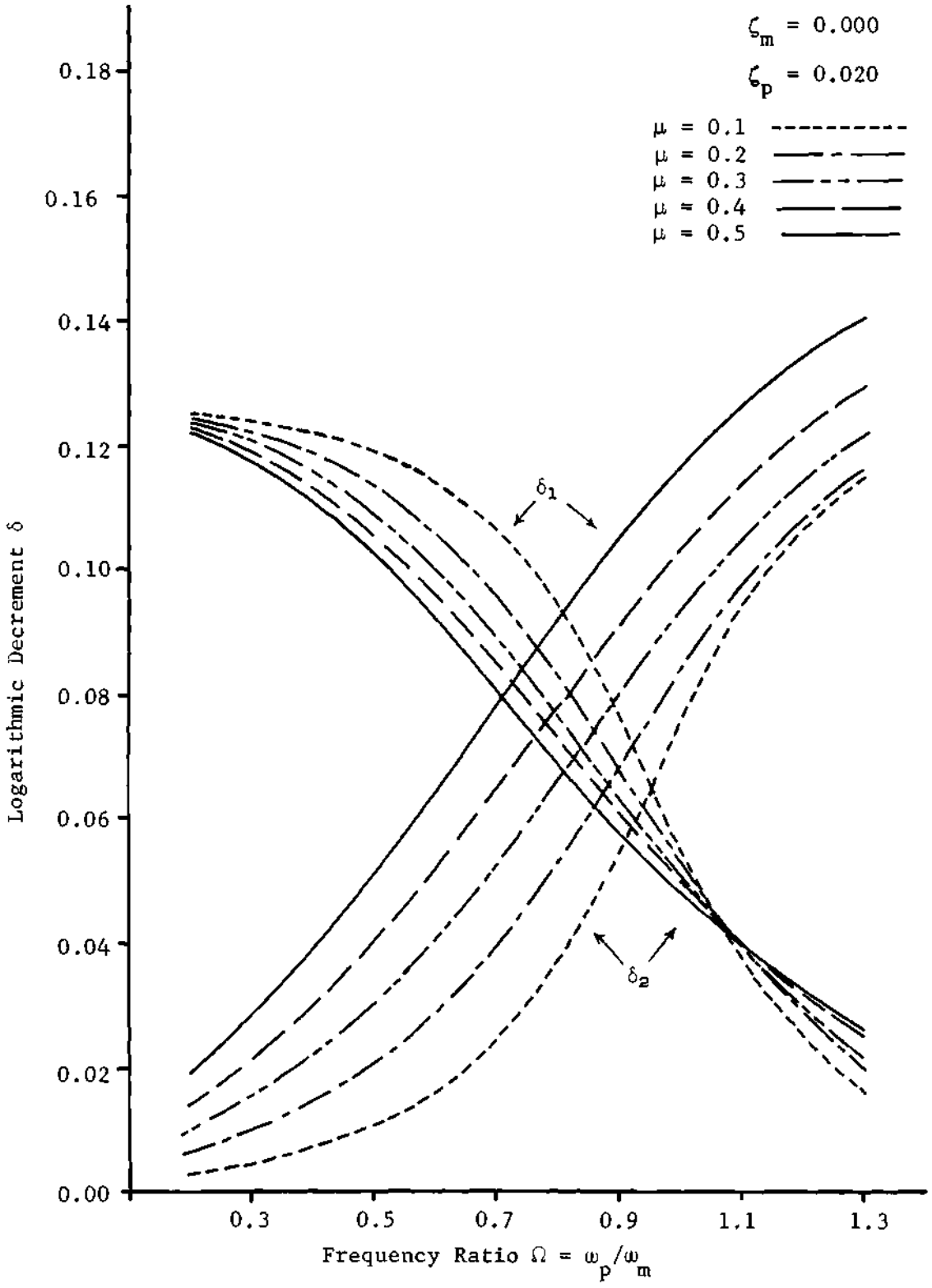

Figure 14. Logarithmic Decrement of Motion ζ_p = 0.02

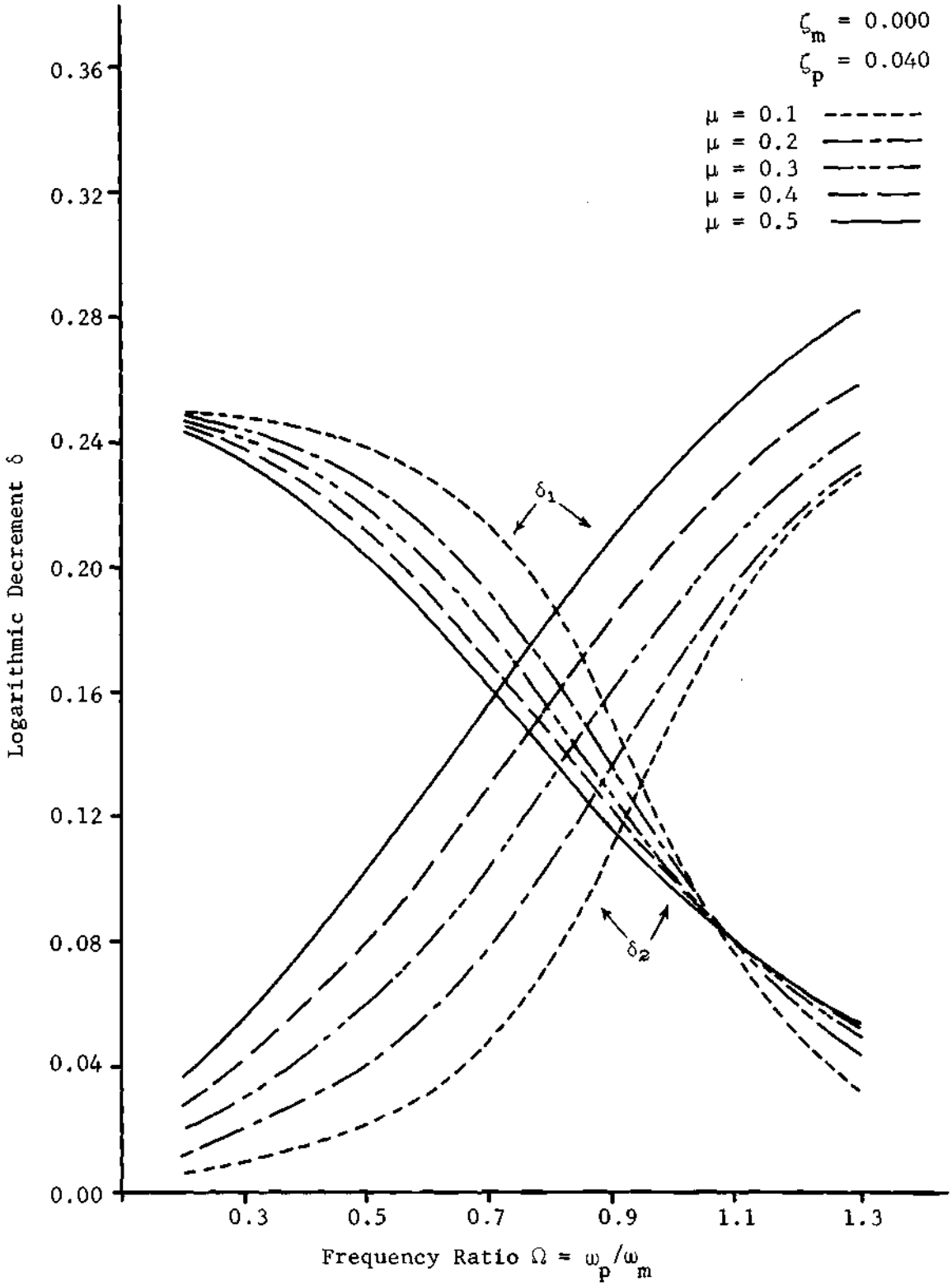

Figure 15. Logarithmic Decrement of Motion ζ_p = 0.04

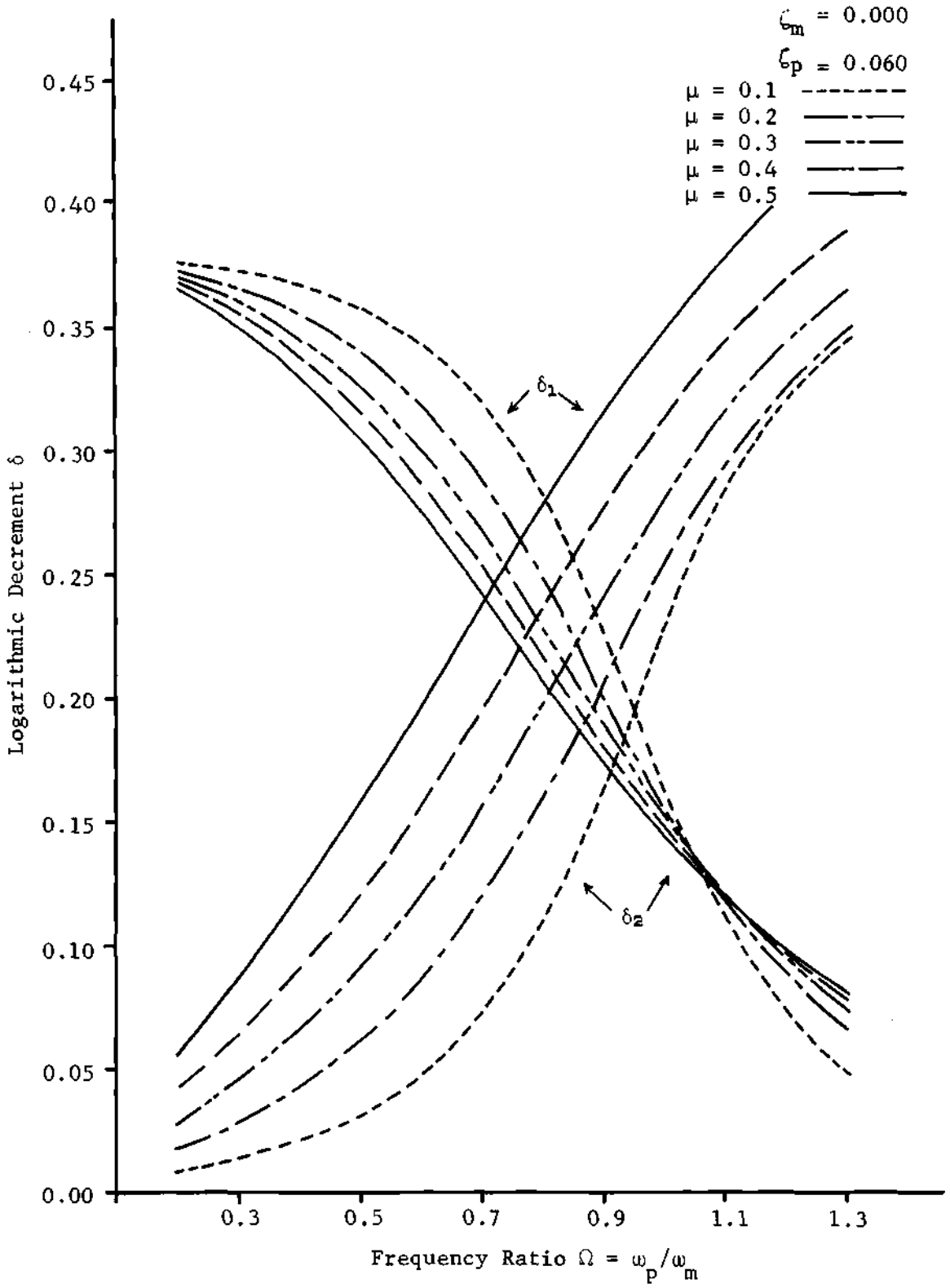

Figure 16. Logarithmic Decrement of Motion ζ_p = 0.06

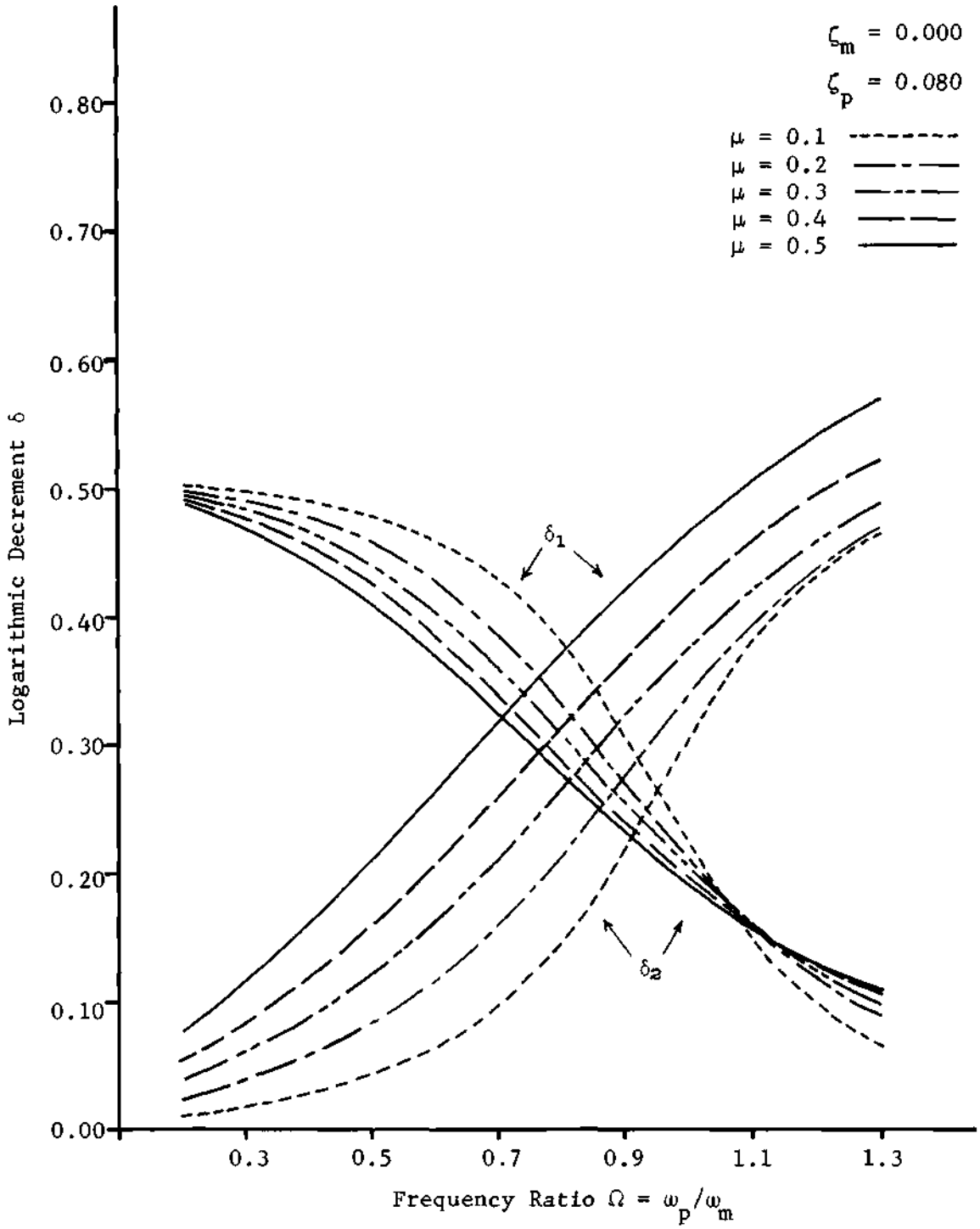

Figure 17. Logarithmic Decrement of Motion ζ_p = 0.08

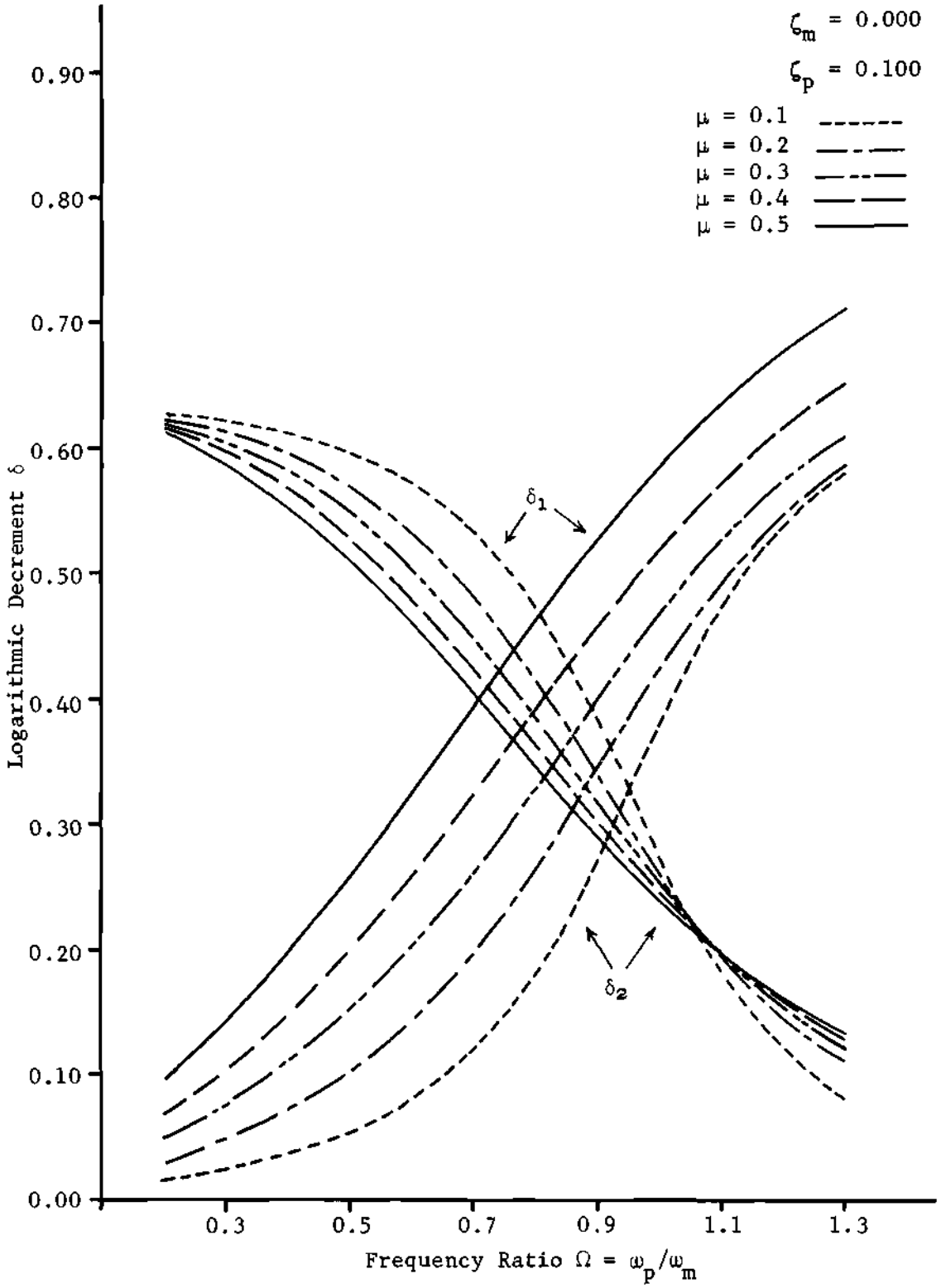

Figure 18. Logarithmic Decrement of Motion ζ_p = 0.10

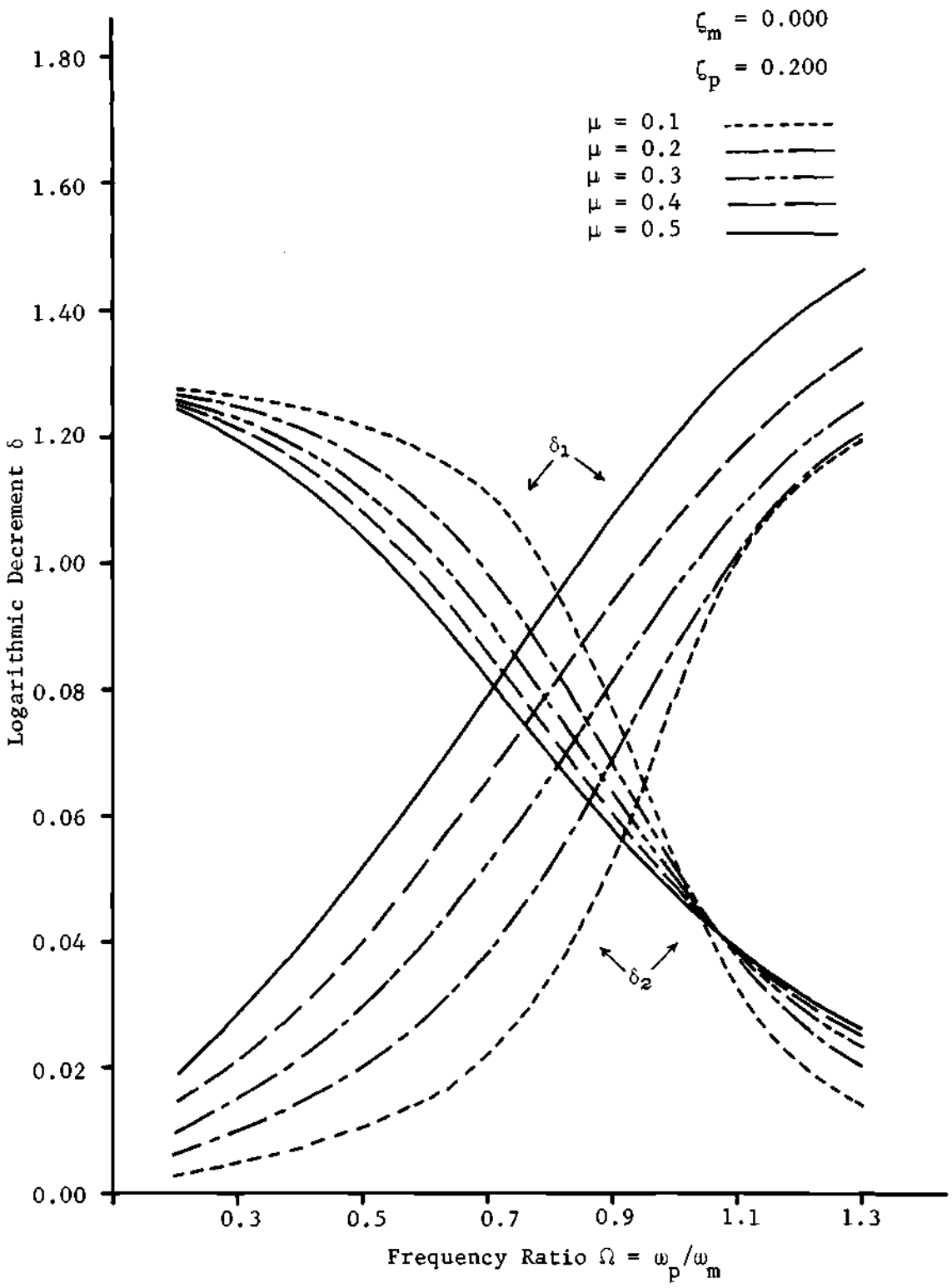

Figure 19. Logarithmic Decrement of Motion ζ_p = 0.20

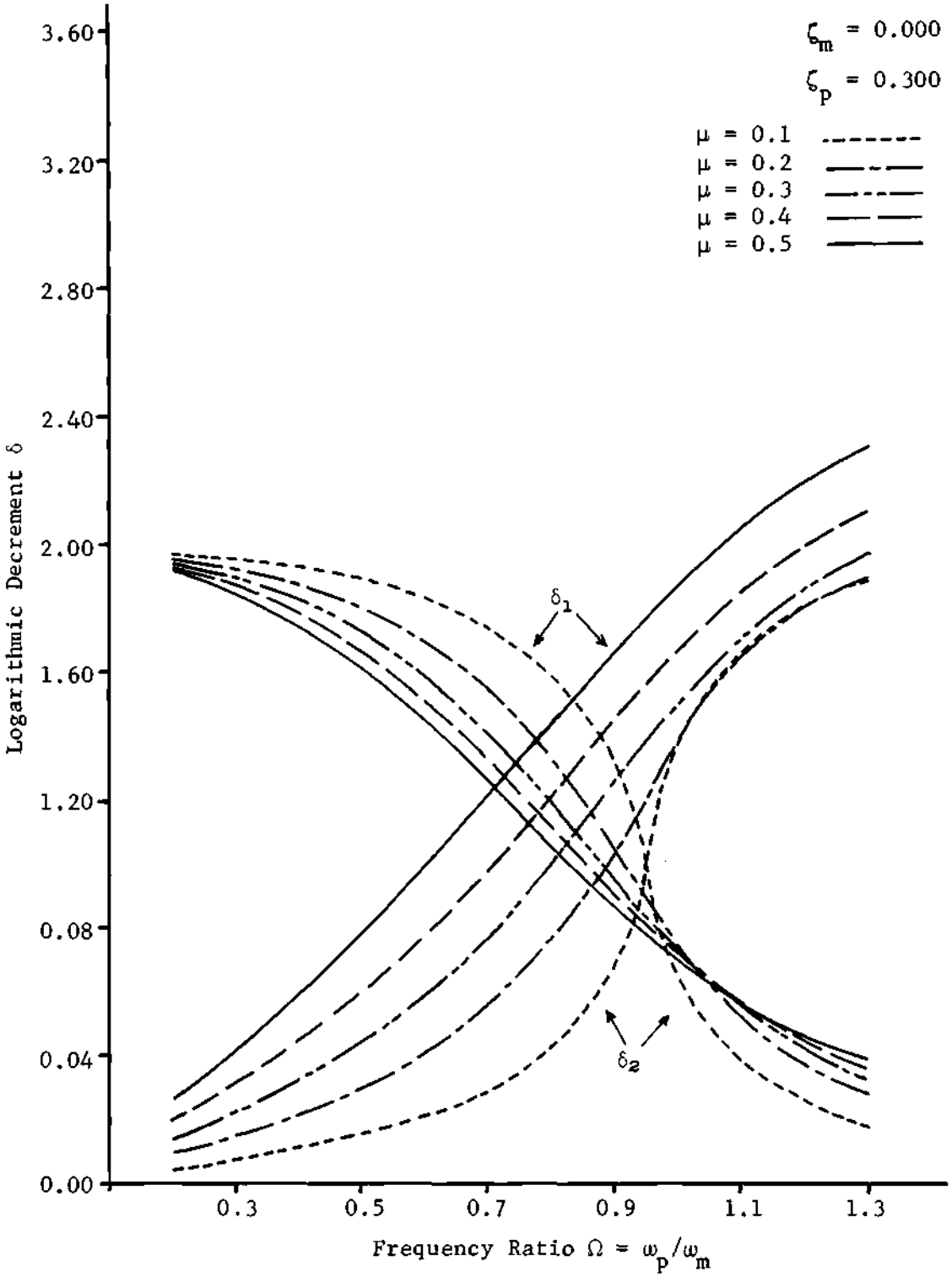

Figure 20. Logarithmic Decrement of Motion ζ_p = 0.30

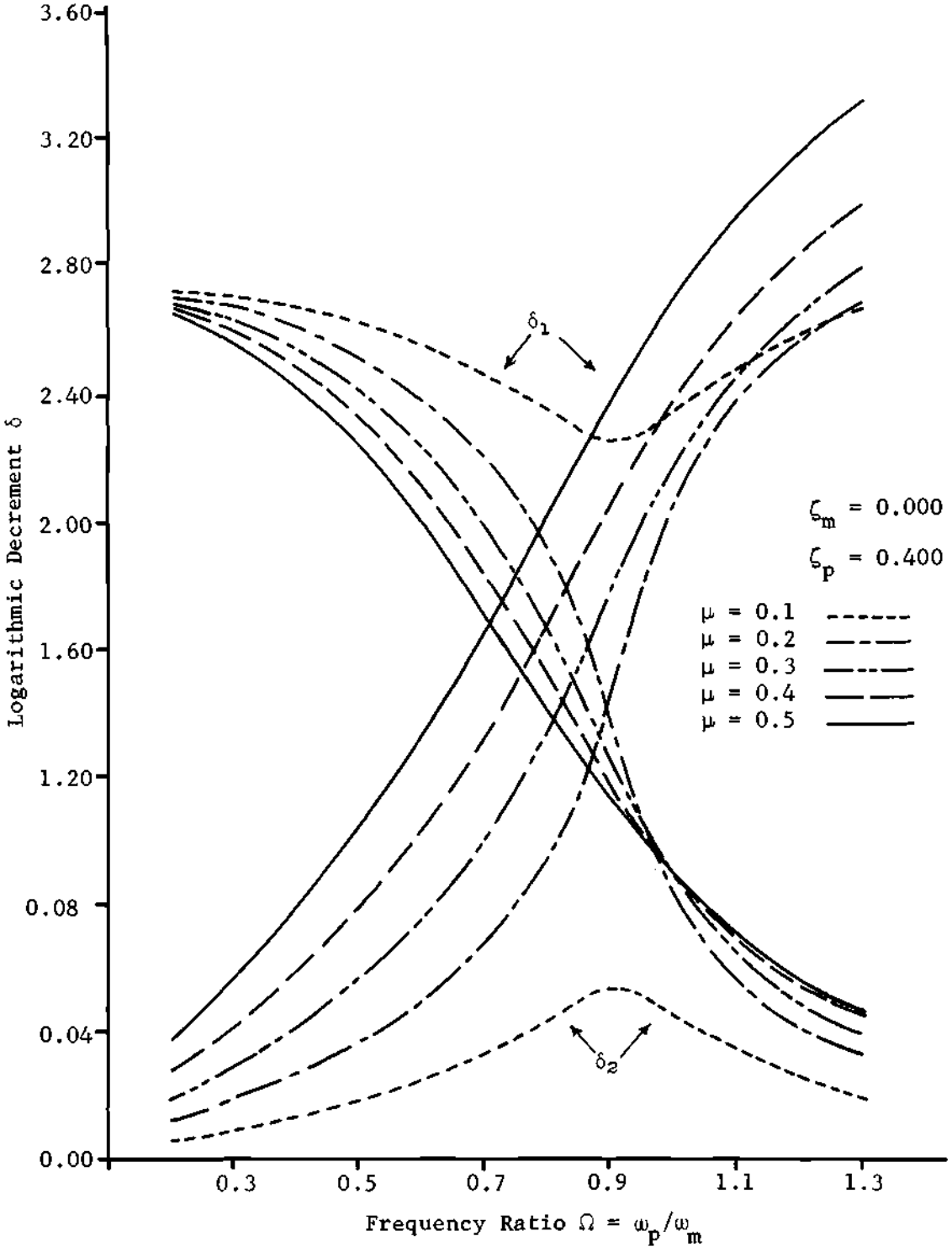

Figure 21. Logarithmic Decrement of Motion $\zeta_p = 0.40$

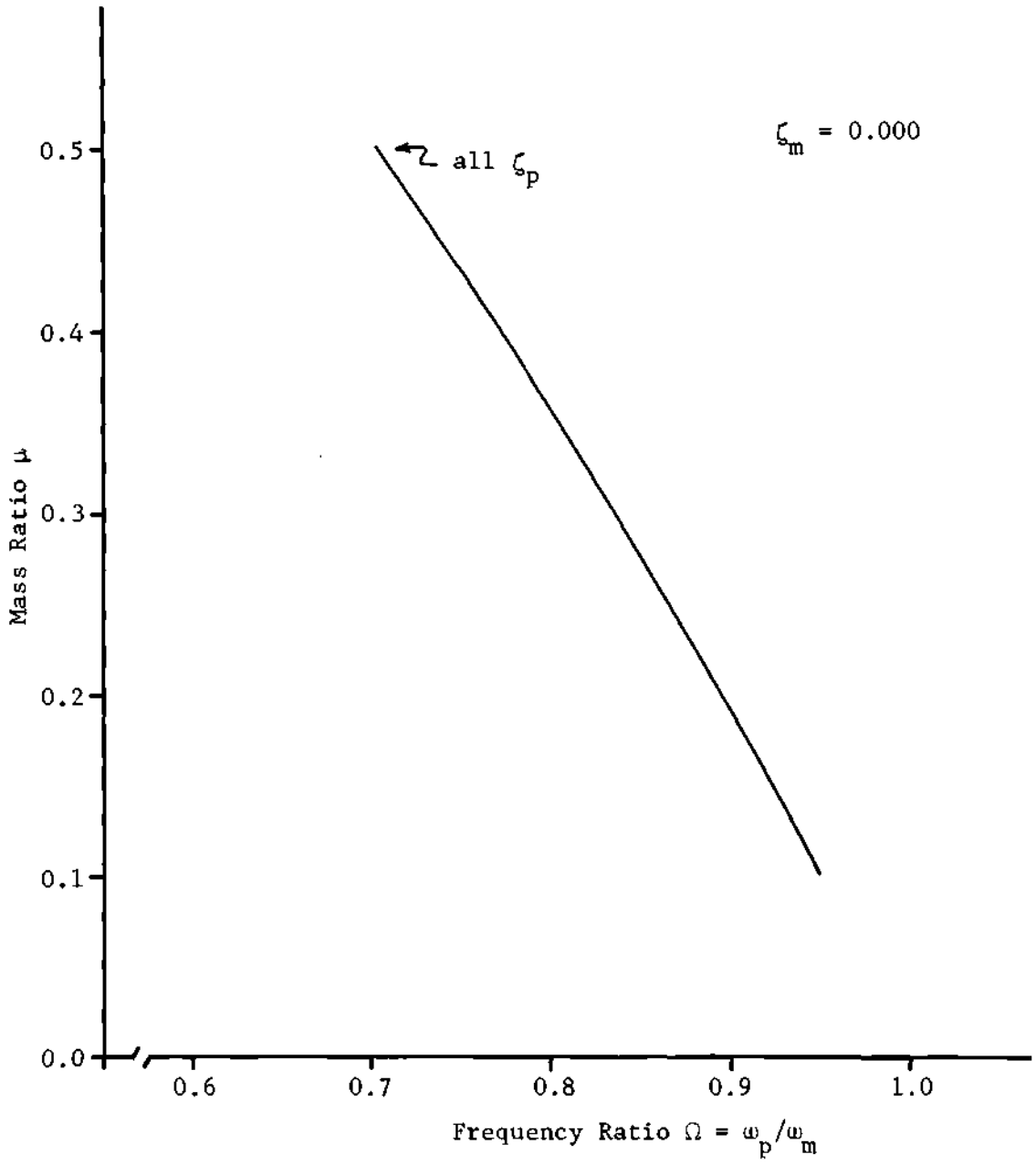

Figure 22. The Effect of Mass Ratio on the Critical Tuning Frequency

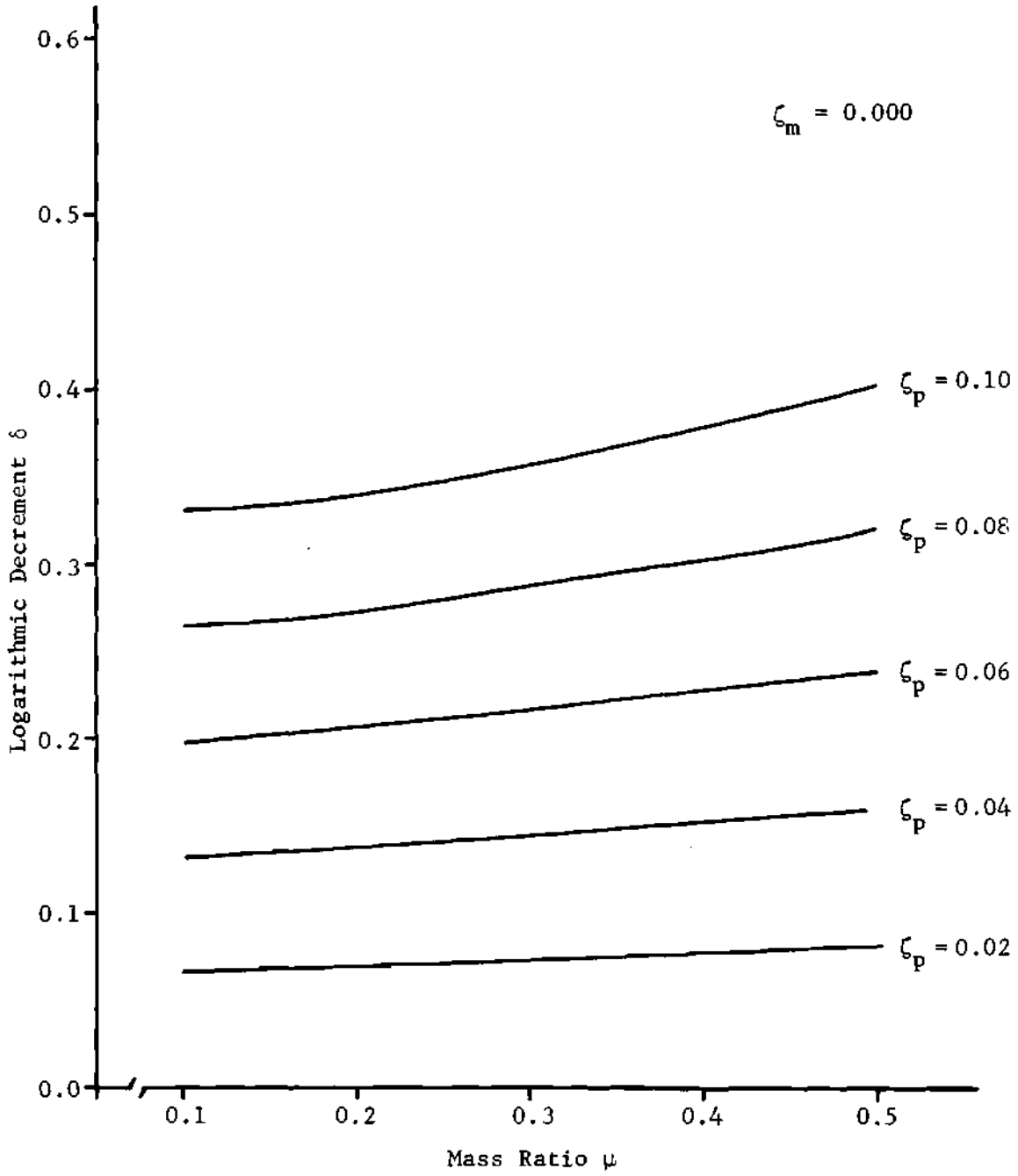

Figure 23. The Effect of Mass Ratio and Viscous Damping on the Damping of the Main System

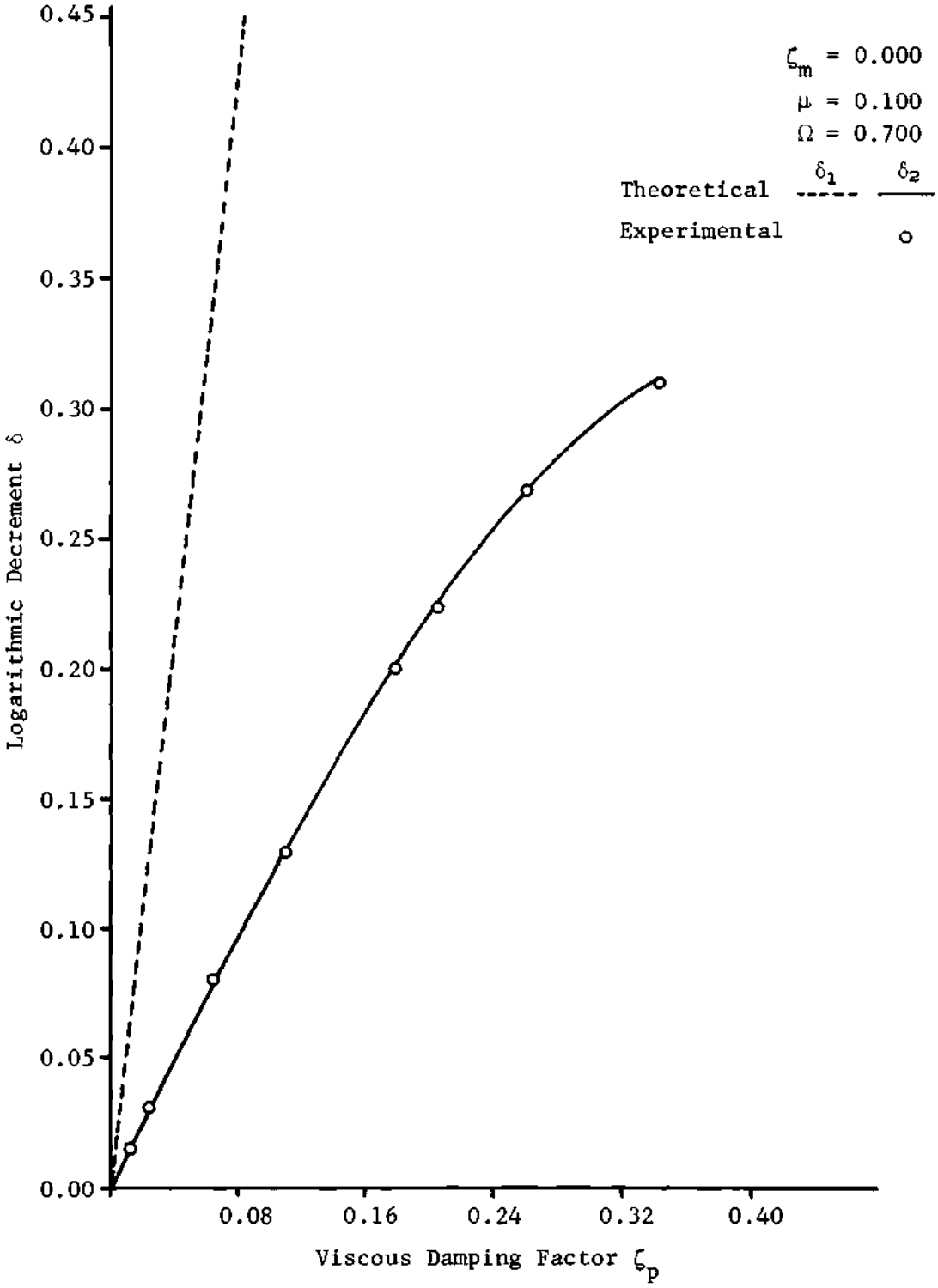

Figure 24. Influence of Viscous Damping on the Damping of the Main System Ω = 0.70

Table 2. Design Specifications and Damping of the Coupled System for $\mu = 0.1$, $\zeta_m = 0$, $\Omega = 0.7$*

		δ (experimental)
water	$K_{m/4} = 0.652$ #/in	0.0149
	$W_w = 0.905$ #	
50% Glycerin	$K_{m/4} = 0.739$ #/in	0.0301
	$W_w = 1.109$ #	
74% Glycerin	$K_{m/4} = 0.779$ #/in	0.0800
	$W_w = 1.216$ #	
85% Glycerin	$K_{m/4} = 0.796$ #/in	0.1297
	$W_w = 1.258$ #	
92% Glycerin	$K_{m/4} = 0.812$ #/in	0.2000
	$W_w = 1.296$ #	
95% Glycerin	$K_{m/4} = 0.820$ #/in	0.2236
	$W_w = 1.300$ #	
97% Glycerin	$K_{m/4} = 0.822$ #/in	0.2680
	$W_w = 1.310$ #	
99% Glycerin	$K_{m/4} = 0.824$ #/in	0.3100
	$W_w = 1.319$ #	

*D = 3.862 inches, H/D = 0.340, $W_t = 0.122$ #, $W_s = 0.616$ #

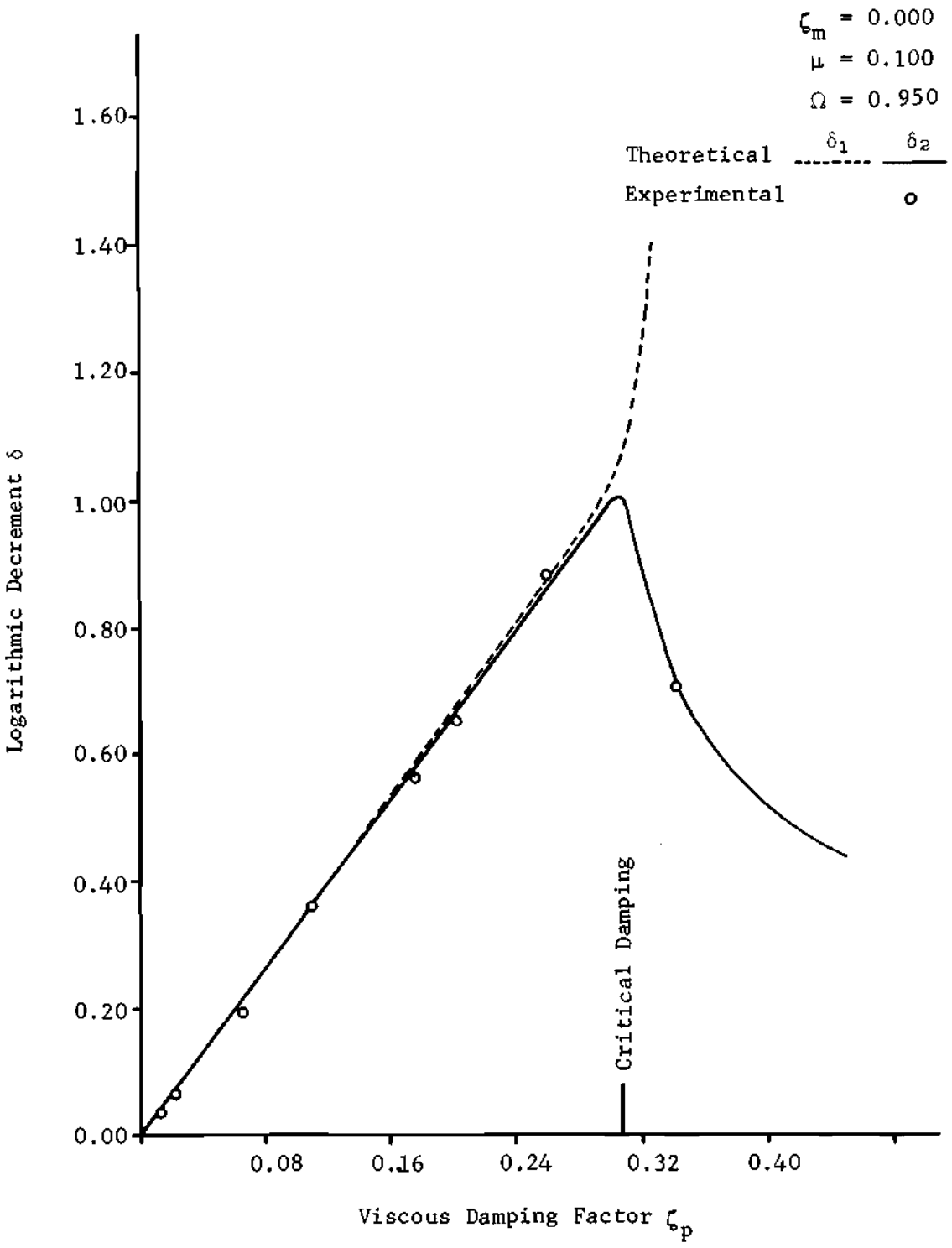

Figure 25. Influence of Viscous Damping on the Damping of the Main System Ω = 0.95

Table 3. Design Specifications and Damping of the Coupled System for $\mu = 0.1$, $\zeta_m = 0$, $\Omega = 0.95$*

		δ (experimental)
water	$K_{m/4} = 0.350$ #/in	0.0379
	$W_w = 0.905$ #	
50% Glycerin	$K_{m/4} = 0.395$ #/in	0.0658
	$W_w = 1.109$ #	
74% Glycerin	$K_{m/4} = 0.420$ #/in	0.1915
	$W_w = 1.216$ #	
85% Glycerin	$K_{m/4} = 0.429$ #/in	0.3595
	$W_w = 1.258$ #	
92% Glycerin	$K_{m/4} = 0.438$ #/in	0.5605
	$W_w = 1.296$ #	
95% Glycerin	$K_{m/4} = 0.440$ #/in	0.6500
	$W_w = 1.300$ #	
97% Glycerin	$K_{m/4} = 0.442$ #/in	0.8800
	$W_w = 1.310$ #	
99% Glycerin	$K_{m/4} = 0.553$ #/in	0.7044
	$W_w = 1.319$ #	

*D = 3.862 inches, H/D = 0.340, $W_t = 0.122$ #, $W_s = 0.616$ #

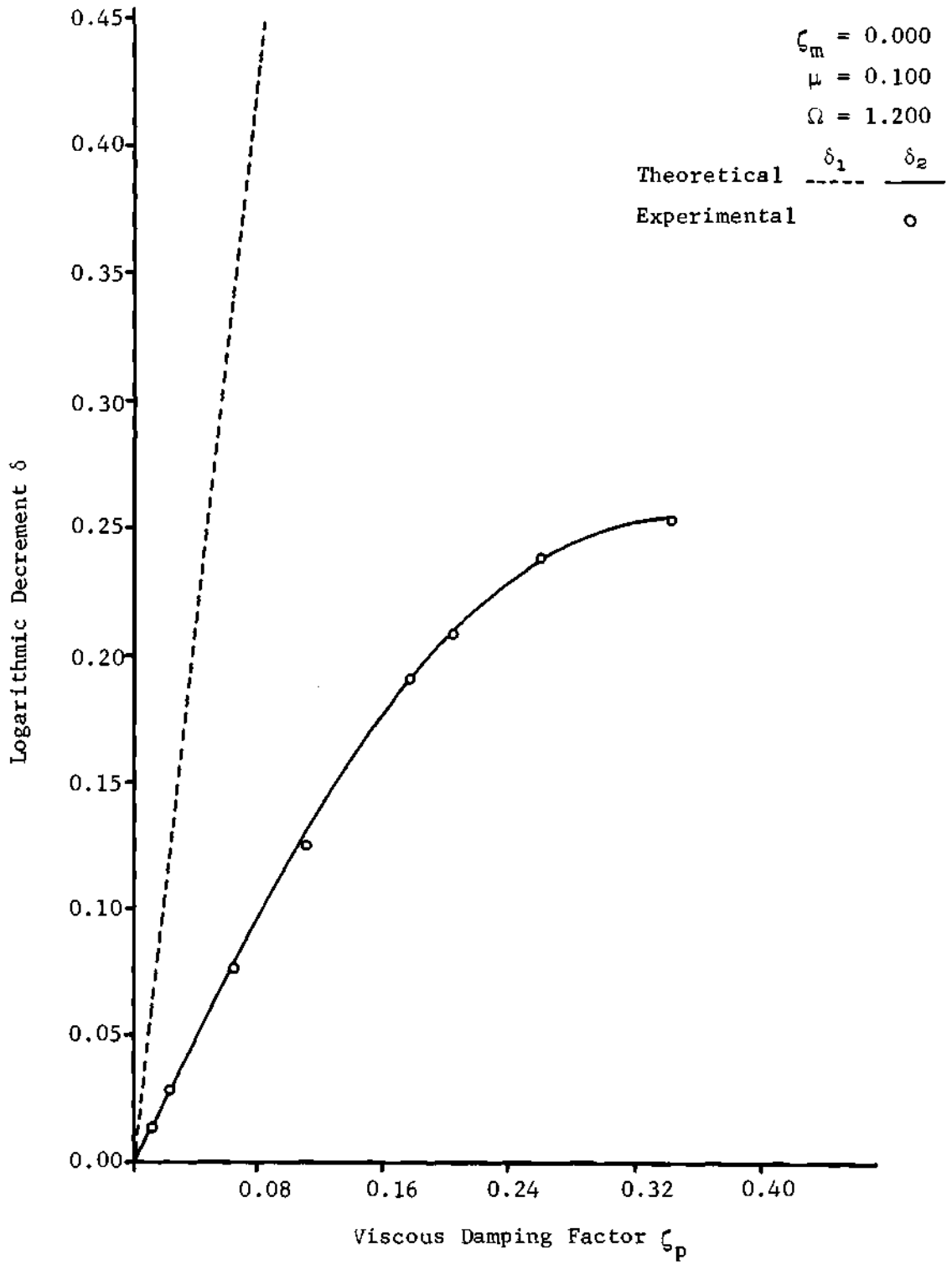

Figure 26. Influence of Viscous Damping on the Damping of the Main System Ω = 1.20

Table 4. Design Specifications and Damping of the Coupled System for $\mu = 0.1$, $\zeta_m = 0$, $\Omega = 1.2$*

		δ (experimental)
water	$K_{m/4} = 0.217$ #/in	0.0129
	$W_w = 0.905$ #	
50% Glycerin	$K_{m/4} = 0.245$ #/in	0.0278
	$W_w = 1.109$ #	
74% Glycerin	$K_{m/4} = 0.259$ #/in	0.0770
	$W_w = 1.216$ #	
85% Glycerin	$K_{m/4} = 0.265$ #/in	0.1258
	$W_w = 1.258$ #	
92% Glycerin	$K_{m/4} = 0.270$ #/in	0.1913
	$W_w = 1.296$ #	
95% Glycerin	$K_{m/4} = 0.271$ #/in	0.2077
	$W_w = 1.300$ #	
97% Glycerin	$K_{m/4} = 0.272$ #/in	0.2391
	$W_w = 1.310$ #	
99% Glycerin	$K_{m/4} = 0.273$ #/in	0.2537
	$W_w = 1.319$ #	

*D = 3.862 inches, H/D = 0.340, $W_t = 0.122$ #, $W_s = 0.616$ #

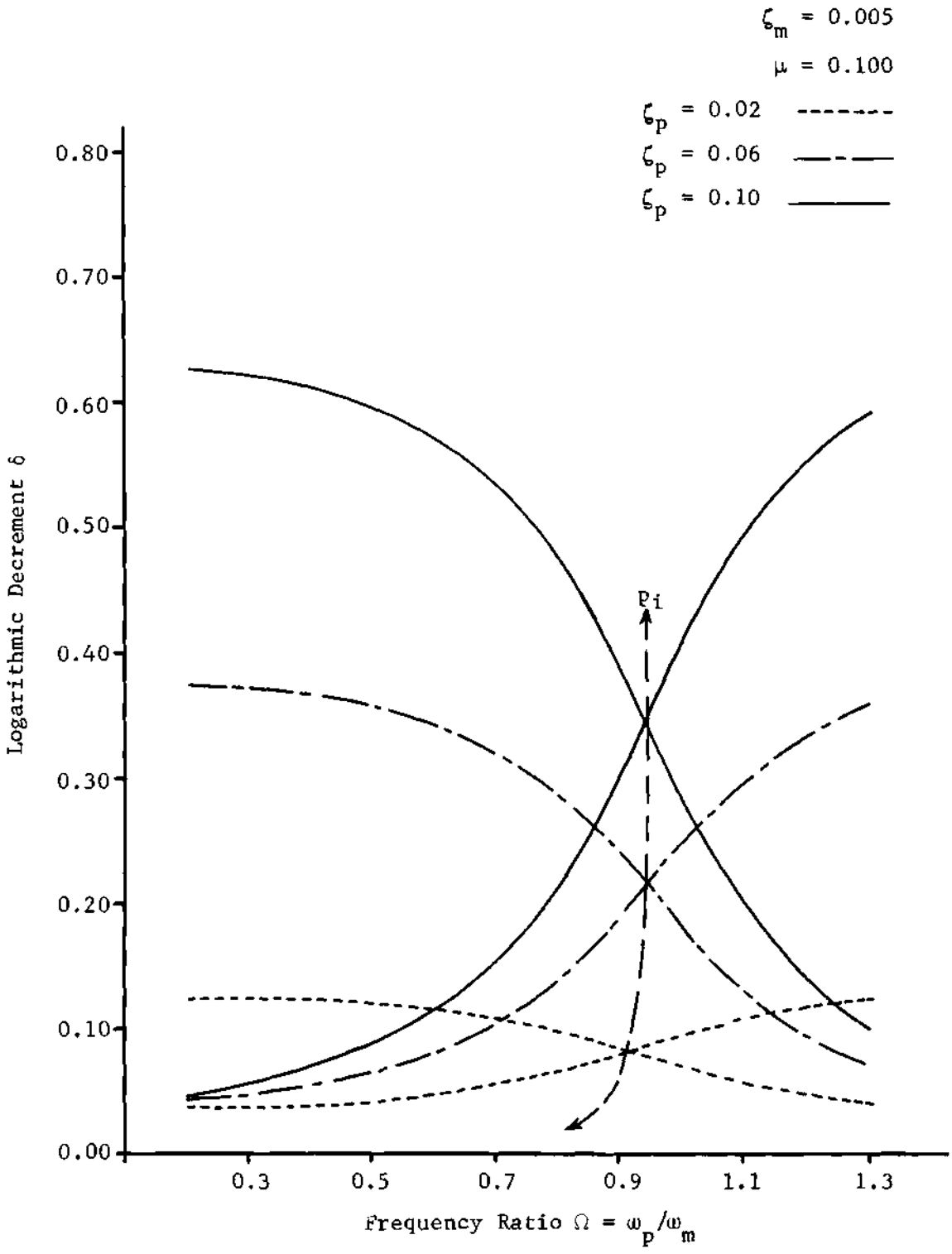

Figure 27. Effect of Small Structural Damping on Resonance Frequency

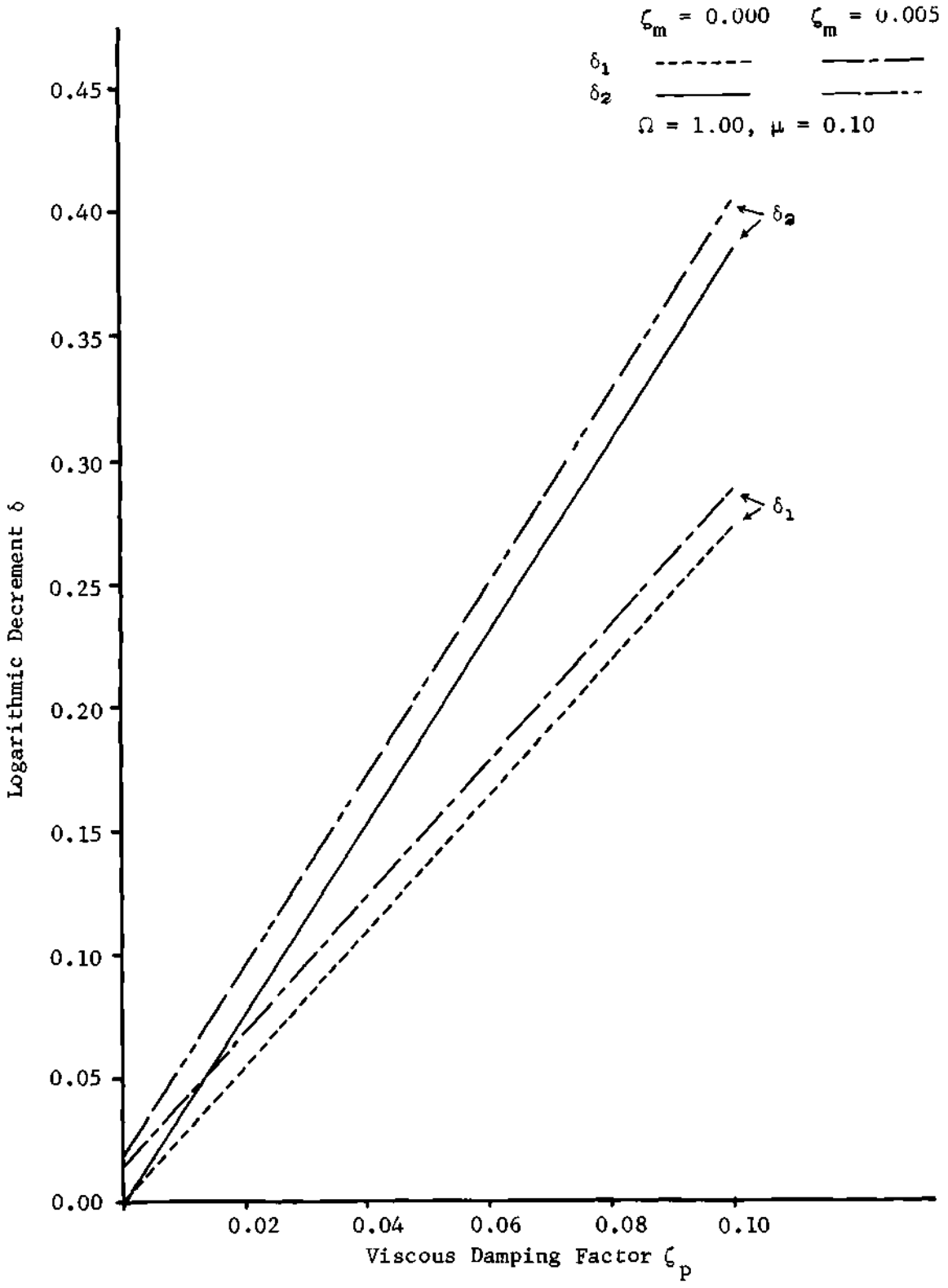

Figure 28. Effect of Small Structural Damping on Logarithmic Decrement

Comparison to Experiments and Analysis of "Beat"

It is understood from the previous analysis that the frequency ratio and the viscous damping of fluid (pendulum) are the two most sensitive parameters contributing to the overall damping of the main system. Since Figures 24 to 26, which are drawn for three arbitrarily selected frequency ratios from the three regions of the frequency domain, demonstrate the improvement in damping of the main system the best, experiments were run (Design Specifications are listed in Tables 2, 3, and 4) and the logarithmic decrements of the main system were calculated from the measured response. The experimental logarithmic decrements are identified by small circles in Figures 24 to 26 and the agreement with the theoretical curves is excellent.

From an observation of experimental response of the main system another important feature of the coupled system was discovered. This feature is the existance of "Beat" at frequency ratios near the critical tuning. Theory also indicates that for a system having two frequencies of different harmonics, one should expect "Beat" to occur when the difference of the frequencies is small. Since the solution of the coupled system (equation 95) contains two frequencies $b_1\omega_m$ and $b_2\omega_m$ and for the frequency ratios close to the critical tuning $(b_1 - b_2)$ is usually small, the theoretical response should also exhibit "Beat." Since it did not seem necessary to plot the response from equation 95 for the linear case, the agreement of the theory will be shown in the next chapter by solving the exact differential equations of motion in the nonlinear form.

The phenomena of "Beat" occurs in physical systems having a weak degree of coupling. In such a case the energy will be transferred from

one system to the other and back to the original system. For the case of negligible damping this transfer of energy will occur indefinitely, but for systems with damping the envelope of beat decays with time. This is exactly what was observed from the experimental records of the response, and it was also found that with the increase in fluid (pendulum) damping the envelope of beat decayed faster and faster. The beat envelope completely disappeared at the critical damping indicated in Figure 25. The reason for decay and disappearance of beat is the dissipation of energy in the fluid such that the fluid receives certain amount of energy from the main system and dissipates part of this energy in the first cycle (depending on the capacity of dissipation). The fluid then gives lesser energy to the main system during the next cycle and during the successive cycles lesser and lesser energy will be transferred between the main and the auxiliary system until all the energy is dissipated. It is then, that the main system comes to a complete stop. In case of high damping ($\zeta_p \geq \zeta_{pc}$) most of the energy is dissipated during the first few cycles and the beat phenomena will not exist.

It is already proved that the maximum damping of the main system occurs at $\Omega = \Omega_p$, but unfortunately this is the region where beat is the most serious and for many applications it may not be desirable to have beat in the response of the main system. In such cases the designer should either use values of viscous damping equal or greater than the critical value or tune the main system at some other frequency ratio and accept lesser overall damping. It is also possible to increase the mass ratio to obtain higher damping but one should accept the weight penalty in this case.

Because of the existence of beat the frequencies and amplitudes of the components of motion (equation 95) combine in some fashion to produce the final response of the main system. It was easy to analyze each component and obtain the logarithmic decrements of motion separately. This method of isolation of components worked well for $\Omega < \Omega_p$ and $\Omega > \Omega_p$ merely because one of the components decays rapidly and the remaining component explains the response and the damping of the main system.

For the case of $\Omega = \Omega_p$ the response and damping of the main system cannot be explained by either of the components of the motion alone. Both components have equal importance and according to equation 95 which is very complicated to solve, one cannot obtain a single easy to handle criteria for determination of the overall damping of the main system, unless further approximations are sought.

The following is a simple approximate solution derived to replace equation 95 because of its simplicity.

Considering equation 95 and realizing that at $\Omega = \Omega_p$ the values of a_1 and a_2 as well as b_1 and b_2 are close to each other, one can assume

$$a_1 \simeq a_2 \simeq \frac{a_1 + a_2}{2} \tag{98}$$

Rewriting equation 95

$$X = e^{-\left(\frac{a_1 + a_2}{2}\right)\tau} [C' \sin(b_1\tau + \varphi_1) + E' \sin(b_2\tau + \varphi_2)] \tag{99}$$

At resonance both components of motion have equal importance, therefore one can assume

$$C' \simeq E' \tag{100}$$

After substitution of equation 100, equation 99 becomes

$$X = E' e^{-\left(\frac{a_1 + a_2}{2}\right)\tau} [\sin(b_1\tau + \varphi_1) + \sin(b_2\tau + \varphi_2)]. \tag{101}$$

Noticing that at the critical tuning frequency which corresponds to the resonance frequency in the case of forced vibration the phase angle is $\varphi_1 \simeq \varphi_2 \simeq \frac{\pi}{2}$, one can rewrite equation 101 as

$$X = E' e^{-\left(\frac{a_1 + a_2}{2}\right)\tau} [\cos b_1\tau + \cos b_2\tau]. \tag{102}$$

Using the initial conditions

$$\tau = 0, \text{ and}$$

$$X = 1, \text{ yields}$$

$$E' = 1/2.$$

Substituting for the sum of cosines and the value of E', equation 102 becomes

$$X = e^{-\left(\frac{a_1 + a_2}{2}\right)\tau} \cos\left(\frac{b_1 + b_2}{2}\right)\tau \quad \cos\left(\frac{b_1 - b_2}{2}\right)\tau \tag{103}$$

Indeed equation 103 is the equation of beat with exponentially decaying envelope. The beat frequency is $\left(\frac{b_1 - b_2}{2}\right)\omega_m$ and the frequency of the main system is $b_1\omega_m \simeq b_2\omega_m \simeq \left(\frac{b_1+b_2}{2}\right)\omega_m$. Equation 103 defines approximately the response of the main system for $\zeta_p \leq \zeta_{pc}$. For $\zeta_p > \zeta_{pc}$ again one of the

components of equation 95 vanishes rapidly ($a_1 \gg a_2$) and the motion will simply be explained by the remaining component as

$$X = e^{-a_2\tau} \cos(b_2\tau + \varphi) \tag{104}$$

From equation 103 a single logarithmic decrement can be calculated to define the damping of the main system. For example, according to Figure 29 and equation 103 one can realize that

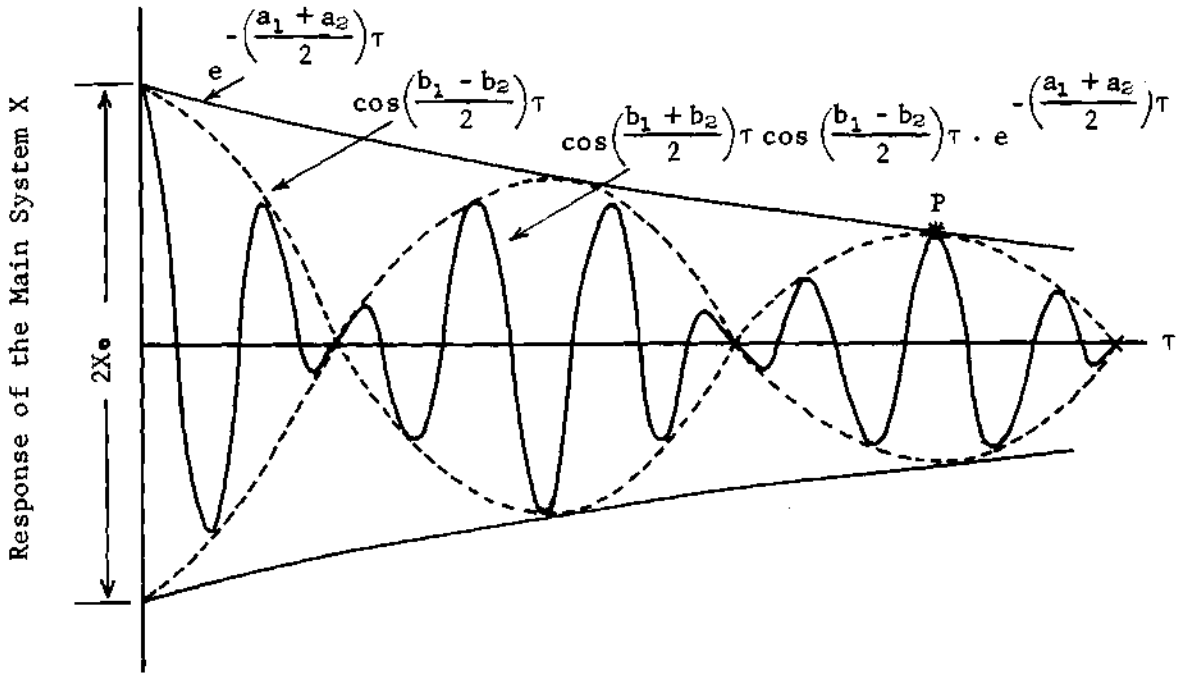

Figure 29. Beat Phenomena

$$X = X_p = X_{max.} = e^{-\left(\frac{a_1 + a_2}{2}\right)\tau_p} \tag{105}$$

when

$$\cos\left(\frac{b_1 + b_2}{2}\right)\tau_p = 1 \ , \qquad \text{and} \tag{106}$$

$$\cos\left(\frac{b_1 + b_2}{2}\right)\tau_p = 1 \ , \tag{107}$$

or when

$$\left(\frac{b_1 + b_2}{2}\right)\tau_p = 2\pi \ , \qquad \text{and} \tag{108}$$

$$\left(\frac{b_1 + b_2}{2}\right)\tau_p = n\pi \ . \tag{109}$$

From equations 108 and 109

$$\frac{n}{2} = \left(\frac{b_1 + b_2}{b_1 - b_2}\right) \ , \qquad \text{and} \tag{110}$$

$$\tau_p = \left(\frac{4\pi}{b_1 - b_2}\right) \ . \tag{111}$$

The logarithmic decrement of the envelope is

$$\delta_{env.} = \ln \frac{X_o}{X_p} = \ln \frac{e^{-\left(\frac{a_1 + a_2}{2}\right)\tau_o}}{e^{-\left(\frac{a_1 + a_2}{2}\right)\tau_p}} \ , \qquad \text{and} \tag{112}$$

for

$$\tau_o = 0$$

$$\delta_{env.} = \left(\frac{a_1 + a_2}{2}\right)\tau_p \ . \tag{113}$$

Substituting equation 111 into equation 113 results

$$\delta_{env.} = 2\pi\left(\frac{a_1 + a_2}{b_1 - b_2}\right) . \tag{114}$$

One can use a new criteria such as equation 114 and determine the damping of the main system from theory (a_1, a_2, b_1 and b_2) and also from experiment as $\ln \frac{X_o}{X_p}$ but it is desirable if a logarithmic decrement based on the decay of each oscillation of the main system is developed. To develop such an expression consider Figure 30 and realize that beat does not occur, but the decaying envelope $e^{-\left(\frac{a_1 + a_2}{2}\right)\tau}$ and the magnitude of response at τ_p remains the same and at the same time the frequency of oscillation is $\left(\frac{b_1 + b_2}{2}\right)\omega_m$. Let the ideal response under this envelope be as

$$X = e^{-\left(\frac{a_1 + a_2}{2}\right)\tau} \cos\left(\frac{b_1 + b_2}{2}\right)\tau , \quad \text{and} \tag{115}$$

let the number of cycles of motion up to P be m, then the logarithmic decrement at p will be

$$\delta_{pm} = \ln \frac{X_o}{X_p} = \ln \frac{e^{-\left(\frac{a_1 + a_2}{2}\right)\tau_o}}{e^{-\left(\frac{a_1 + a_2}{2}\right)\tau_p}} . \tag{116}$$

For

$$\tau_o = 0$$

$$\delta_{pm} = \left(\frac{a_1 + a_2}{2}\right)\tau_p . \tag{117}$$

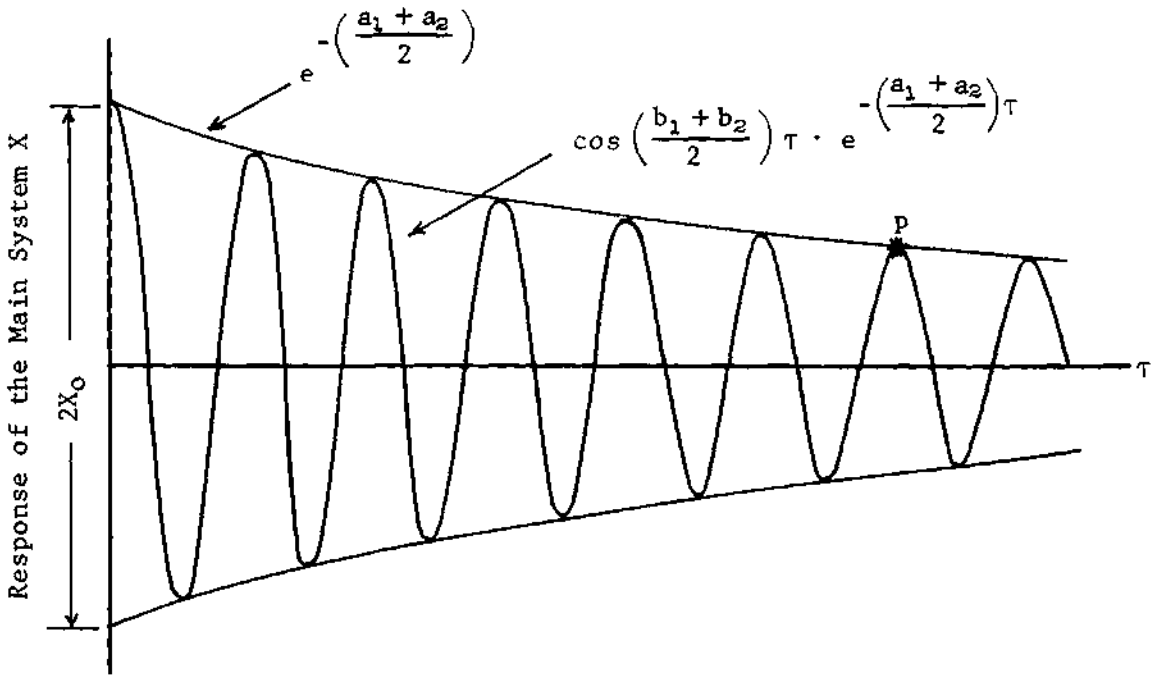

Figure 30. Ideal Response (if the beat does not exist).

Substituting for τ_p from equation 111 results

$$\delta_{pm} = \delta_{env.} = 2\pi\left(\frac{a_1 + a_2}{b_1 - b_2}\right) . \tag{118}$$

Equation 116 can also be written as

$$\delta_{pm} = \ln \frac{X_o}{X_p} = \ln \left(\frac{X_o}{X_1} \cdot \frac{X_1}{X_2} \cdot \frac{X_2}{X_3} \cdot\cdot \frac{X_{m-2}}{X_{m-1}} \cdot \frac{X_{m-1}}{X_p}\right) . \tag{119}$$

Assuming the dissipation over each cycle to be constant and m to be the number of cycle up to p

$$\frac{X_o}{X_1} = \frac{X_1}{X_2} = \frac{X_2}{X_3} = \text{---} = \frac{X_{m-1}}{X_m} \quad . \tag{120}$$

Substituting equation 121 in equation 120 yields

$$\delta_{pm} = \ln\left(\frac{X_i}{X_{i+1}}\right)^m = m \ln \frac{X_i}{X_{i+1}} \tag{121}$$

Letting the logarithmic decrement based on any successive cycles be δ and substituting in equation 121 one gets

$$\delta = \frac{1}{m} \delta_{pm} . \tag{122}$$

Substituting equation 118 in equation 122 the desired logarithmic decrement will be obtained

$$\delta = \frac{2\pi}{m} \left(\frac{a_1 + a_2}{b_1 - b_2}\right) . \tag{123}$$

The number of cycles up to point p being

$$m = \frac{n}{2} = \left(\frac{b_1 + b_2}{b_1 - b_2}\right) , \tag{124}$$

when substituted into equation 123 yields

$$\delta = 2\pi \left(\frac{a_1 + a_2}{b_1 + b_2}\right) . \tag{125}$$

Logarithmic decrements from equation 125 were calculated for the values of a_1, a_2, b_1 and b_2 obtained from the solutions of the characteristic equation and the magnitudes were found to be identical to the curves of Figure 25 up to $\zeta_p = \zeta_{pc}$. Identical values were calculated from the measured response by taking the logarithmic decrements of successive amplitudes assuming the peaks to lie on the exponential curve. In some cases logarithmic decrements of the envelope ($\delta_{env.} = \delta_{pm}$) were also

calculated and by use of equation (122) were converted to δ.

Although some of the assumptions and approximations made were crude, the expressions developed give fairly reasonable and simple analysis of the coupled system. Of course for exact analysis one has either to solve equation 95 or to solve the exact differential equations in the nonlinear form as has been done in the next chapter.

CHAPTER VI

NONLINEAR FLUID (PENDULUM) MOTION

Equations of Motion

The subject of nonlinear fluid motion under forced vibration was discussed in the first two chapters and the significance of a nonlinear theory seemed essential for the analysis of large amplitudes of motion. Many interesting phenomena, such as the softening characteristic of fluid, rotational motion, jump, and the accuracy of the pendulum model were studied. In free vibration when the motion of fluid is coupled to the main system, there exists a mutual influence of one upon the other. The parameters of the coupled system determine the relative influence mentioned above. For example the fluid develops large amplitudes close to the critical tuning frequency ($\Omega \simeq \Omega_p$) for relatively lower initial amplitudes of the main system,while for the same fluid amplitudes away from Ω_p very large initial displacement of the main system is needed. Suppose one concentrates at frequency ratios Ω_p, still the amplitude of fluid motion depends on the amount of viscous damping present. For the same initial displacement and frequency ratio, the developed amplitude is lesser in a highly viscous fluid in comparison to a low viscosity fluid, especially if the viscosity is such that $\zeta_p \geq \zeta_{pc}$, very large initial displacements are required to produce large amplitude (nonlinear) fluid motion. It should be emphasized that even if large amplitude fluid motion is developed in case of large ζ_p the amplitude in the next

cycle will be significantly reduced due to large damping. Therefore for large damping of the fluid (pendulum) the linear theory holds for considerably large initial displacements of the main system. For the case of low damping the developed nonlinear fluid motion will last only a few cycles depending on the amount of damping present.

For small mass ratios even the nonlinear fluid motion will not effect the motion of the main system significantly, while for large mass ratios the motion of the fluid dominating the motion of the coupled system could produce nonlinear response of the main system.

The analysis of Chapter V suggests the use of small mass ratios and large viscous damping at critical tuning frequencies for the optimum design of slosh dampers (the use of such suggested values in designing slosh dampers is shown and a sample calculation is given in Appendix E). Under such circumstances the fluid amplitudes remain small and the use of nonlinear theory does not seem necessary, but to show some of the above mentioned features of coupled motion, the nonlinear differential equations 79 and 80 are solved numerically and compared with experiments for certain special cases.

Because of the nonlinear terms in equations 79 and 80, a closed form solution does not exist and one solves the equations of motion by a numerical method. The Runge-Kutta method of numerical integration seems the best and the most standard method for the class of differential equations

$$X'' = f(X', X, \theta', \theta, \tau) \tag{126}$$

$$\theta'' = g(\theta', \theta, X', X, \tau) \tag{127}$$

Equations 79 and 80 are not quite in this form but by slight manipulations they could be transformed in this form.

Multiplying equation 79 by $\epsilon \cos\theta$ and subtracting equation 80 from it, one obtains

$$\theta'' = \frac{-2\zeta_m \epsilon X' \cos\theta - \epsilon X \cos\theta + \mu\, \acute{\theta}^2 \sin\theta \cos\theta + 2\zeta_p \Omega\, \acute{\theta} + \Omega^2 \sin\theta + \Omega^2 \xi \theta^3}{\mu \cos^2\theta - 1} . \tag{128}$$

Also by multiplying equation 80 by $(\mu/\epsilon)\cos\theta$ and subtracting equation 79 from it, one obtains

$$X'' = \frac{-(\mu/\epsilon)[\acute{\theta}^2 \sin\theta + 2\zeta_p \Omega \theta' \cos\theta + \Omega^2 \sin\theta \cos\theta + \Omega^2 \xi \theta^3] + 2\zeta_m X' + X}{\mu \cos^2\theta - 1} . \tag{129}$$

Equations 128 and 129 being of the form of equations 126 and 127, can be solved by the Runge-Kutta method.

In connection with the solution of equations 128 and 129 the following initial conditions are to be used.

$$\tau = 0,$$

$$X = 1.0,$$

$$X' = 0.0,$$

$$\theta = 0.0, \text{ and}$$

$$\theta' = 0.0. \tag{130}$$

Digital Computer Program and Analysis

Unless the equations of motion (equations 128 and 129) are solved for the linear or small oscillation case, the criteria of logarithmic decrement is meaningless, therefore it is intended to solve equations 128 and 129 for the response, over several cycles of motion and plot the response for each combination of parameters. The experimental response can be then compared to the theoretical response and the agreement or disagreement can be checked as well.

Equations 128 and 129 can also be written as a set of four first order differential equations.

Assigning the following variables for the four variables of equations 128 and 129, one can write

$$Y(1) = \tau$$

$$Y(2) = X$$

$$Y(3) = X'$$

$$Y(4) = \theta$$

$$Y(5) = \theta' \tag{131}$$

and from equations 128, 124 and 131

$$X' = \frac{dY(2)}{d\tau} = Y(3) \tag{132}$$

$$X'' = \frac{dY(3)}{d\tau} = f(Y(2),Y(3),Y(4),Y(5)) \tag{133}$$

$$\theta' = \frac{dY(4)}{d\tau} = Y(5) \tag{134}$$

$$\theta'' = \frac{dY(5)}{d\tau} = g(Y(2),Y(3),Y(4),Y(5)) \tag{135}$$

Equations 132 through 135 are the four first order equations that could be solved together with the initial conditions 130 that could also be written in terms of the new variables as

$$Y(1) = 0.0$$

$$Y(2) = 1.0$$

$$Y(3) = 0.0$$

$$Y(4) = 0.0$$

$$Y(5) = 0.0 \tag{136}$$

Equations 132 and 134 are abvious, but equations 133 and 135 are the same as equations 128 and 129 written in terms of the new variables.

A program written in Fortran and called RKDE in the UNIVAC 1108 MATH-PACK is employed to solve the four first order differential equations 132, 133, 134, and 135 together with the four initial conditions 136.

A copy of the program and a sample of the output solutions are provided in Appendix F.

Theoretical and Experimental Analysis

In the course of analysis it was discovered that extremely large initial displacements (in comparison to the excitation amplitude of the forced vibration) are needed to produce any nonlinear fluid motion, especially if the viscous damping is high.

Experiments were run on three different fluids of increasing

viscosities namely water, 85% and 95% aqueous solutions of glycerin. The container diameter was selected to be 3.862" and the fluid height of 0.340 was used. The remaining parameters were selected such to obtain $\mu = 0.1$ and $\Omega = 0.95$. For the three fluids, different initial displacements (ϵ) were used and for the two largest initial displacements ($\epsilon = 0.128$ and $\epsilon = 0.192$), the experimental curves were plotted as shown in Figures 31, 32 and 33. For the same parameters computer solutions of the nonlinear equations were also obtained and plotted on the same figures. Figures 31 through 33 show good agreement between the theoretical and experimental response, but as noticed from the experiments and from the theory, neither the amplitudes of the fluid built up considerably nor a significant improvement in damping was noticed. If the same auxiliary system is uncoupled and studied under forced vibration, the fluid amplitudes will grow very large, even for an excitation amplitude much lesser than the initial displacements used. But because of the coupling in contrast to the constant input energy of the forced vibration, the amplitudes remained small. This suggests that the frequency-amplitude relations obtained for forced vibration do not hold for the case of coupled free vibration. Therefore the values of ϵ used are large in comparison to the corresponding forced vibration case, but for the coupled free vibration they are not large enough to produce strong nonlinear fluid response.

Still the effect of larger initial displacements on damping remained to be studied. To obtain high values of ϵ without using large initial displacements (not exceeding the linear range of the displacement transducer) a smaller container of 2.288 inches in diameter was employed. Since the nonlinearity is more pronounced for higher values

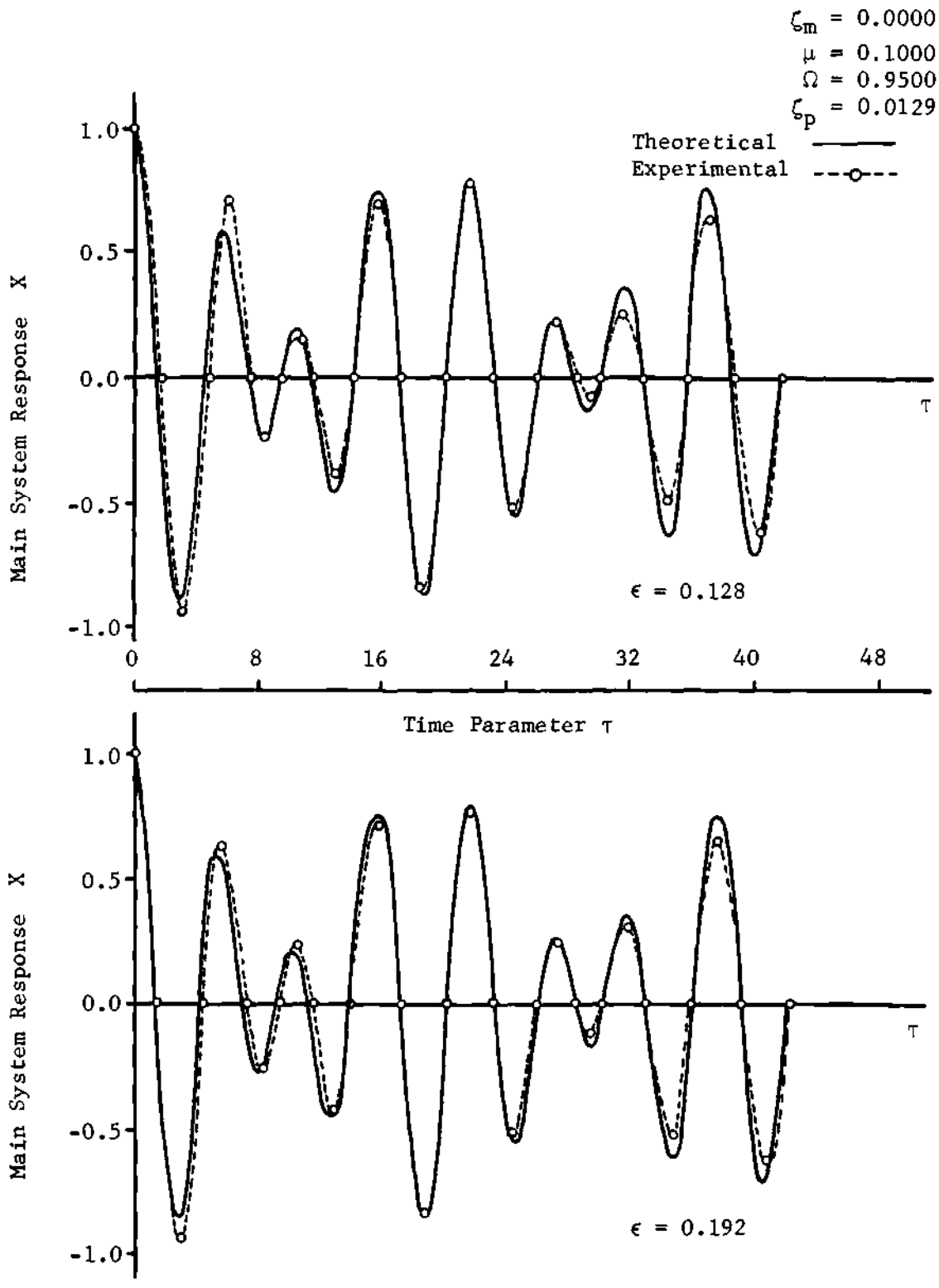

Figure 31. Theoretical and Experimental Response of the Main System for Large Initial Displacements ζ_p = 0.0129

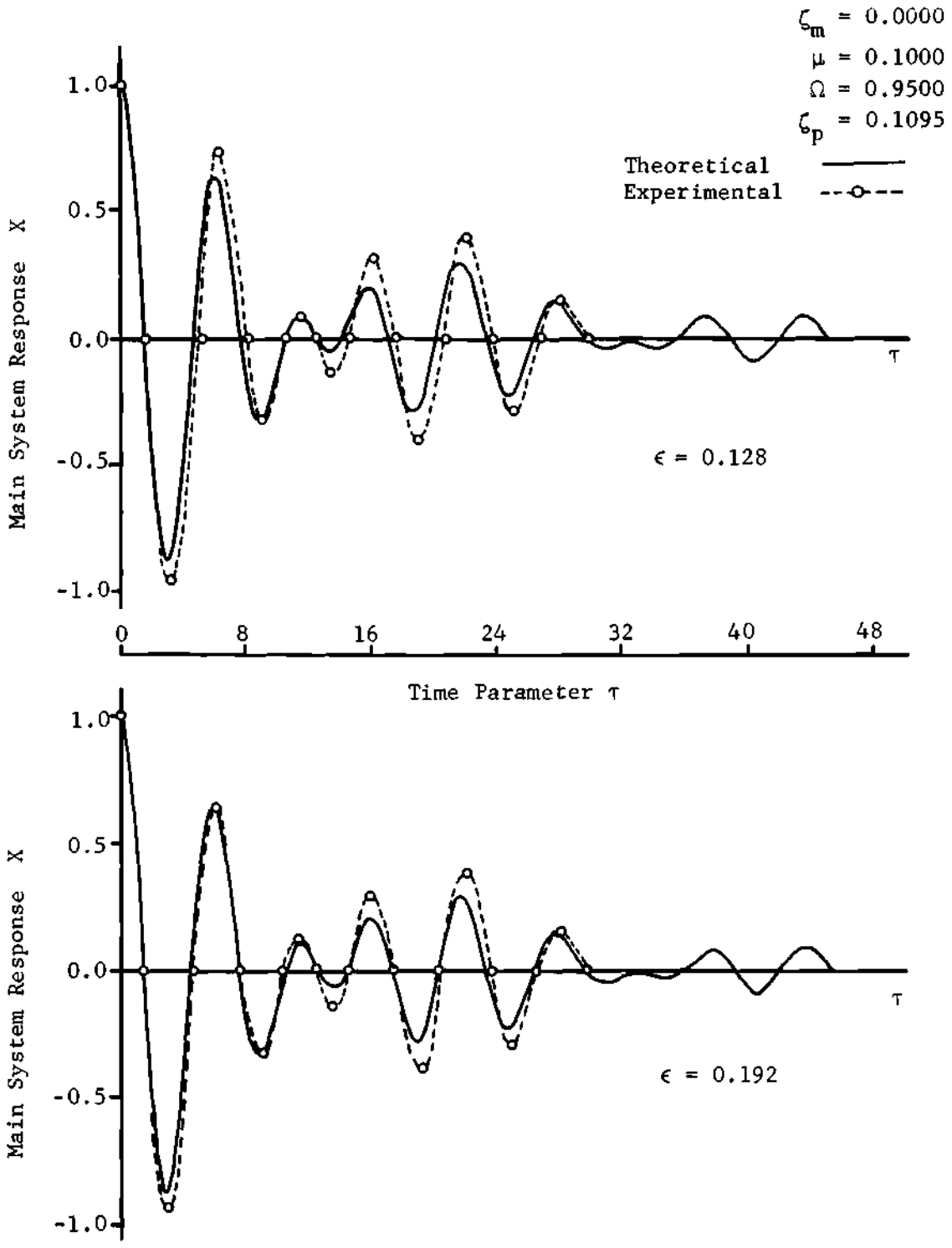

Figure 32. Theoretical and Experimental Response of the Main System for Large Initial Displacements ζ_p = 0.1095

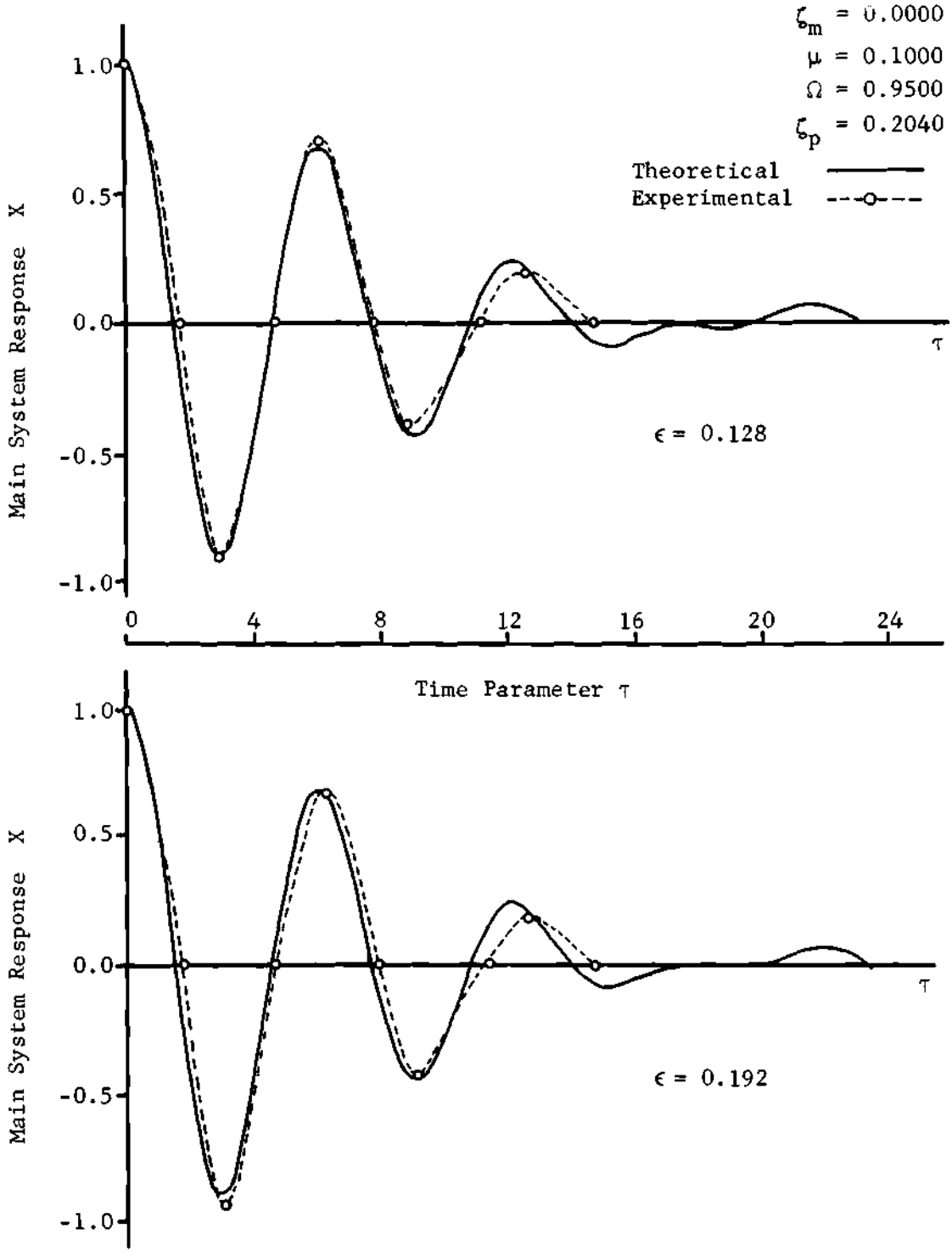

Figure 33. Theoretical and Experimental Response of the Main System for Large Displacements ζ_p = 0.2040

of fluid height and lower values of fluid viscosity, a half full container with water as the fluid medium was used. For the range of parameters indicated in Figures 34 and 35, experiments were run for frequencies higher and lower than the critical tuning frequency ($\Omega = \Omega_p$).

Figures 34 and 35 indicate improvement in damping due to increase in the initial displacement. The decrease in beat as can be seen in Figure 34-b and 34-c in comparison to Figure 34-a, indicates that at the corresponding initial displacements the critical tuning frequency is moving further away from the tuned frequency $\Omega = 0.907$. At the same time the increase in beat as shown in Figures 35-b and 35-c in comparison to Figure 35-a indicates that the critical tuning frequency is approaching the tuned frequency $\Omega = 1.140$.

In Figure 34-b the fluid was observed to exhibit nonplanar motion with large amplitudes while in Figure 34-c even swirl was observed, and due to the transfer of energy in the coupled system the duration of swirl was very short. Unfortunately for such cases the theory of a plane pendulum (modified and unmodified) will fail to predict the response and for a better analysis the employment of spherical pendulum is suggested. On the other hand, in Figure 35-b only large amplitude planar motion of fluid was observed that could be analyzed by the nonlinear theory of plane pendulum, but for the initial displacement of Figure 35-c the fluid exhibited nonplanar motion.

It is worthy of mentioning that the criteria of concentration of beat at the critical tuning frequency was already discovered in the text of the linear analysis and it is assumed that similar phenomena exists for the nonlinear analysis.

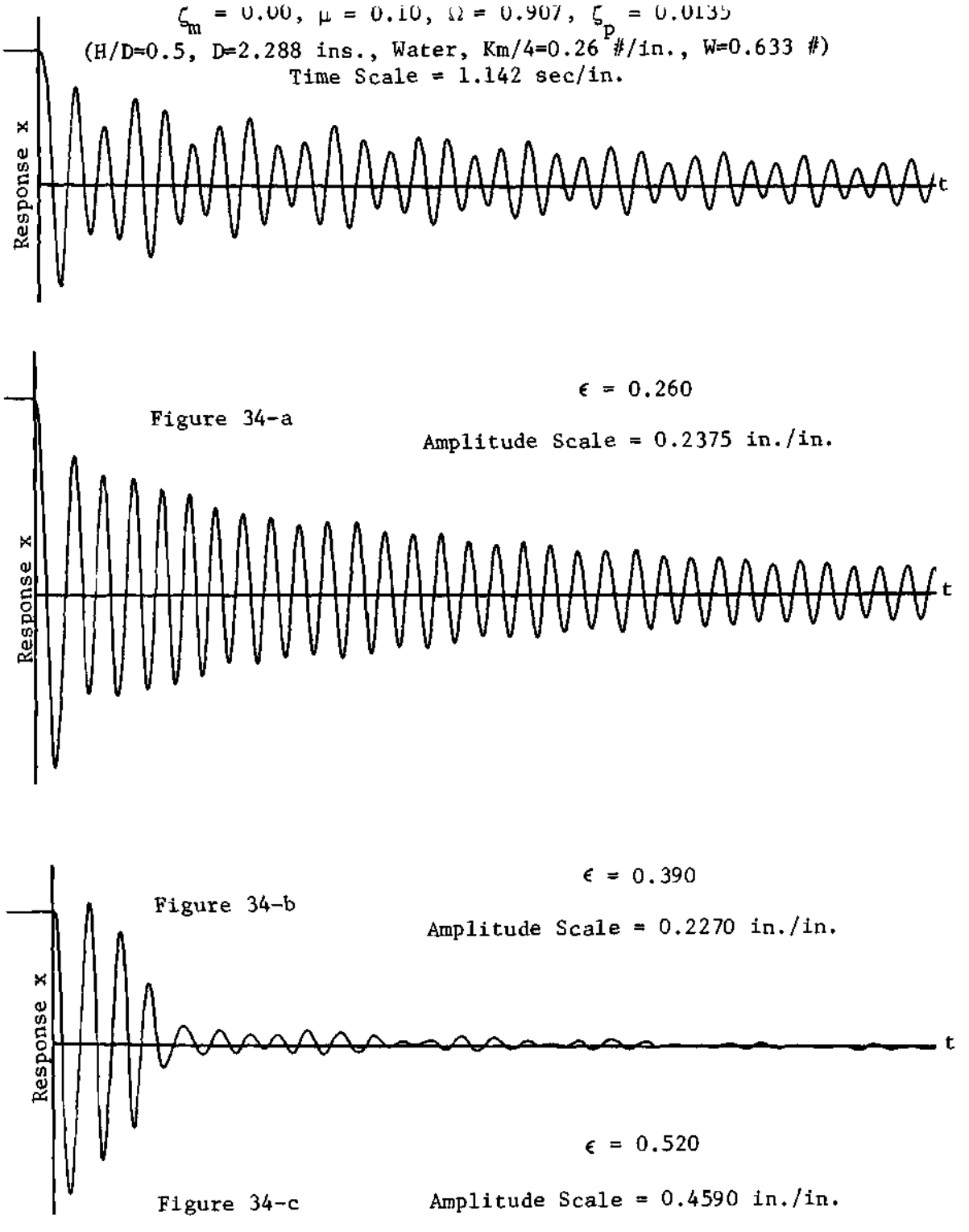

Figure 34. Experimental Response of the Main System for Large ϵ, $\Omega < \Omega_p$

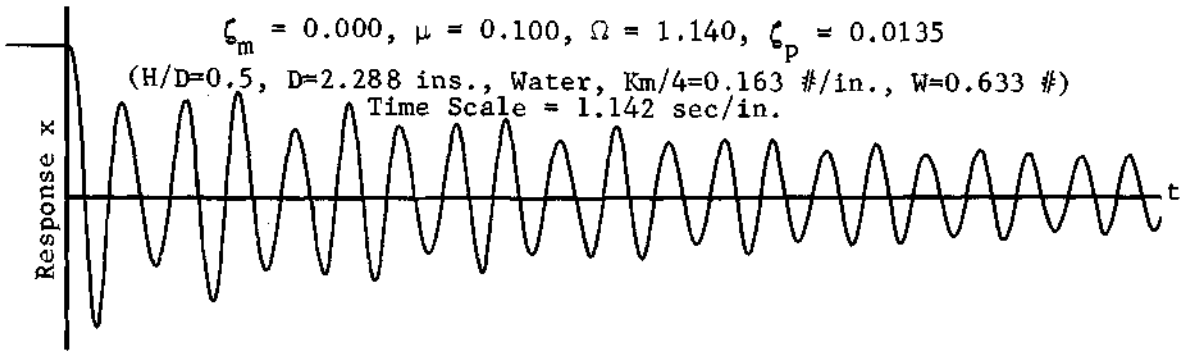

ϵ = 0.260

Figure 35-a Amplitude Scale = 0.2375 in./in.

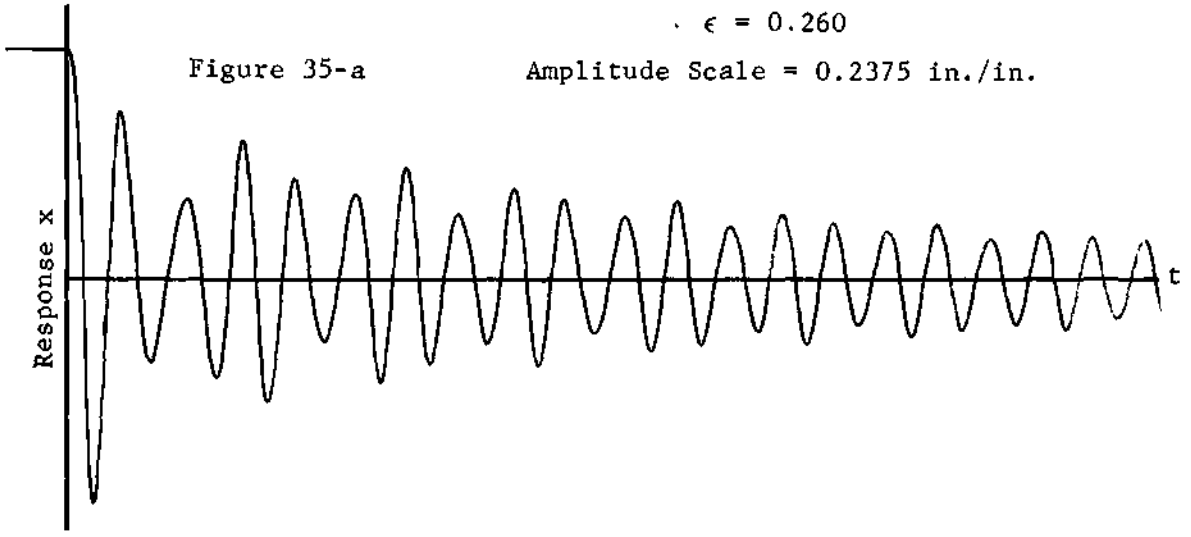

ϵ = 0.390

Figure 35-b Amplitude Scale = 0.2270 in./in.

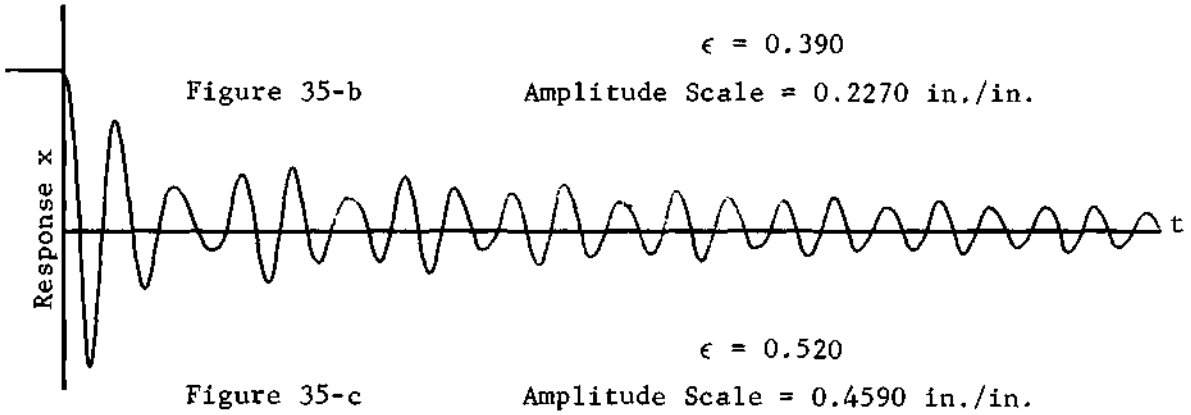

ϵ = 0.520

Figure 35-c Amplitude Scale = 0.4590 in./in.

Figure 35. Experimental Response of the Main System for Large ϵ, $\Omega > \Omega_p$

Since Figure 35-b qualified for a nonlinear treatment by being close to the critical tuning frequency and still remaining in the plane of oscillation, the nonlinear differential equations were solved both for plain pendulum and for the modified pendulum and the theoretical and experimental responses are compared in Figure 36. The agreement of the modified pendulum with the coefficient of added cubic spring equal to -0.14 read from Figure 9 is much closer to the experimental output in comparison to the plain pendulum. This proves once again that the modification made in Chapter II is justified. Since the present nonlinear analyses cover only a few specific cases, it is not advisable to draw any general conclusion in regard to a limiting value of ϵ above which the planar fluid motion ceases and the plane pendulum is not applicable. But the existence of a critical value of ϵ as such can be certified for any particular set of parameters. For the design parameters of Figure 34 this value is slightly smaller than 0.390 and for the design parameters of Figure 35 it is slightly larger. Since no significant damping due to increase in ϵ was noticed up to this critical value of ϵ, further investigation did not seem as fruitfull as in the case of linear analysis.

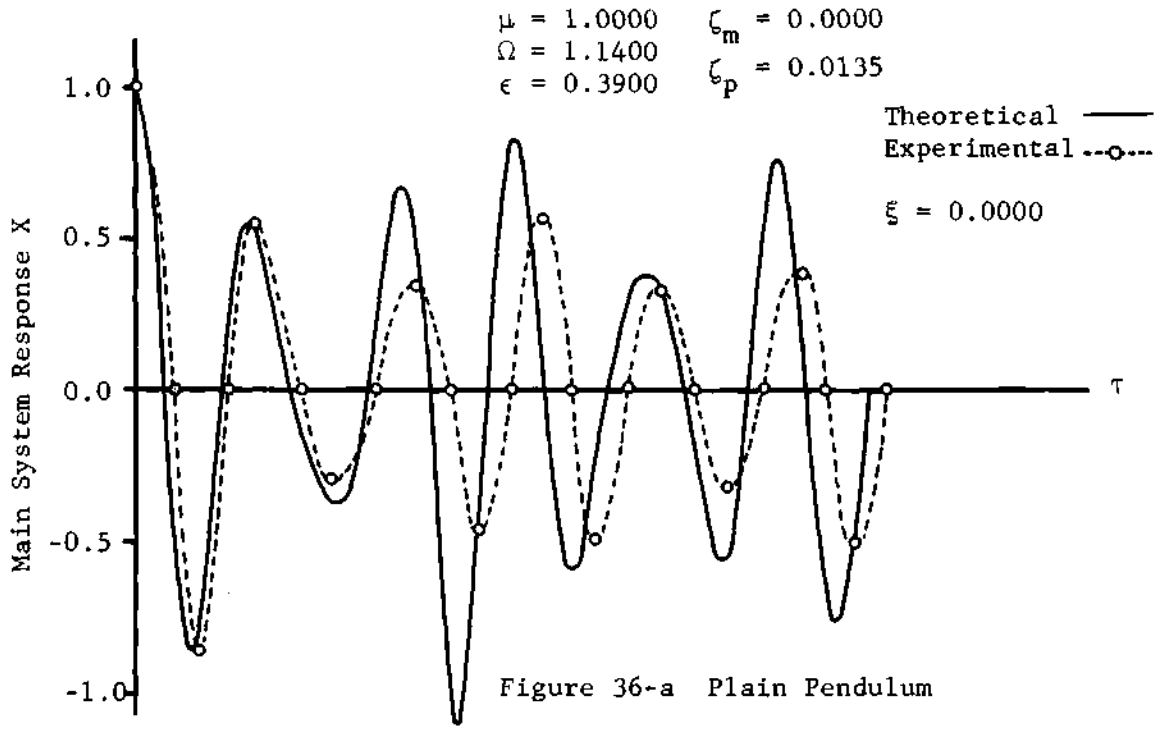

Figure 36-a Plain Pendulum

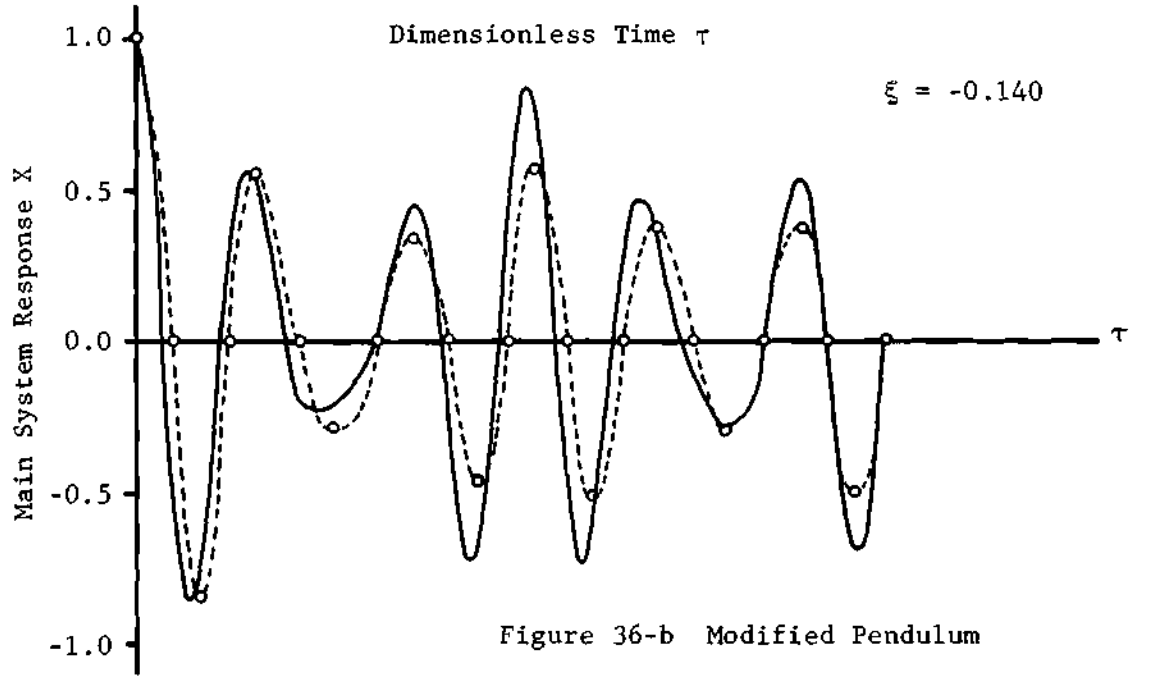

Figure 36-b Modified Pendulum

Figure 36. Nonlinear Response for Plain and Modified Pendulum

CHAPTER VII

EXPERIMENTATION

Forced Vibration (Single Degree of Freedom)

The main objective in the case of forced vibration was to measure the hydrodynamic force (slosh force) that the moving fluid exerts on the container. The simplest method to achieve this objective was to use a load cell similar to the experimental setup of Sumner [9]. Since the main interest was to understand only the horizontal component of the total force, only one load cell seemed sufficient. Three other subsystems were to be built to complete the entire setup as shown in Figure 37.

1. To avoid any axial load normal to the sensitive axis of the load cell and to carry the dead weight of the fluid, the fluid container, and its support, they were suspended by means of four steel wires of considerable lengths. The wire lengths were selected so as to minimize the interference with the frequency of oscillation. At the same time, to avoid any reaction in the horizontal component of the force, the long wires were suspended vertically from a rigid frame. The frame was built of wood with the joints rigidly screwed and for further rigidity gussetts were used at the corners.

2. To provide a forcing function a 25 pound dynamic shaker was rigidly fastened to the frame and connected to a power amplifier and a low frequency oscillator.

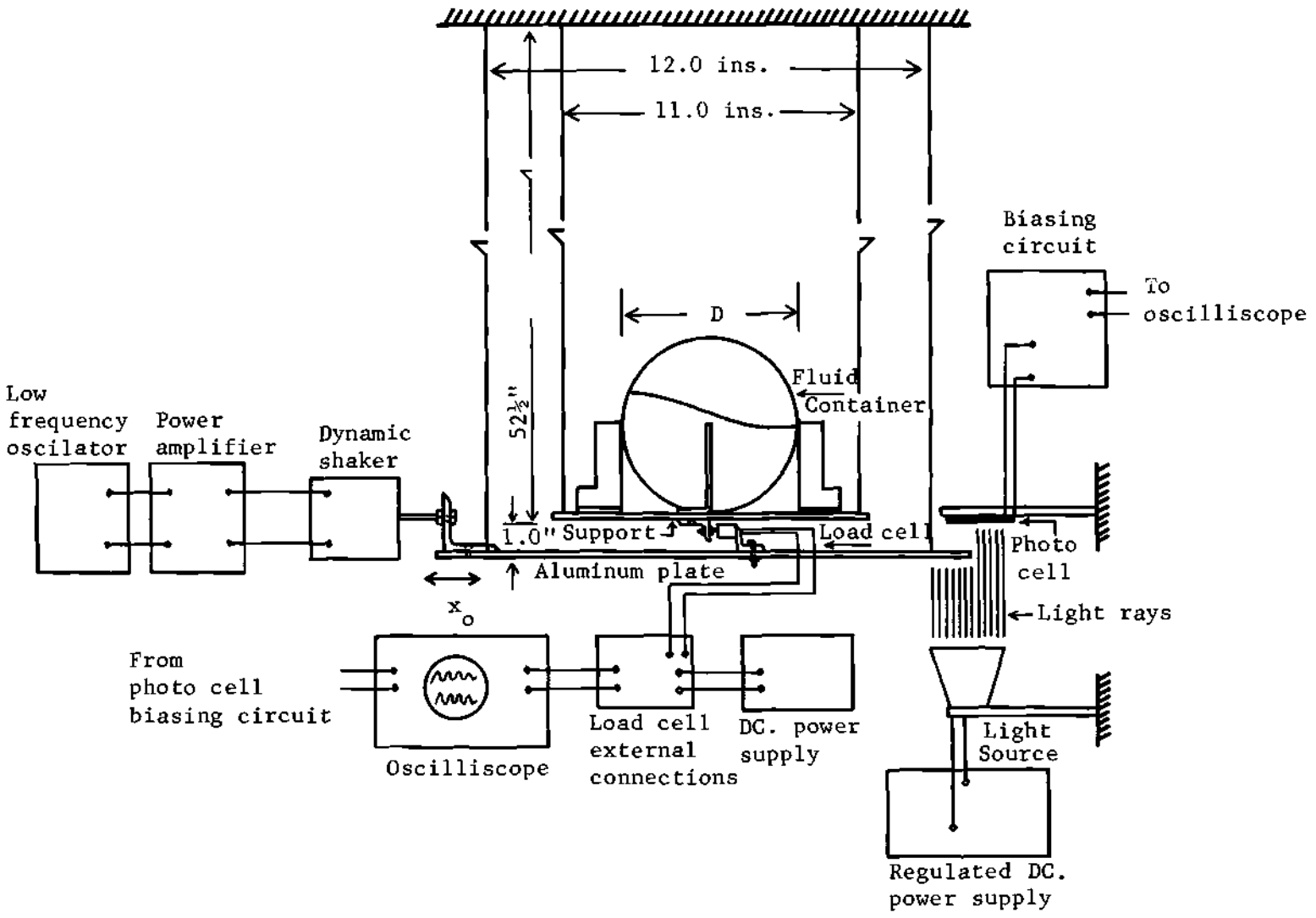

Figure 37. Experimental Setup for Forced Vibration

3. To measure the excitation amplitude and keep it constant for any phase of the operation a displacement transducer was built. The displacement transducer consisted of a photo cell (solar battery) and mounting, a light source with fixed and uniform intensity together with a power supply providing constant voltage for the light source and a 1½ volts dry cell battery in connection with a potentiometer to provide the proper biasing for the photo cell.

The fluid containers were transparent plastic spheres (D_o = 7.00") both with the without splitters which were fastened rigidly to the supporting plate. Since the containers were to be removed frequently for changing the fluid height, L-shaped aluminum plates were rigidly connected to the support plate and the clearance was small enough to ensure perfect contact and grip with the container. The L-shaped plates were mounted in the direction of maximum moment of inertia of the area to insure the rigidity and prevent bending under the dynamic loads.

The parts and instruments used are listed in Table 5. For detailed explanation of the instrumental setup as shown in Figure 37, it seems sufficient to concentrate on the two transducers only.

Load Cell

The load cell used was a semiconductor strain gage type, in which the gages were electrically connected to form a wheatstone bridge. The circuit is shown in Figure 38 and its calibration is given in Figure 39. The calibration curve was obtained by fixing one end of the transducer to a clamp and hanging weights from the other end, and recording the output voltage from the osciliscope.

Table 5. Instrumentation and Equipment List

Low Frequency Oscillator	Hewlet Packard 202 C
Power Amplifier	MB Electronics 2125 MB
Dynamic Shaker (Exciter)	MB Electronics PM-25
Dual Beam Oscilloscope	Tektronix Type 502A
Power Supply (Regulated)	Heathkit Model IP-27
DC Power Supply	Hewlett Packard 6204 B
Load Cell	Bytrex Division and Co. JP-10
Selenium Photo Cell (Solar Battery)	Tandy Corp. 276-115
Potentiometer 40K, 10 Turns	Helipot 5v, 7223-151-1
Potentiometer 0.5 Meg, 1 Turn	AB Type J, 47266 A
Potentiometer 150 Ohms, 1 Turn	Clarostat Mgf. AN3155-50-150
Light Bulb 12 Volts and 6 Volts	Car Tail Light
DC Battery 1½ Volts (Two)	Everdady No. 735 Neda 90v
Spherical Plastic Containers	Toys
Support Plates 11 $in.^2$ and 12 $in.^2$	Cut to Size (Aluminum)
Music Wire Size 009	Allegheny Ludlum Steel Corp.

X-Y Plotter with Time Base	Moseley Model 2-D
AC Motor 1/3 HP, 1725 R.P.M.	Bodine Electric Co. No. 280TA043
Speed Control	Minarik Electric Co. Model SH-53

Displacement Transducer

Although many precision instruments were available for measuring displacement, most of them had a minimum frequency limit which was higher than the range of frequencies to be measured. Therefore the photo cell transducer which is linear [20] at low frequencies was employed in the measurement of the displacement.

The selenium photo cells are sensitive to incident light and have the property of converting the light energy into a potential difference across its terminals. The amount of the potential difference being proportional to the area illuminated and the intensity of the incident light. To further increase the output potential difference and the linearity of the output signal a biasing circuit as suggested by Alvord [21] seemed essential.

The displacement transducer circuit and arrangement are shown in Figure 40. The light source used, was a car tail light bulb fixed in a reflector and covered with several layers of wax paper to assure the uniform distribution of light. The bulb was energized by 12 volt DC provided by a regulated power supply.

The following steps were taken in the biasing and calibration of the transducer:

1. The entire area of the photo cell was illuminated.

2. The gain resistance R was reduced until the output voltage was read zero on the oscilloscope.

3. The gain resistance was still reduced slightly to improve the linearity [21].

4. The transducer was calibrated by means of displacing the

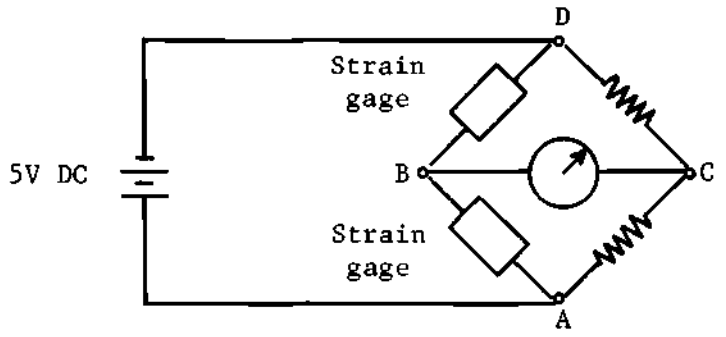

Figure 38-a Load Cell Bridge Circuit

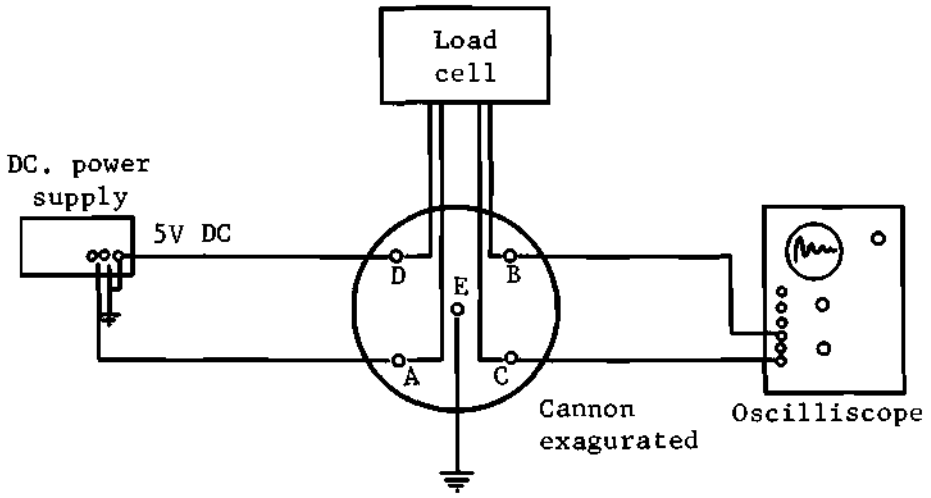

Figure 38-b Load Cell External Connections

Figure 38. Load Cell Bridge Circuit and External Connections

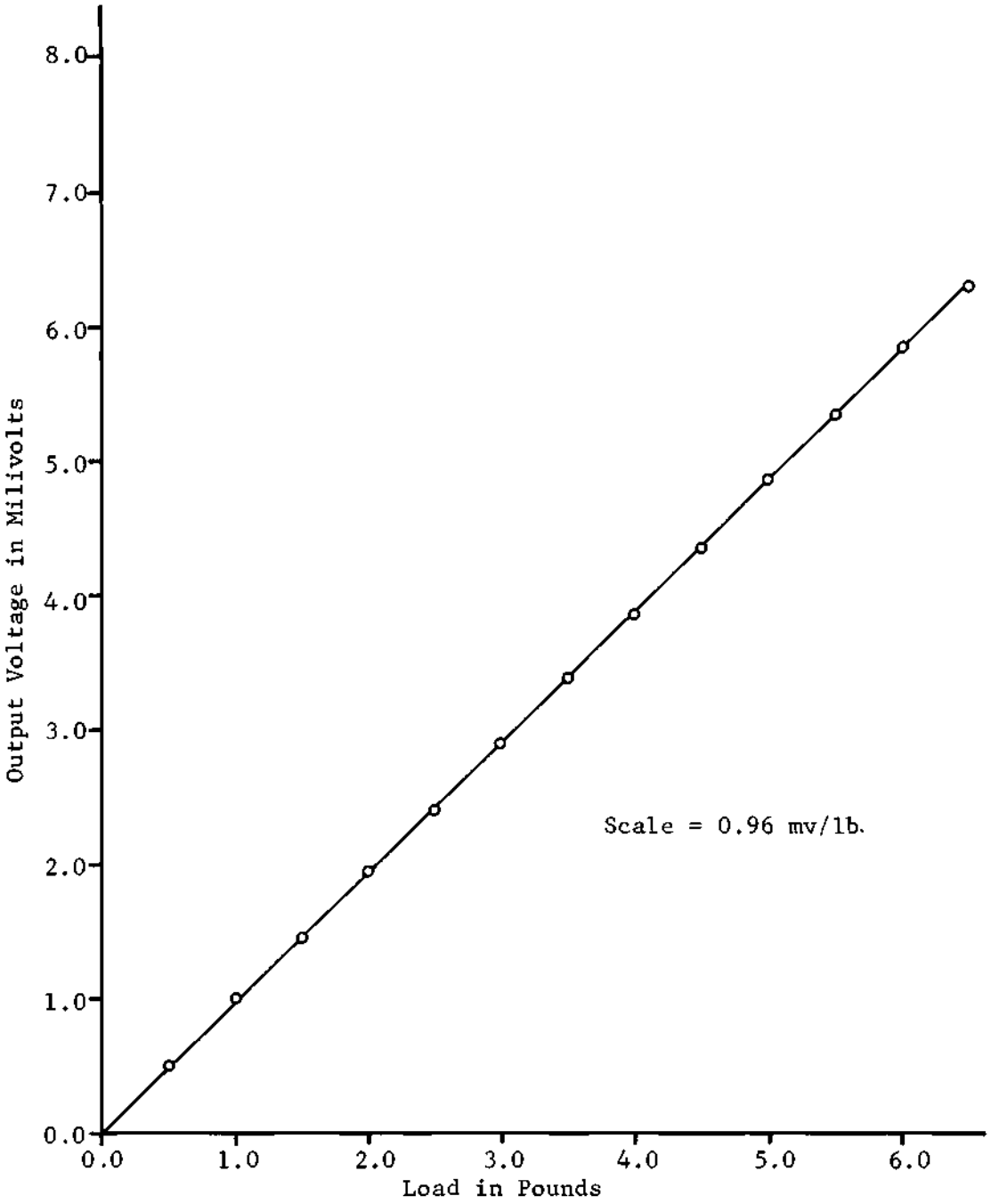

Figure 39. Load Cell Calibration Curve

shutter plate statically and measuring the output voltage on the oscilloscope.

The calibration curve is plotted in Figure 41 and the linear range of operation is marked.

Since the displacement to be measured is generally of an oscillatory nature and one has to measure positive and negative displacements, the output signal was zeroed at the center of the linear range as shown in Figure 41. To zero the output signal at the cneter of the linear range a constant voltage (780 mv) was subtracted from the signal at the oscilloscope terminal. The constant voltage was provided by a 1.5 volts dry cell battery which was connected to a potentiometer as shown in Figure 40.

With the arrangement shown in Figure 37 three different measurements were made under forced vibration.

1. Stability Boundaries

A spherical container of seven inches in diameter without splitter plate was mounted and for each fluid height (seven fluid heights were tested) five excitation amplitudes were tried. For each excitation amplitude selected, the excitation frequency was increased through small intervals and the force output of the load cell was recorded. Approaching the resonance frequency, for each excitation amplitude a frequency parameter was reached at which the fluid oscillation departed from the plane of excitation and with further increase in frequency the swirl or rotation of fluid was observed. The locus of these points determined the lower stability boundaries and are shown in Appendix B. To determine the upper boundaries, the fluid was excited with the same excitation amplitude but with an excitation frequency larger than the resonance and as the

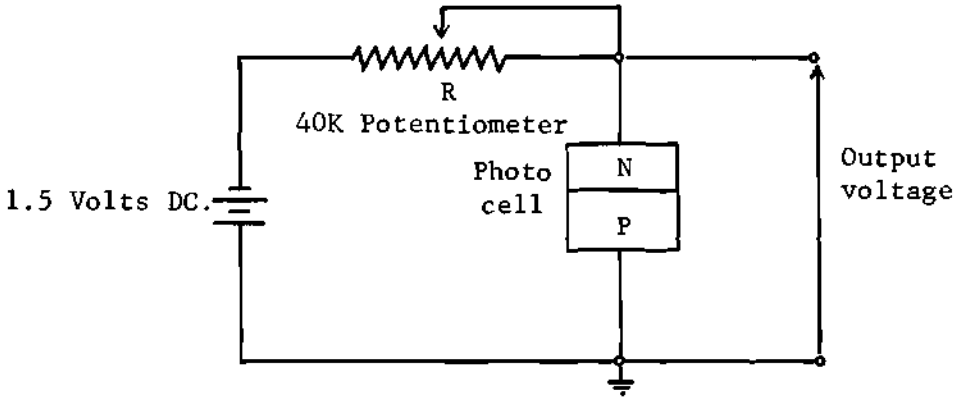

Figure 40-a. Displacement Transducer Circuit

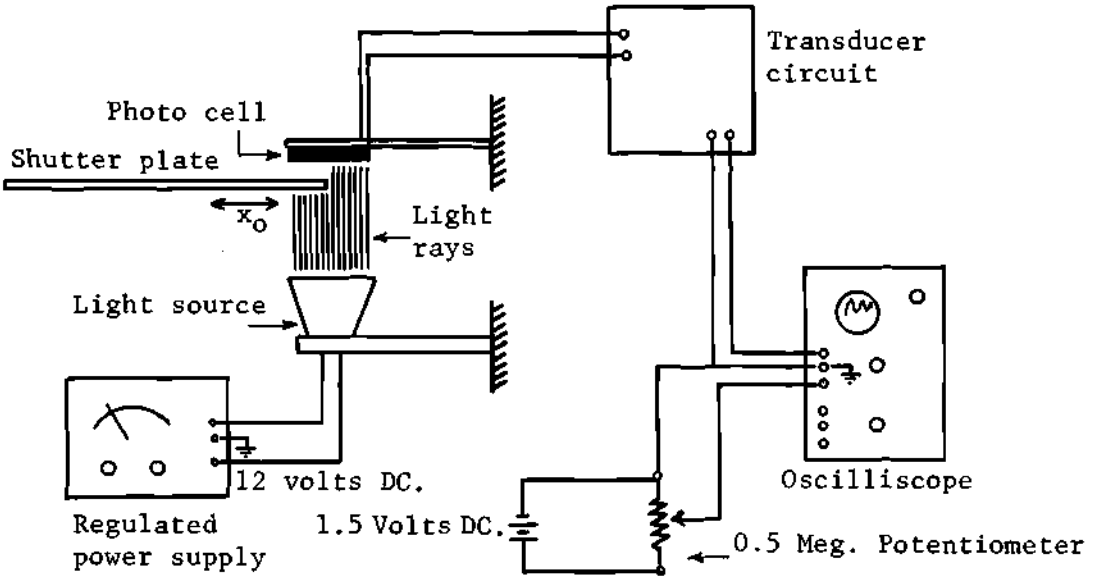

Figure 40-b. Displacement Transducer External Connections

Figure 40. Displacement Transducer Circuit and External Connections

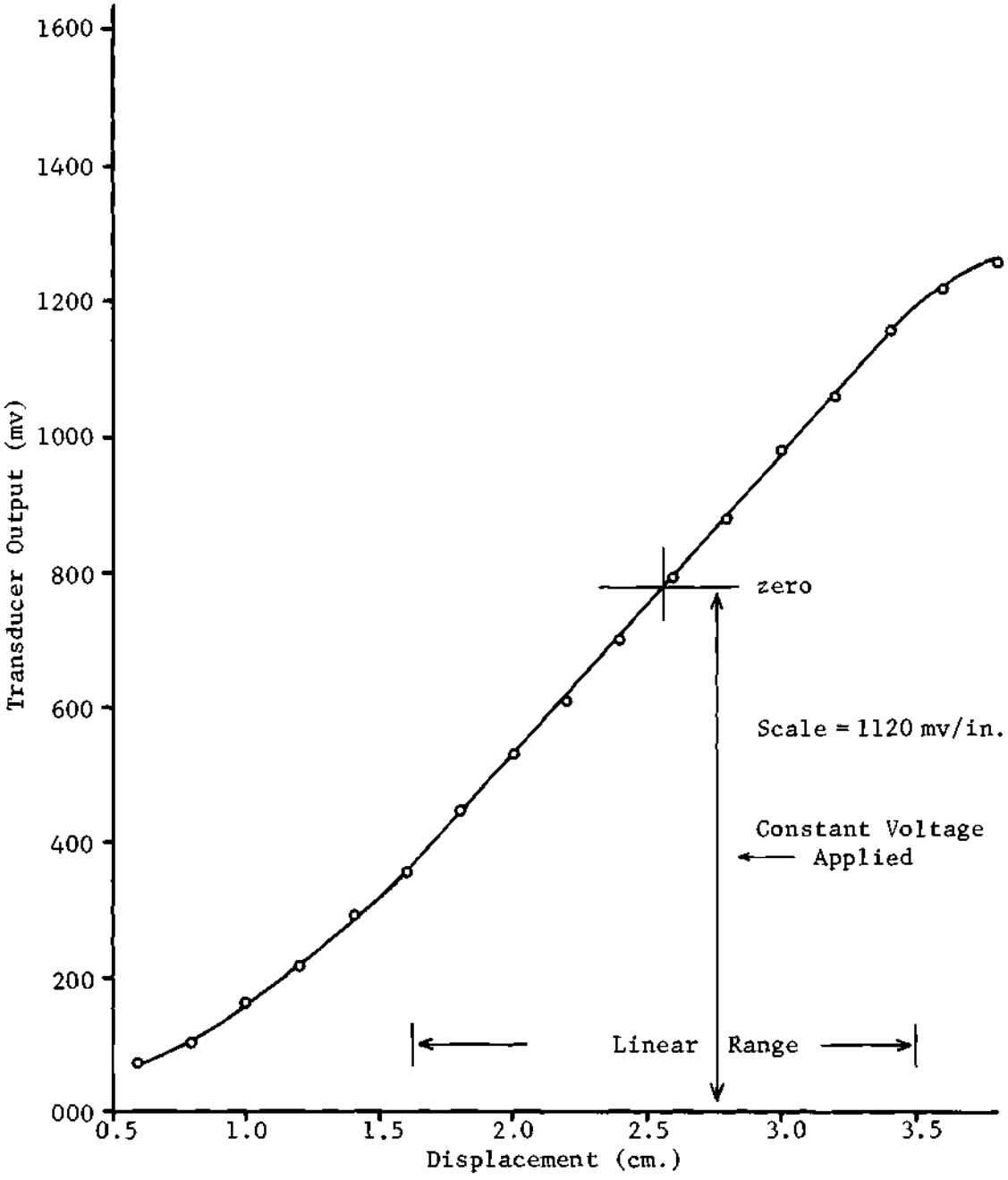

Figure 41. Displacement Transducer Calibration Curve

frequency was decreased through intervals the force outputs were recorded. Approaching the resonance frequency the force, frequency and amplitude of excitation corresponding to the stability boundary were recorded as shown in Appendix B. Similar procedure was used for each of the remaining fluid heights and excitation amplitudes.

2. Natural Frequencies

Because of fluid rotation at resonance frequency it was not possible to measure a steady force amplitude. A splitter plate was installed in the fluid container parallel to the direction of excitation in order to suppress the rotational motion, then for very small excitation amplitudes the maximum force in the frequency domain near resonance was measured. For slight increase in excitation amplitude another value of the maximum force was measured. If the straight line passing through the two maxima was vertically upward the corresponding frequency was considered to be at resonance and the oscillation was linear. The experimental natural frequencies as compared to the natural frequencies of the mathematical pendulum and those of Stofan's [5] are plotted in Figure 42 and the agreement is very good.

3. Force Measurement Near Resonance

By installing the vertical splitter it was possible to measure force values at all frequencies except at a narrow band at which the jump phenomena appears. At this narrow band of frequency the force jumps from a low magnitude to a high magnitude for increasing frequency and jumps from a high value to a low value for decreasing frequency. The force outputs for variation in excitation amplitude and frequency are plotted for each fluid heights in Appendix C.

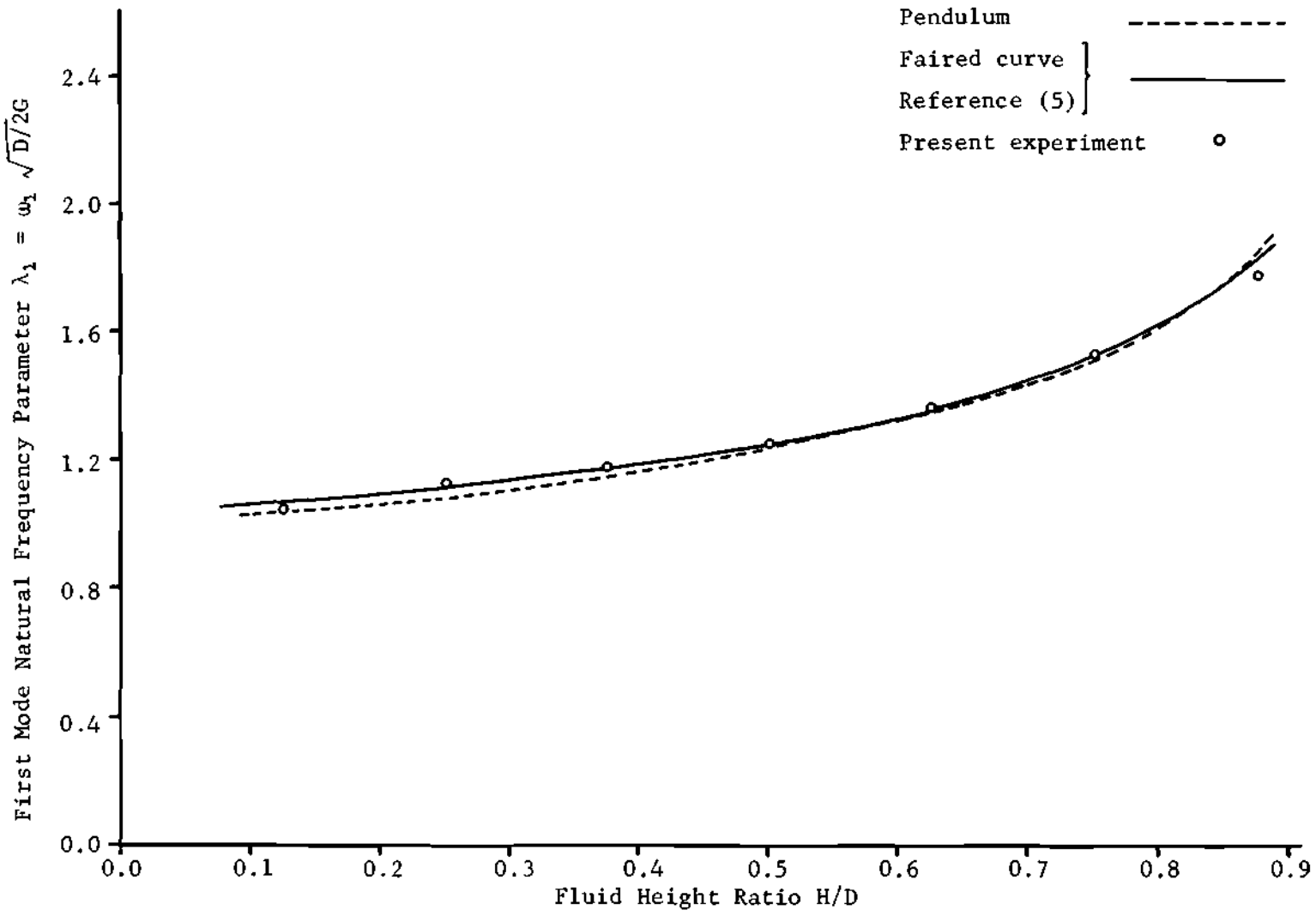

Figure 42. Variation of the Natural Frequency as a Function of Fluid Height

Free Vibration
(Two Degree Freedom)

The main objective in the analysis of free vibration was to measure the response (displacement) of the main system after it is released from a preassigned initial value. The instrumentation, being similar to Figure 37, is shown in Figure 43.

The displacement transducer is identical to the one used for forced vibration except for the selinium photo cell which was replaced by a larger one to provide wider linear range. The calibration curve for this transducer is shown in Figure 44.

The initial displacements were set by means of a string which was pulled until the desired initial displacement was read on the oscilloscope screen, then after holding the string for a short while (for the small oscillation of the fluid to vanish) the string was released and the oscillation was recorded by an X-Y plotter having a built in time base. The time scale generally used was calibrated and the calibrated scale found to be 1.142 sec/in. It would be interesting to study some recorded responses of the main system for several important cases studied in Chapter V.

1. Figure 45 substantiates the statement that one component of motion vahish rapidly on either side of the critical tuning frequency and that both components have equal importance at the critical tuning frequency ($\Omega = \Omega_p$).

2. Figure 46 illustrates the disappearance of beat with increasing the viscous damping at critical tuning frequency.

3. Figure 47 demonstrates the improvement in damping when the

response of the main system is compared before and after the application of the slosh damper.

In the measurement of response curves, small initial displacements were used to insure the linearity of the output.

Viscous Damping and Viscosities

Viscous Damping

Empirical equations for viscous damping in spherical containers are presented by Sumner [7] and Mikishev [22] which disagree considerably. The comparison is made by Abramson [1] and the reason for the disagreement is explained to be in the nonlinear relation which exists between the force and amplitude of oscillation.

To understand which one of the equations apply to the analysis of this program, it seemed necessary to run a few experiments and obtain the logarithmic decrements to be compared with the two equations. The experimental setup is shown in Figure 48 and the test procedure is as follows:

Containers of seven inches in diameter with and without splitter were used, and for an excitation amplitude of $X_o/D = 0.0109$ the fluid was set in motion to produce large amplitudes (the excitation frequency was set close to resonance by adjusting the motor speed control device). As soon as the fluid developed large amplitudes, the motor was quickly stopped and the force output was recorded on the plotter. This process was repeated for different fluid heights for the two spheres and the logarithmic decrements were calculated from the force response as

$$\delta = \ln \frac{F_n}{F_{n+1}} \tag{137}$$

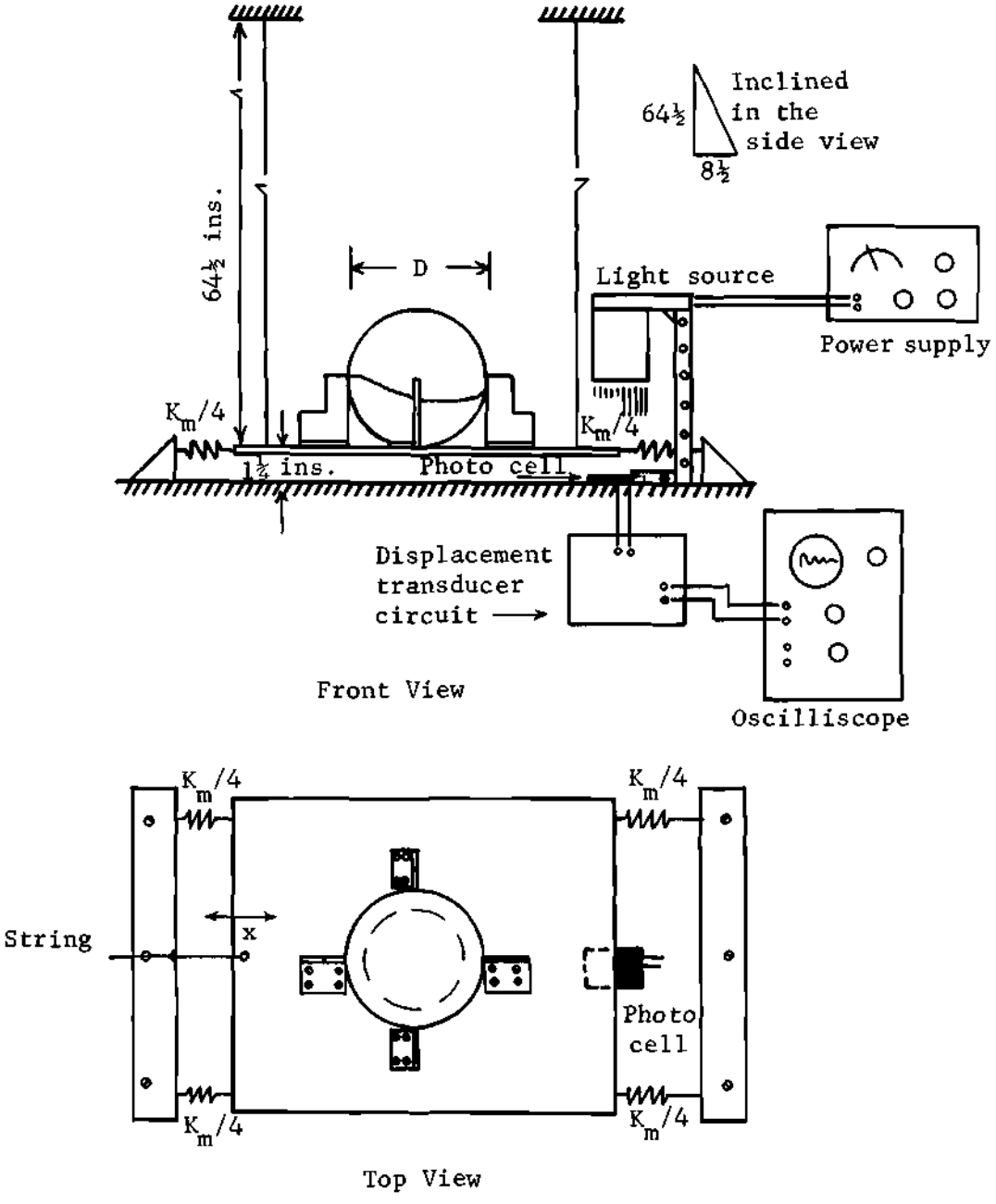

Figure 43. Experimental Setup for Free Vibration

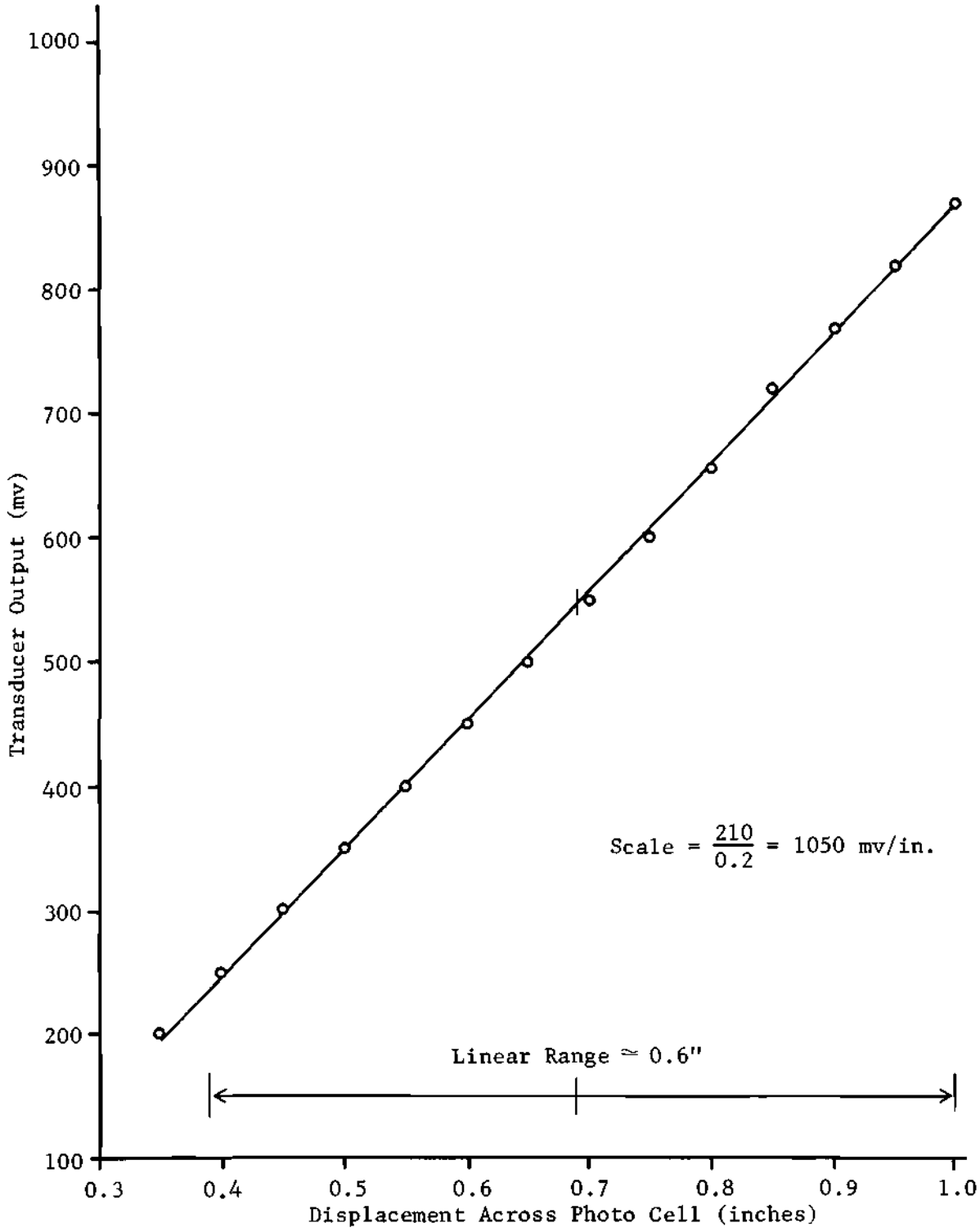

Figure 44. Displacement Transducer Calibration Curve

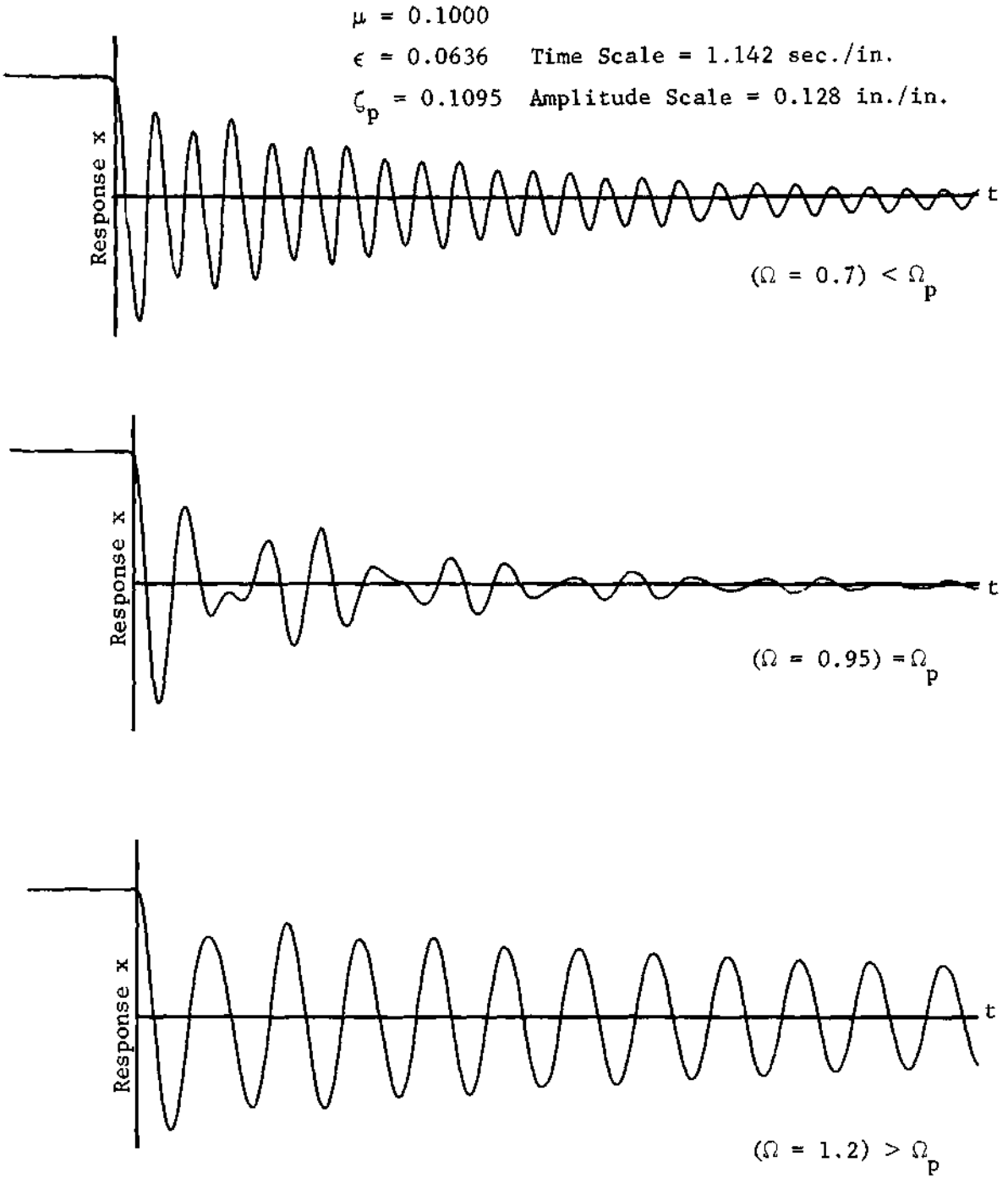

Figure 45. Response of the Main System at, and on Either Sides of the Critical Tuning Frequency

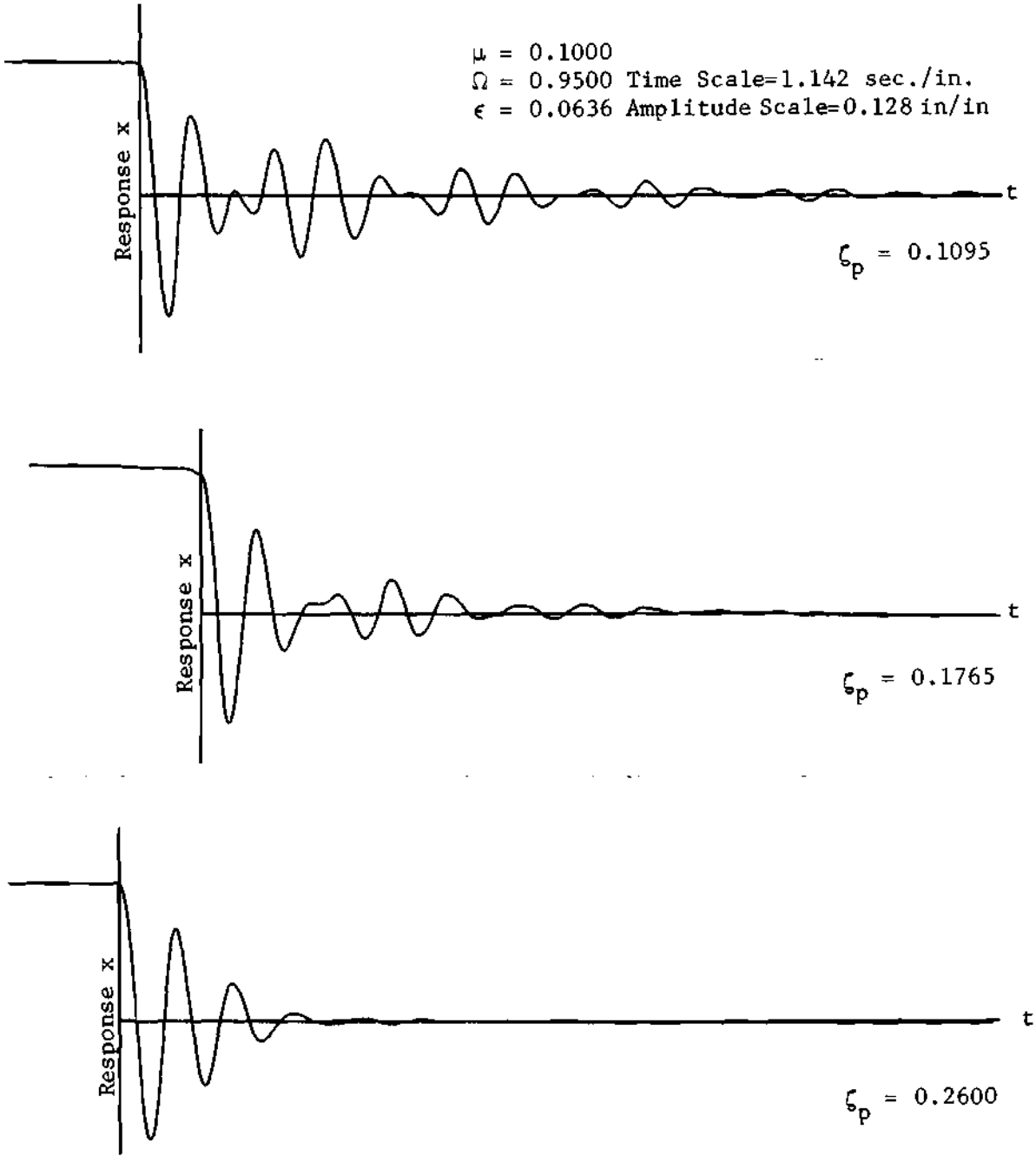

Figure 46. Disappearance of Beat with Increase in Viscous Damping at Critical Tuning Frequency.

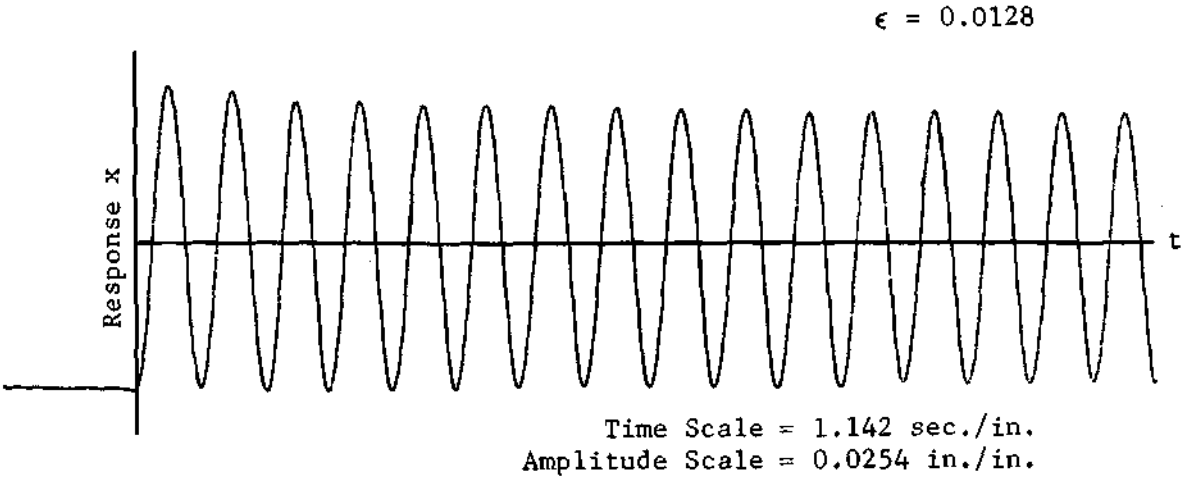

Figure 47-a Without Slosh Damper

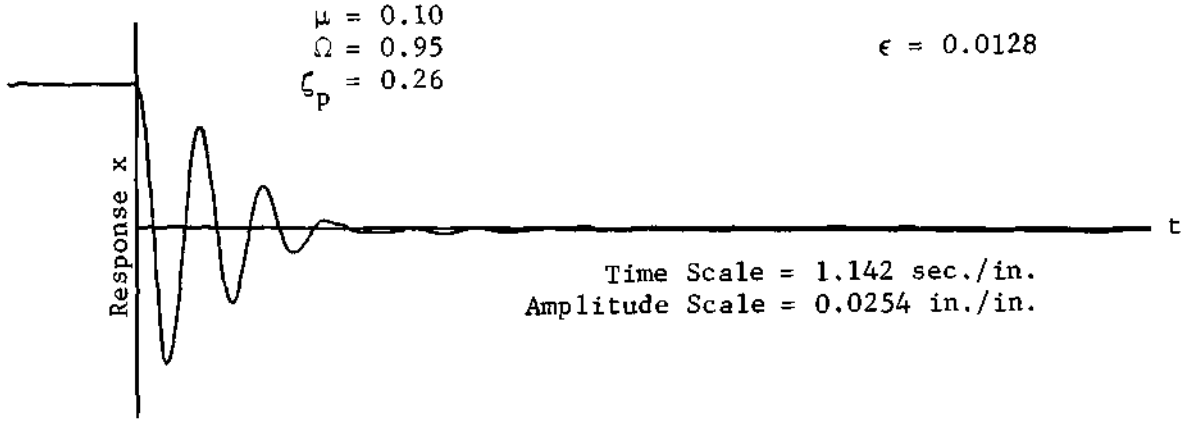

Figure 47-b With Slosh Damper

Figure 47. Response of the Main System Before and After the Application of Slosh Damper

The average values of the logarithmic decrements are plotted in Figure 49 together with the solutions of the two empirical equations of Sumner [7] and Mikishev [22].

The magnitudes of viscous damping seems to agree closely with the empirical equation of Sumner [7], while the variation with respect to fluid height have a similar form to that of Mikishev [22]. It should be mentioned that Sumner's [7] analysis covers only one particular fluid height (H/D = 1/2). The difference in magnitude is almost twice as much between Mikishev's equation and the present experiment as well as with Sumner's equation.

Instead of reruning similar experimental programs as those run by Sumner and Mikishev it seemed reasonable to correct Mikishev's equation which is already in a general form to fit the present experimental results as well as to agree with Sumner for the particular fluid height of one half. Mikishev's equation when multiplied by 2.15 seems to agree much closer at fluid heights in the neighborhood of one half and be fairly acceptable at the other fluid heights.

It is obvious from Figure 50 that even the adjusted empirical equation of Mikishev [22] is not the best representative of actual damping in the fluid. In view of the disagreements in the literature this subject deserves further investigation that could be made the subject of another program. For analysis completed in Chapters V and VII which was performed at fluid heights in the neighborhood of one half the damping values obtained from the adjusted empirical equation seem reasonably accurate.

The adjusted empirical equations are

for $0.05 < H/D \leq 0.50$

$$\delta_p = 0.08974 \left(\frac{\nu \times 10^4}{\sqrt{G} D^3} \right)^{\frac{1}{2}} / (H/D) \tag{138}$$

and for

$$H/D \geq 0.50$$

$$\delta_p = 0.08974 \left(\frac{\nu \times 10^4}{\sqrt{G} D^3} \right)^{\frac{1}{2}} \left[\frac{1 + 0.92(1 - (H/D))}{1.46(1 - (H/D))} \right] \tag{139}$$

To check the agreement at a different container size, experiments were run for a container of 3.862 inches in diameter and water was used as the fluid medium. The results of present experimentations and those calculated from equations 138 and 139 are plotted in Figure 50.

Fluid Viscosities

In the course of analysis of linear motion (Chapter V) it was desired to analyze the coupled motion for large viscous camping. To obtain large viscous damping equations 138 and 139 suggest four possibilities:

1. To use very small containers.
2. To use highly viscous fluids.
3. Very low or very high fluid heights.
4. Some combination of the above.

Since the intention was to use fluid heights in the neighborhood of half full, the third possibility was ruled out. It seemed easier to fix the diameter of the container and use fluids of different viscosities.

The simplest method to obtain fluids of different viscosities was

to use glycerin-water mixtures. If viscosities higher than 100% glycerin were needed, different grades of silicon oils were also available.

The specific gravities and viscosities of aqueous solutions of glycerin [23] are plotted in Figures 51 and 52 and several mixtures in sufficient quantities were prepared in the range of desired viscosities. The viscosities of the mixtures were tested by the use of different grades of viscometers and the measured values are marked by small circles on Figure 52. The slight disagreement of tested values initiate from two facts:

1. The tests were carried at a higher temperature compared to that of Reference [23].

2. The pure glycerin available was not exactly 100% pure.

The viscosities measured are converted in the unit ft/sec^2 for direct use in equations 138 and 139 and are presented in Table 6. The viscous damping factors used in the text of this program are calculated from equation 140

$$\zeta_p = \delta_p/2\pi \tag{140}$$

where δ_p is calculated from equations 138 and 139. The approximation 140 holds up to a value of $\zeta_p \simeq 0.3$. This approximation is explained in any standard vibration book.

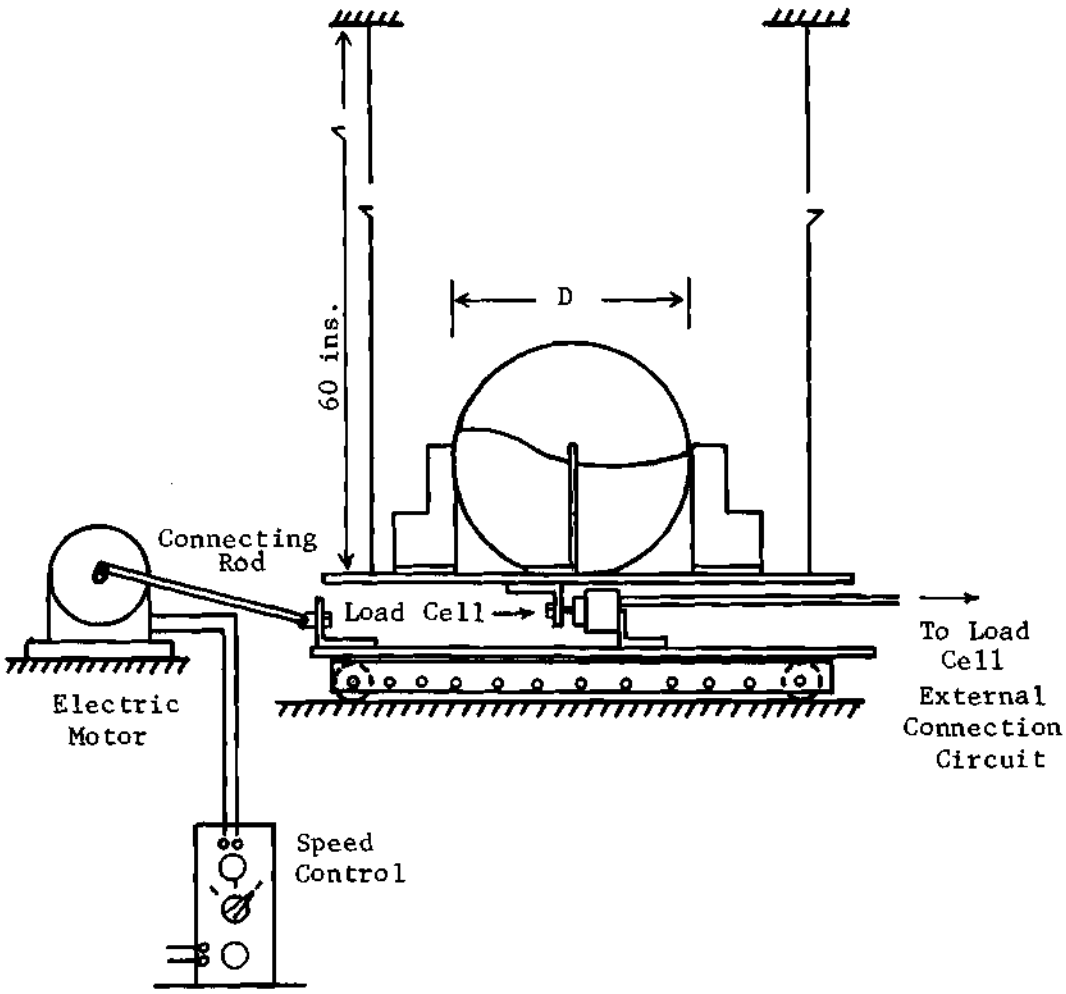

Figure 48. Experimental Setup for Measuring Viscous Damping

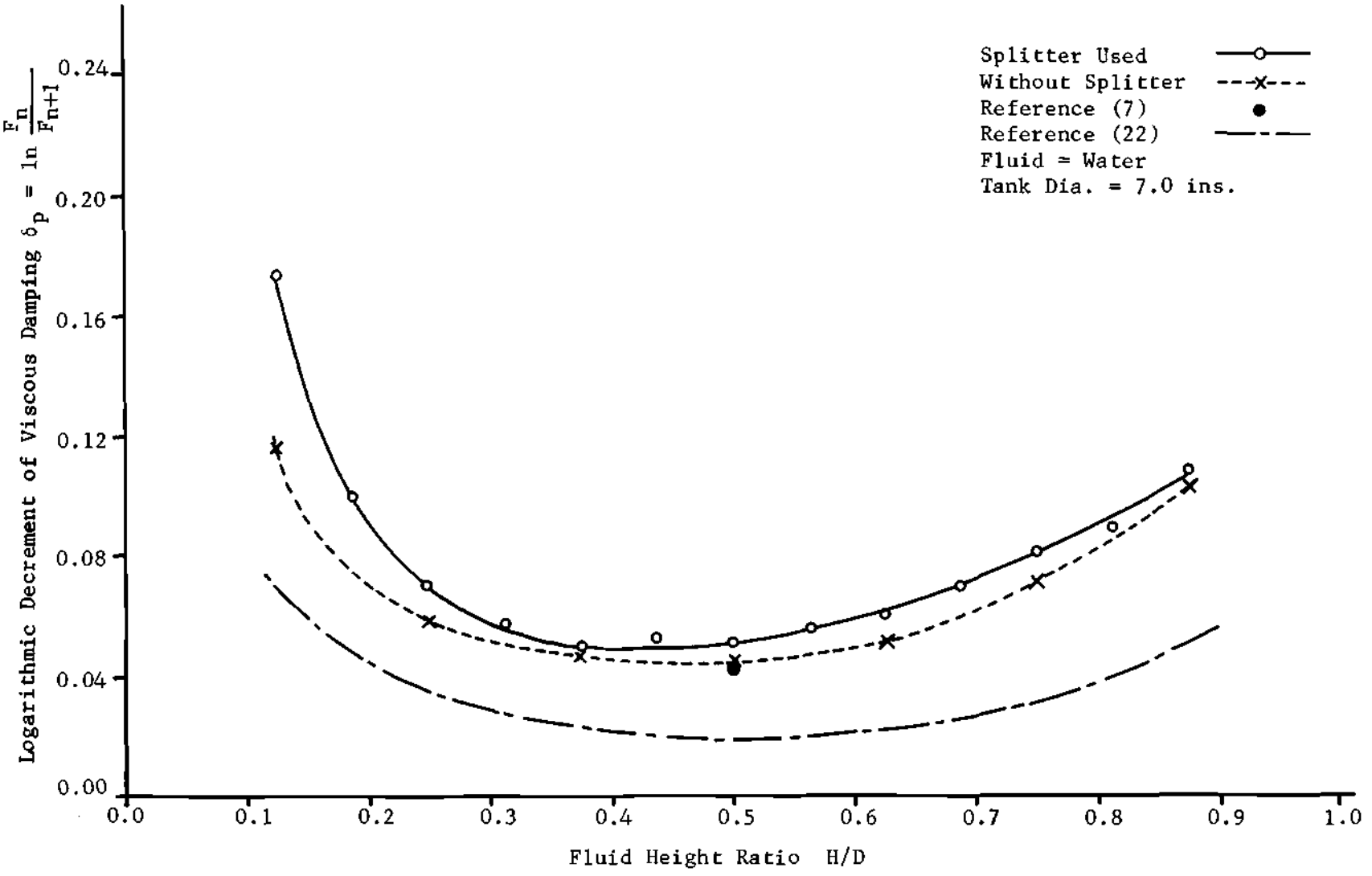

Figure 49. Viscous Damping for Fluid Sloshing in Spherical Containers

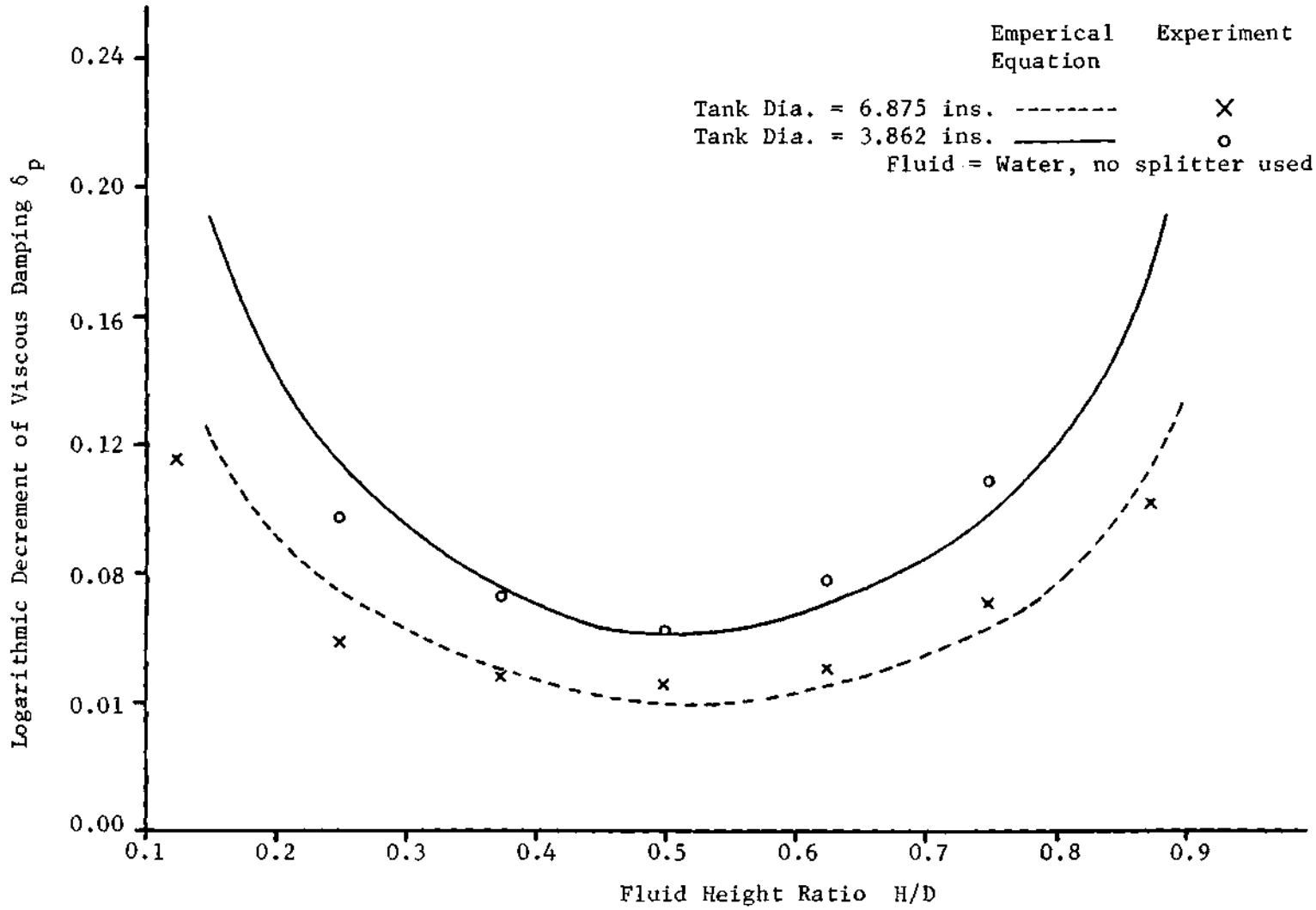

Figure 50. Viscous Damping for Fluid Sloshing in Spherical Containers

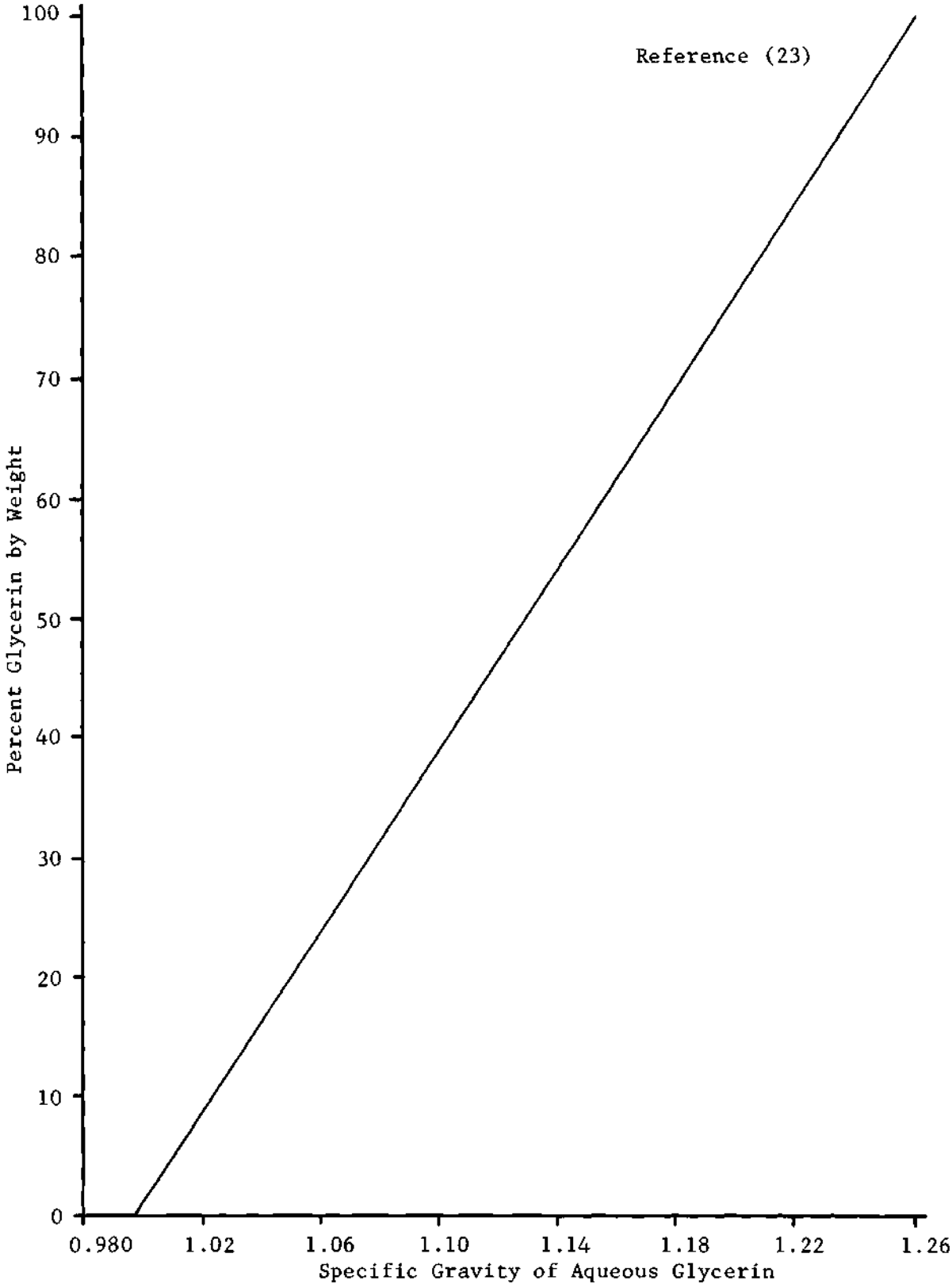

Figure 51. Specific Gravity of Aqueous Glycerin

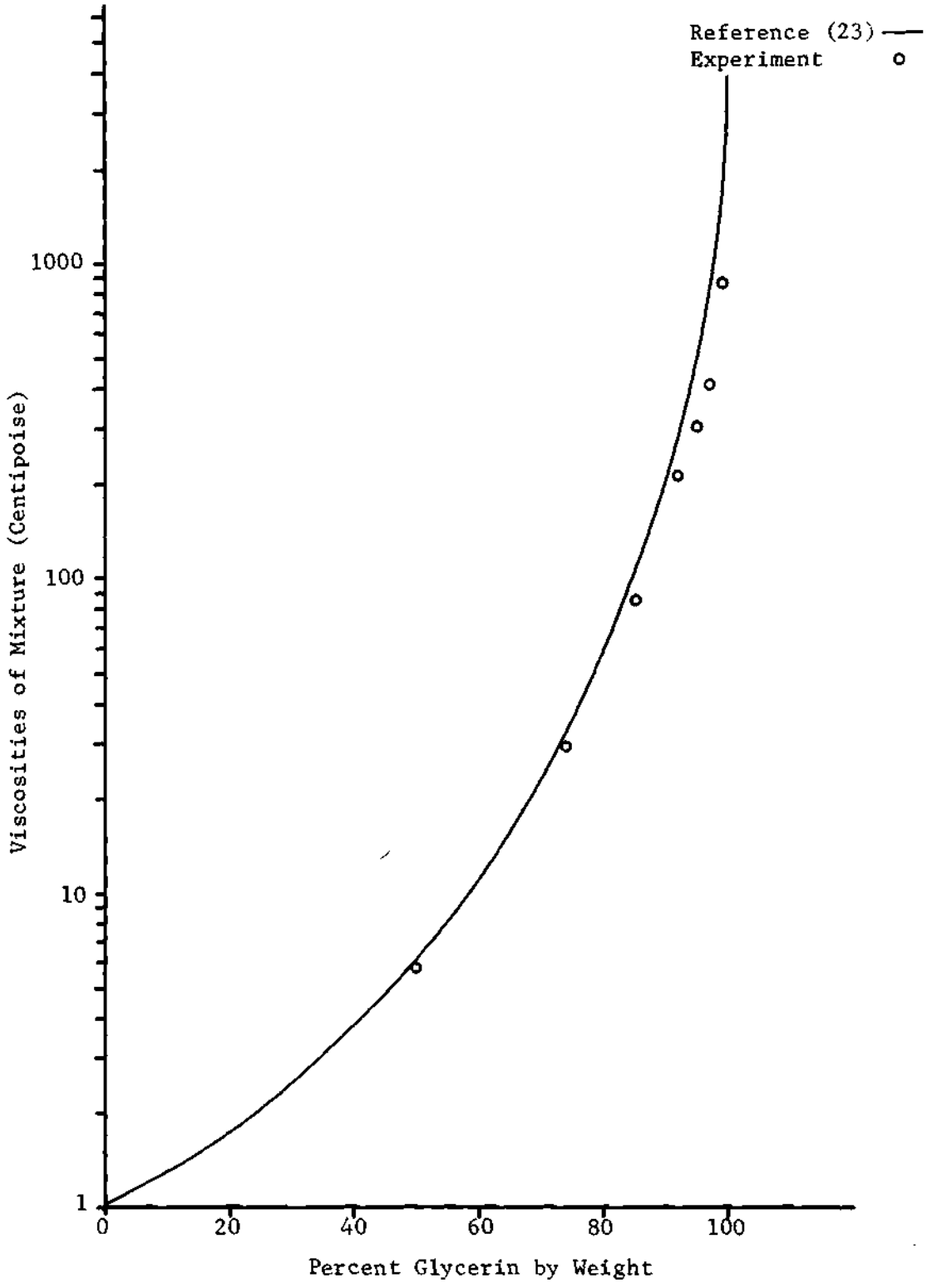

Figure 52. Dynamic Viscosities of Aqueous Glycerin

Table 6. Kinematic Viscosities of Aqueous Glycerin and the Corresponding Specific Weights

Fluid	Kinematic Viscosity (ft^2/sec)	Specific Weight ($\#/ft^3$)
Water	1.059×10^{-5}	62.3
50% Glycerin	5.59×10^{-6}	70.4
74% Glycerin	2.64×10^{-4}	74.4
85% Glycerin	7.63×10^{-4}	76.10
92% Glycerin	1.99×10^{-3}	77.40
95% Glycerin	2.63×10^{-3}	77.80
97% Glycerin	4.26×10^{-3}	78.20
99% Glycerin	7.45×10^{-3}	78.50

CHAPTER VIII

CONCLUSIONS AND REMARKS

Since most of the subjects are discussed in detail in the text of this program, and many conclusions are drawn when theoretical and experimental results are discussed, it seems sufficient to summarize only the important conclusions.

Forced Vibration

1. The regions of instability of the fluid sloshing in spherical containers have been compared to the regions of instability of an analogous spherical pendulum system. The boundaries of these regions have been determined experimentally (Figures 57 through 63) and compared with those derived by Miles [14]. The agreement is good and the comparison is shown in Figure 2.

2. In order to obtain force-frequency response of the sloshing fluids, it seemed necessary to install a splitter plate parallel to the direction of excitation. The force-frequency plots obtained are shown in Figures 64 through 72 in Appendix C. The plots indicate strong softening characteristics for the nonlinear range of oscillation for all the fluid heights tested.

3. Fluids oscillating in a shperical container under forced vibration exhibit jump phenomena in the nonlinear range of fluid motion (Figures 64 through 72).

4. The maximum slosh forces obtained from Figures 64 through 72 were compared to the corresponding forces of a pendulum model. The comparison as shown in Figure 5 indicates some disagreements in the nonlinear range of fluid motion for most of the fluid heights tested.

5. There exists a critical fluid height (H/D = 0.340) at which the pendulum duplicates fluid response for the entire range of fluid oscillations.

6. For the nonlinear range of fluid motion the pendulum was modified by inclusion of a cubic spring. This nonlinear spring constant has been determined for various fluid heights and is shown in Figure 9. The maximum force response agreed well after the modification was made (Figure 10).

7. For the modification imposed on the pendulum model, the stability boundaries still remained in close agreement (Figure 12).

Free Vibration

Linear Analysis

1. The free vibration of the coupled system has been analyzed and the characteristic equation of the coupled linear differential equations was derived. The solutions (roots) of the characteristic equation were obtained in numerical form and for the range of parameters covered, the roots were always complex conjugates with a negative real part.

2. The effect of frequency ratio on logarithmic decrement of the main system has been evaluated and is shown in Figures 14 through 21. As a result of the analysis, damping of the main system is maximum at

certain critical tuning frequencies (Ω_p).

3. The effect of mass ratio on logarithmic decrement of damping has been investigated and is shown in Figures 14 through 21. The analysis indicates that there was little increase in the damping of the main system due to increase in mass ratio (also Figure 23).

4. The critical tuning frequency decreases with increase in mass ratio (Figure 22).

5. The effect of fluid viscous damping on the logarithmic decrement of the main system has been evaluated and is shown in Figures 14 through 21. According to the analysis the damping of the main system increases with increase in viscous damping (Figure 23).

6. At the critical tuning frequency the increase in damping is linear up to a critical value of viscous damping (ζ_{pc}) as shown in Figure 25.

7. At other tuning frequencies ($\Omega > \Omega_p$ and $\Omega < \Omega_p$) the linearity is only up to about one half of the critical value of viscous damping as shown in Figures 24 and 26.

8. The existence of the critical value of damping has been shown experimentally and analytically in Figures 24, 25, and 26. The damping of the main system decreases if ζ_p increases beyond this critical value.

9. Beat phenomena exists in the neighborhood of critical tuning frequency and it is intense at the critical tuning frequency .

10. Beat becomes less intense for frequencies higher and lower than the critical tuning frequency.

11. Beat disappears for viscous damping higher than the critical value ($\zeta_p > \zeta_{pc}$).

12. It has been found that small structural damping shifts the critical tuning frequency if the viscous damping is in the same order of magnitude (Figure 27).

13. It has been found that the effect of small structural damping on the damping of the main system is simply additive.

14. Slosh dampers if designed properly, are excellent devices for damping vibrations. For a better design it is suggested that a partially filled container with low mass ratio be tuned at the critical tuning frequency. The viscous damping should be equal to the critical value ($\zeta_p = \zeta_{pc}$).

15. For the uncoupled fluid sloshing in spherical containers, the logarithmic decrement of damping of the force response has been studied experimentally. The results are compared to other investigators and the comparison is shown in Figure 49. An emperical expression for damping as a function of other parameters is given in Chapter VII. According to the analysis, the fluid exhibits large damping for fluid heights far removed from the half full container.

Nonlinear Analysis

16. The derivation of the nonlinear differential equations are given. The method of numerical solution of this system of equations is shown. The coupled system is analyzed experimentally and analytically for ranges of initial displacements, comparisons are made for various values of ϵ (displacement ratio). It has been found that the pendulum model excellently represents the motion of the sloshing fluid in the coupled system for low values of ϵ (Figures 31, 32, and 33).

17. It has been found that there exists a critical value of ϵ

above which the motion of the fluid becomes complex (combination of swirl, beat and planar oscillation).

18. It has been found that for $\epsilon < \epsilon_c$, the constrained pendulum model (modified or unmodified) sufficiently represents the transient motion of the fluid in the coupled system (Figures 31, 32, 33, and 46).

19. It has been found that the agreement between the theory and experiment greatly improves if the cubic spring constant β is included in the nonlinear pendulum model for fluid heights other than the critical value (H/D = 0.340). This comparison is shown in Figure 36.

20. It is recommended that for fluids of low viscosity (if used as slosh dampers at large displacements) a splitter plate be included in the container to suppress the fluid rotation. In such cases a planar pendulum model is a better mathematical representation.

Recommendations

In the course of analysis of fluid slosh dampers several interesting problems came to the author's attention.

1. One possible continutation of this program is to analyze slosh dampers with a single spherical particle submerged in the fluid [07]. For a fixed container size, fluid viscosity and fluid height one can study the variation in damping of the main system for various particles. In a subsequent program the number of solid particles can also be varied.

2. It would be interesting to study a cluster of spheres partially filled with fluid, each representing a single degree of freedom and replace the single slosh damper with a number of smaller partially filled spheres.

3. The application of other container geometries in fluid slosh damping may have equal importance. The relative improvement, if there is any, deserves an investigation.

4. It was observed that the fluid slosh dampers exhibit marked improvement when the fluid develops large amplitudes and possibly when the swirling motion dominates. This condition of fluid motion may be modeled as a spherical pendulum or an impacting mass with viscous dissipation.

5. When $\Omega \ll \Omega_p$, higher modes of fluid motion will be excited, this suggests the applicability of slosh dampers at relatively higher frequencies and may have to be remodeled.

6. The viscous damping as investigated by Sumner [7] and Mikishev [22] do not agree and the reason for the discrepancy as well as an accurate experimental analysis can be made the subject of a program.

7. Fluid slosh dampers under forced vibration can be modeled as damped vibration absorbers. The steady state oscillation of the main system can be studied for possible variation in viscous damping, frequency ratio and other parameters.

APPENDICES

APPENDIX A

PENDULUM ANALOGY

The pendulum analogy as obtained from Sumner's [9] analysis is presented for easy reference. The mass and length of the pendulum can be determined for any container diameter and fluid height from Figures 53, 54, and 55.

If Figure 53 is used the stationary mass M_o, can be calculated from the following relation:

$$M_o + M_p = M_f$$

However, it is more convenient to use Figure 54 to calculate the pendulum mass and Figure 56 to calculate the stationary mass.

Sumner's analysis indicate the hinge point location to be at the geometric center of the sphere for all fluid heights.

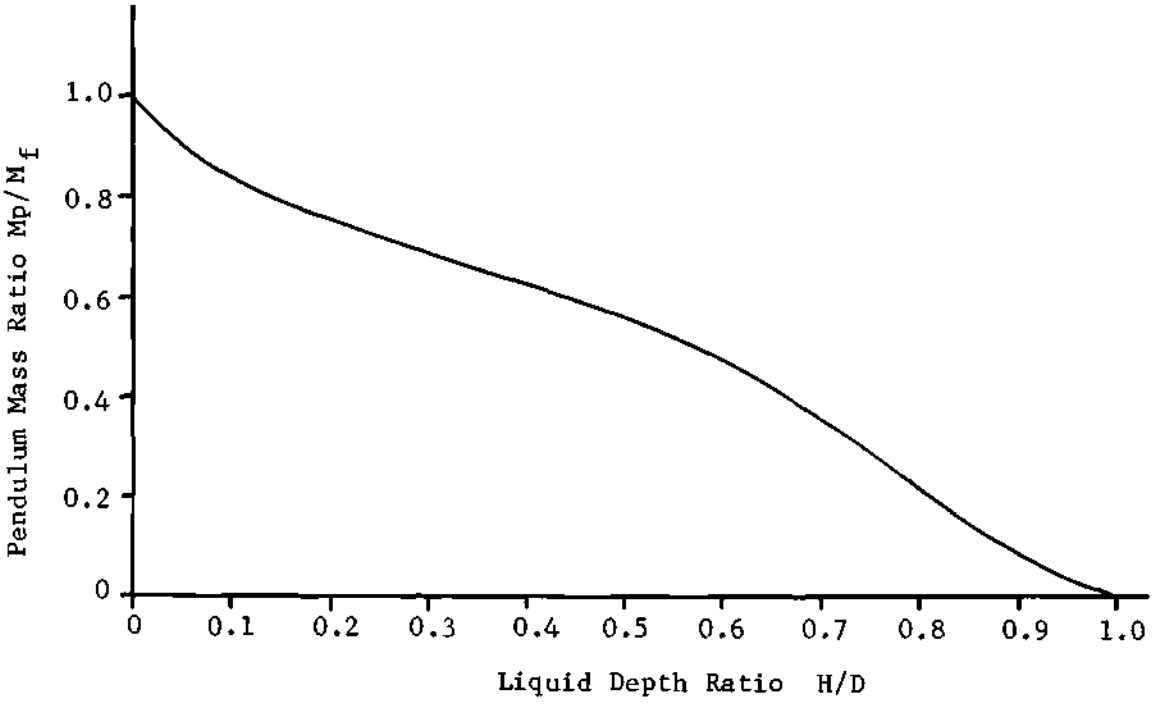

Figure 53. Ratio of Pendulum or Sloshing Mass to Total Liquid Mass in Partially Filled Containers

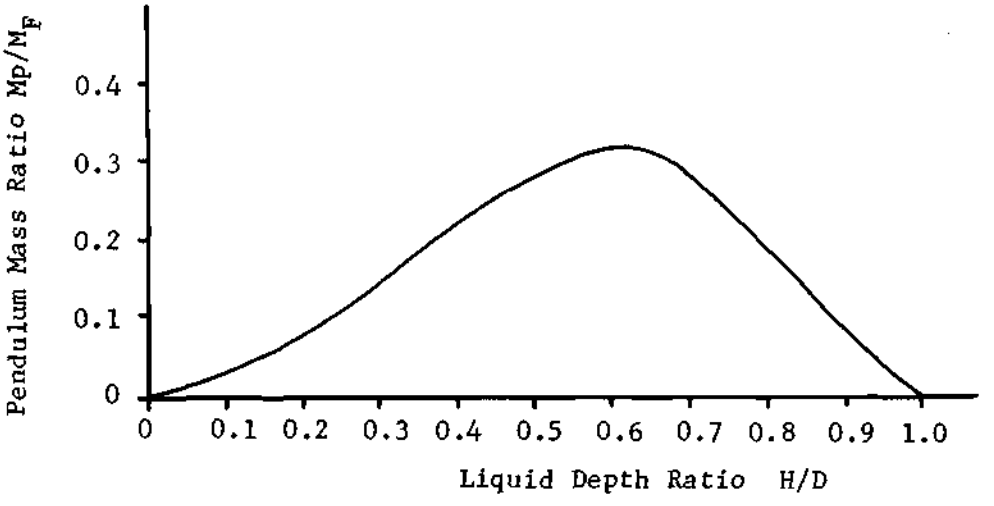

Figure 54. Ratio of Pendulum or Sloshing Mass to Total Liquid Mass in Completely Filled Containers

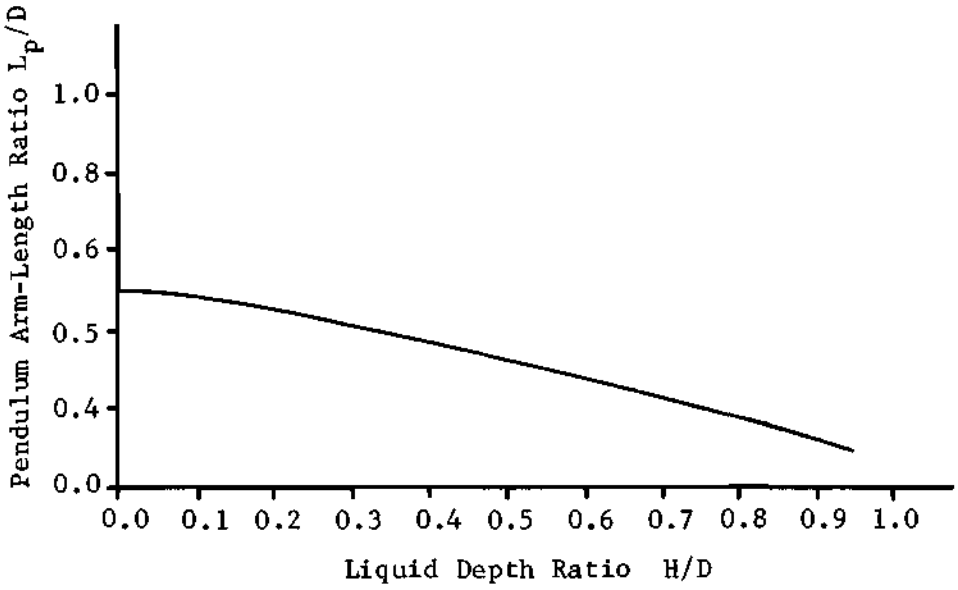

Figure 55. Pendulum Arm-Length Ratio

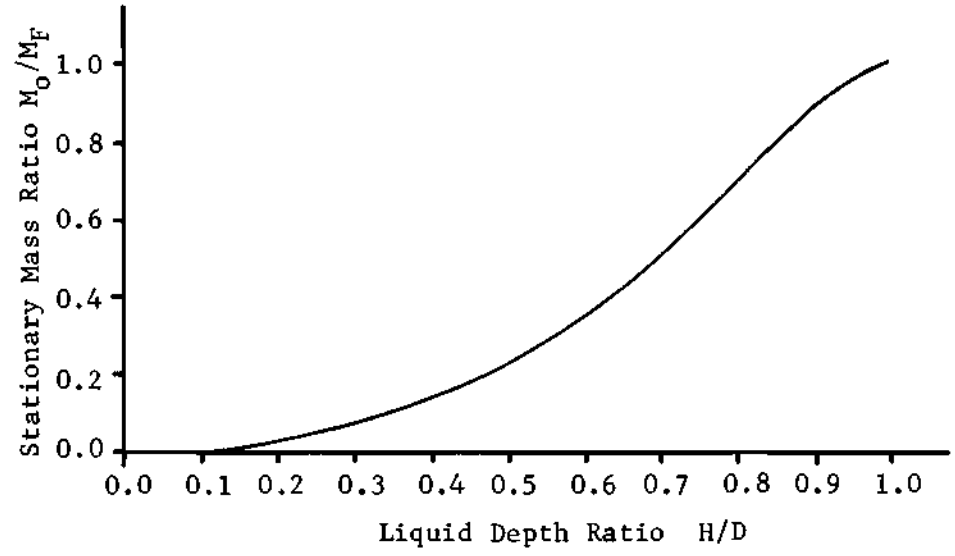

Figure 56. Stationary or Non-Sloshing Mass Ratio

APPENDIX B

EXPERIMENTAL STABILITY BOUNDARIES

This appendix contains the force-frequency plots of fluid (water) sloshing in spherical tanks (D_i = 6.875 inches, without splitter plate) under forced vibration. The stability boundaries are marked and the unstable region at which fluid first departs from the plane of excitation are shaded.

There are two bands of frequencies in the shaded area which are not shown.

1. Nonplanar fluid oscillation.
2. Nonplanar fluid rotation (swirl).

The two bands of frequencies are very close and narrow and it was not the interest of this program to distinguish the bounds.

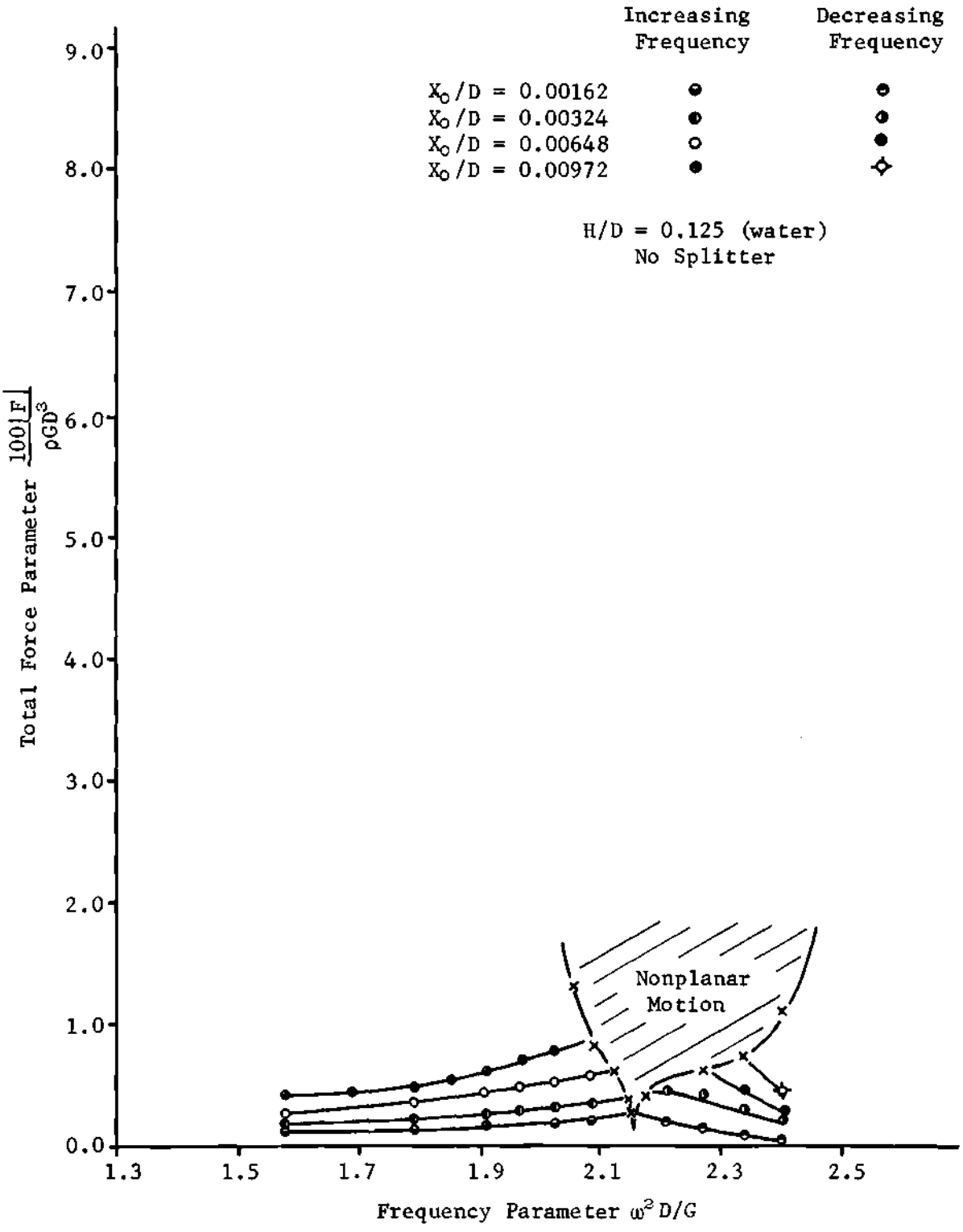

Figure 57. Stability Boundaries (H/D = 1/8)

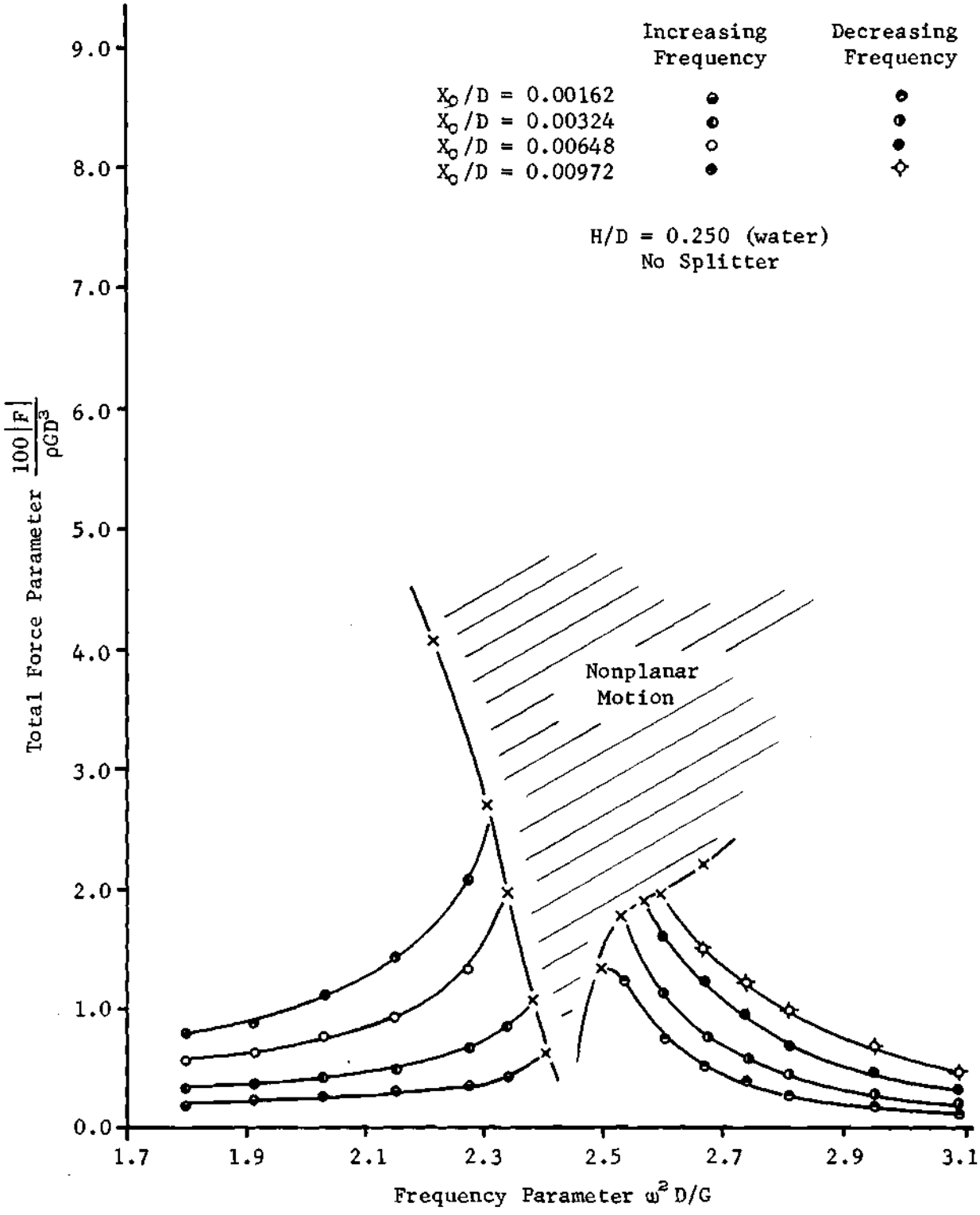

Figure 58. Stability Boundaries (H/D = 1/4)

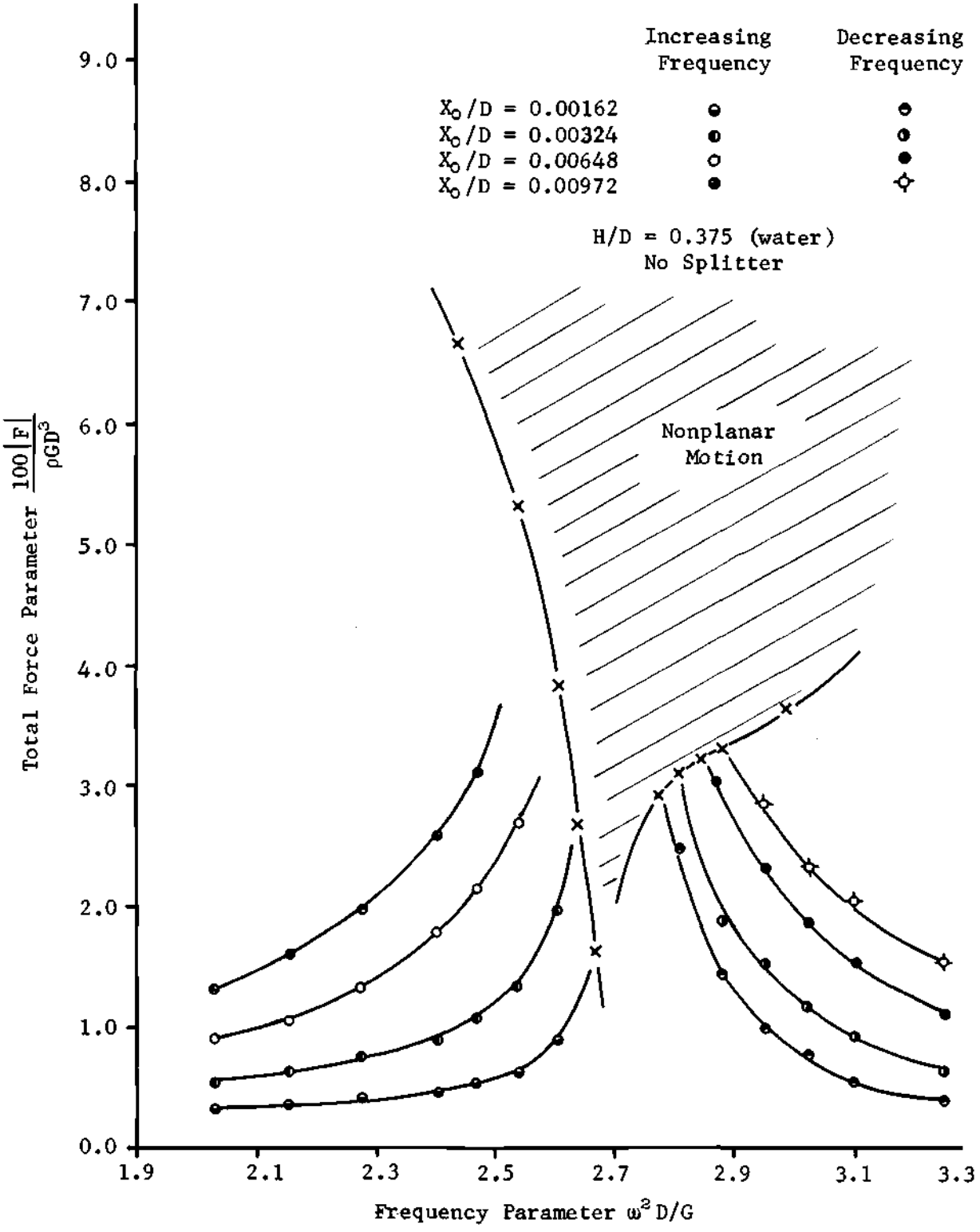

Figure 59. Stability Boundaries (H/D = 3/8)

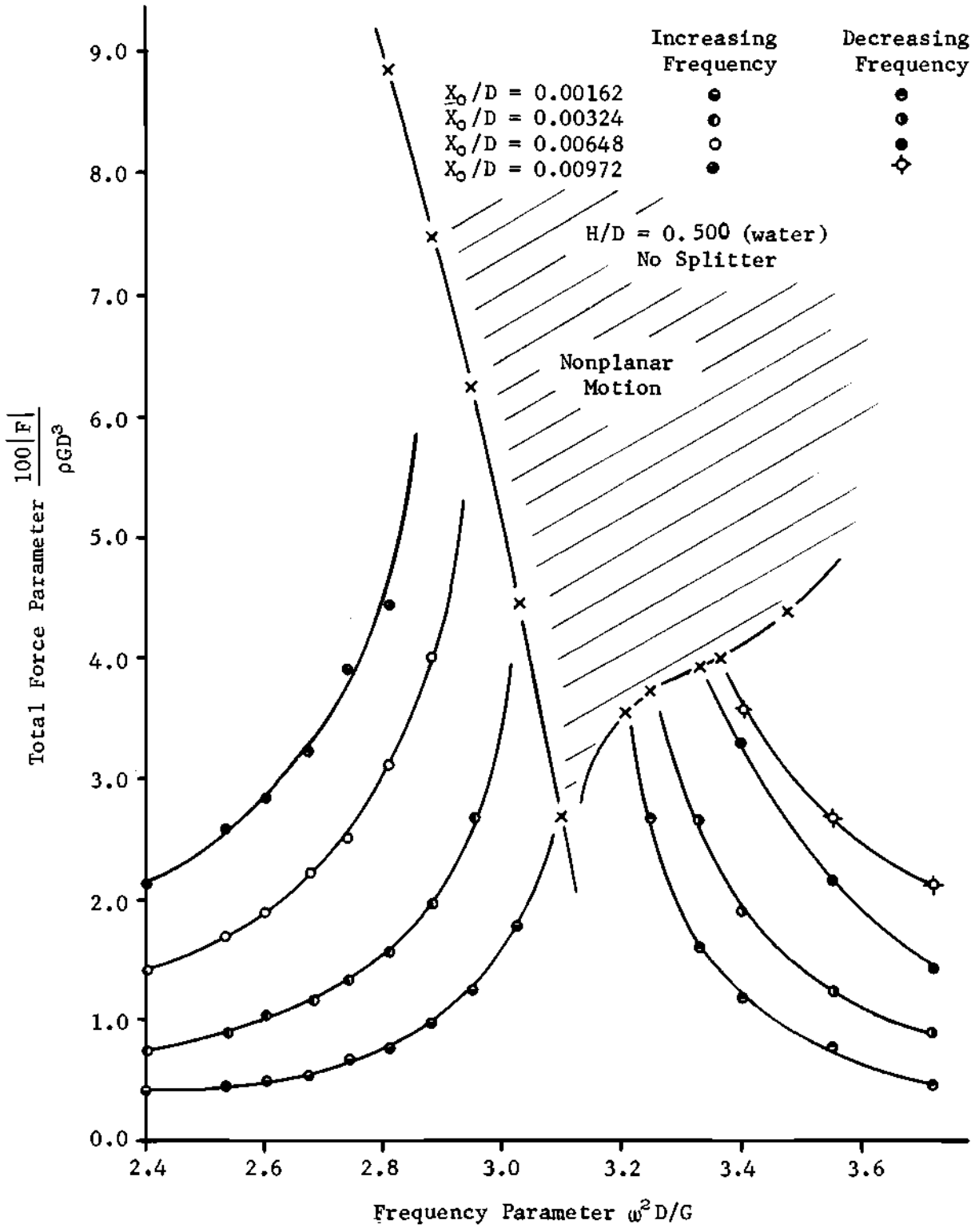

Figure 60. Stability Boundaries (H/D = 1/2)

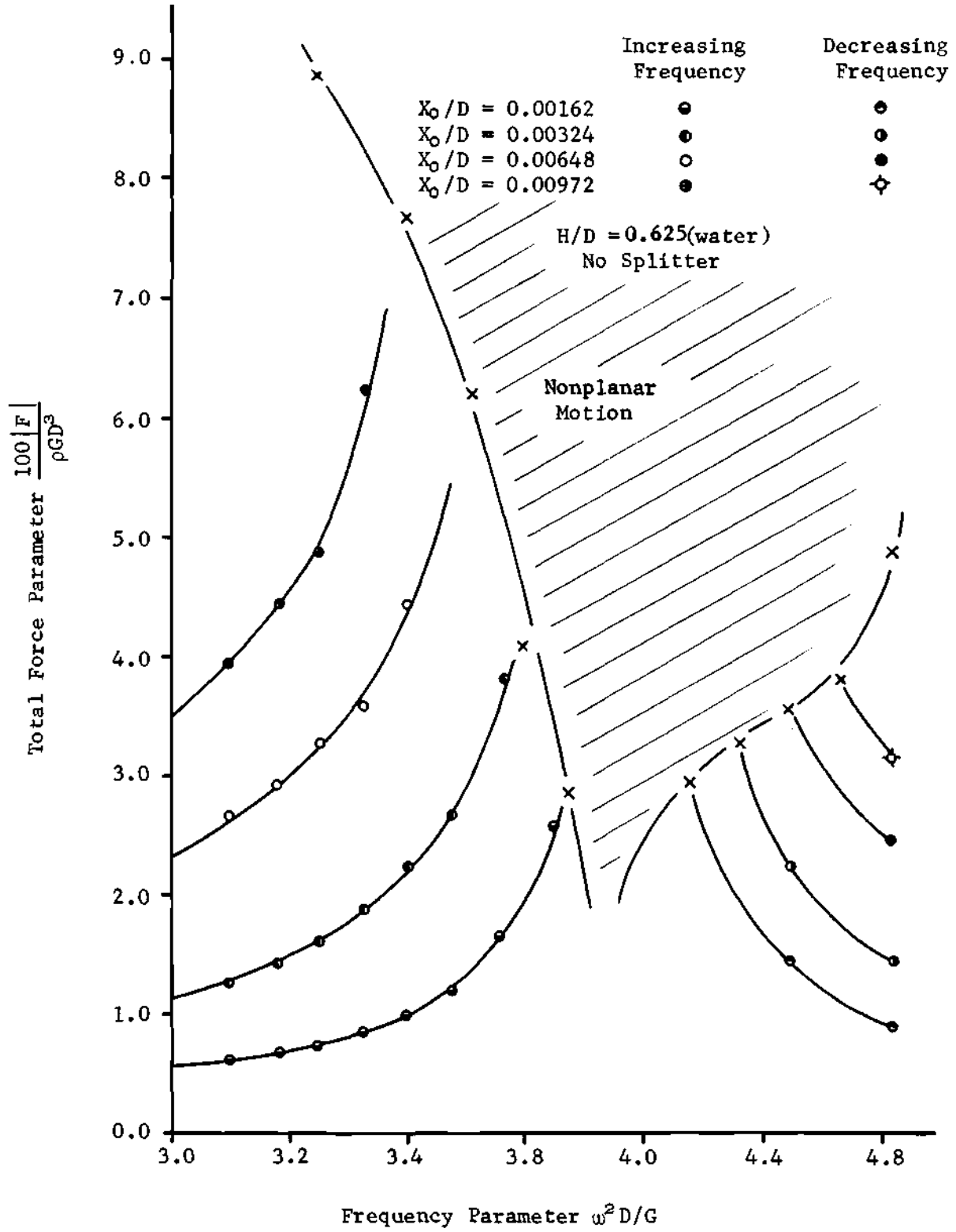

Figure 61. Stability Boundaries (H/D = 5/8)

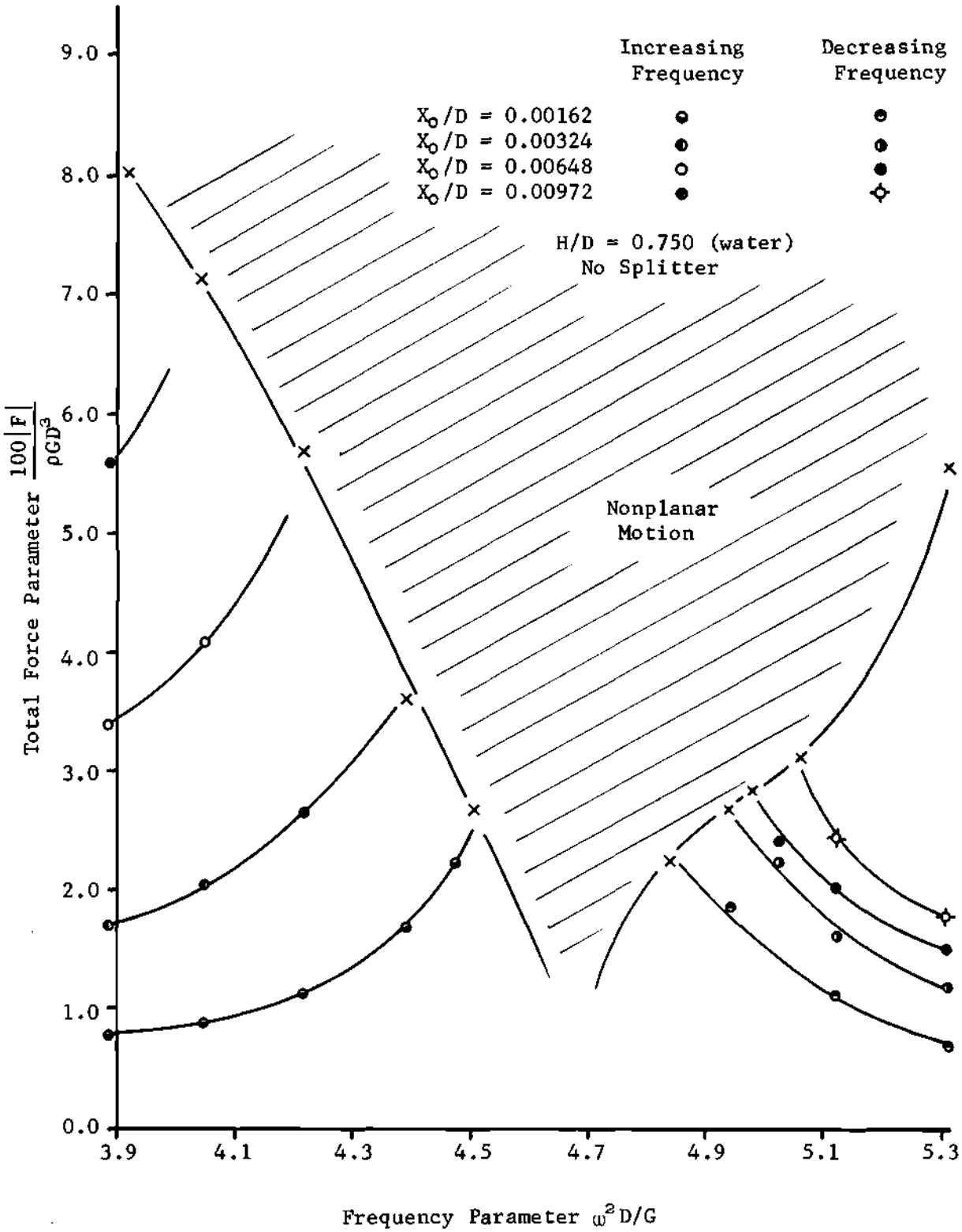

Figure 62. Stability Boundaries (H/D = 3/4)

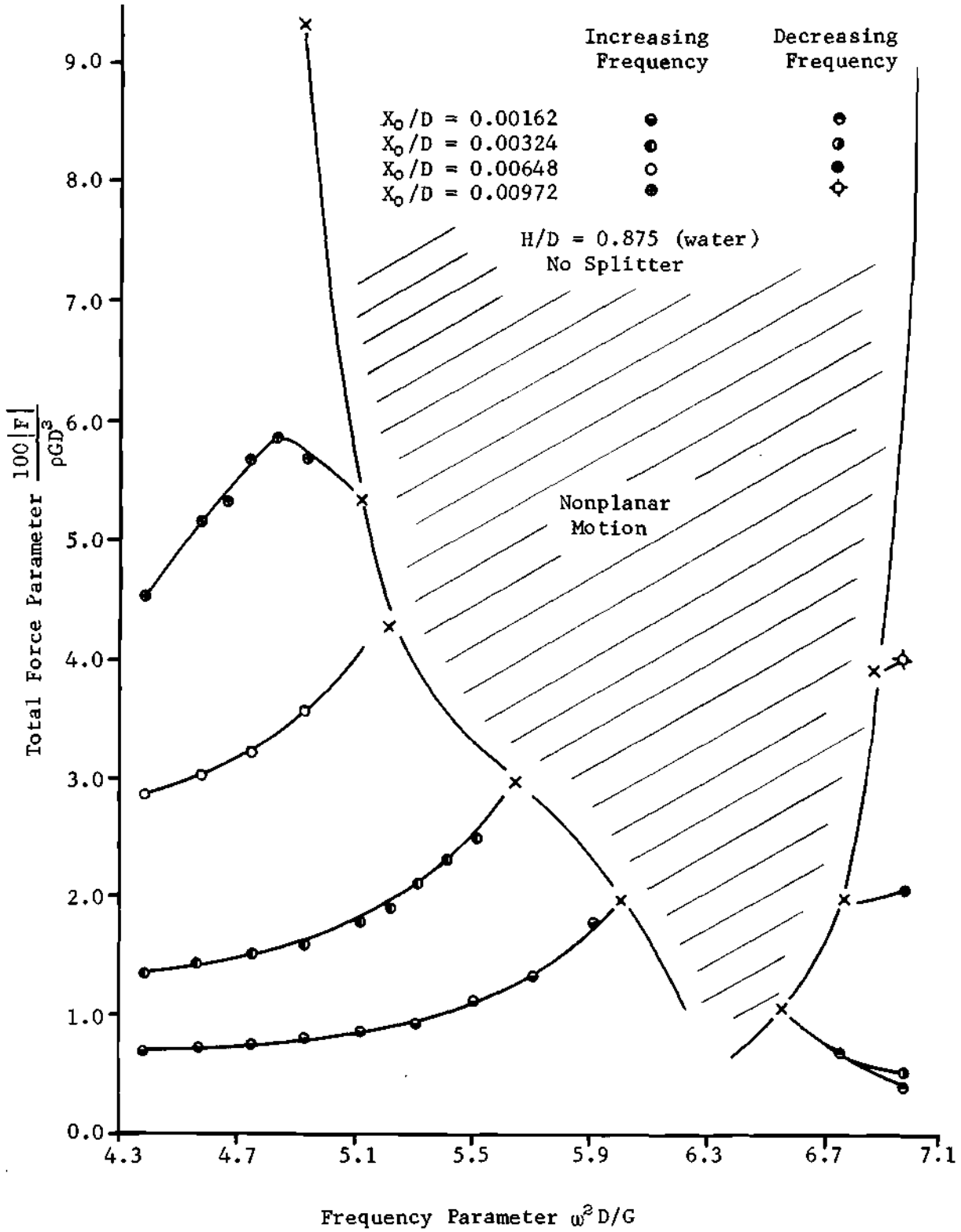

Figure 63. Stability Boundaries (H/D = 7/8)

APPENDIX C

EXPERIMENTAL FORCE-FREQUENCY PLOTS

This appendix contains force-frequency plots of fluid (water) sloshing in spherical containers (D_i = 6.875 inches, with the use of splitter plate parallel to the direction of excitation) under forced vibration.

Conclusions

1. The case of empty container (Figure 64) and completely filled container (Figure 72) indicate rigid body motion.

2. The general characteristic of fluid motion in the nonlinear range is always softening.

3. The fluid oscillations exhibit jump phenomenon.

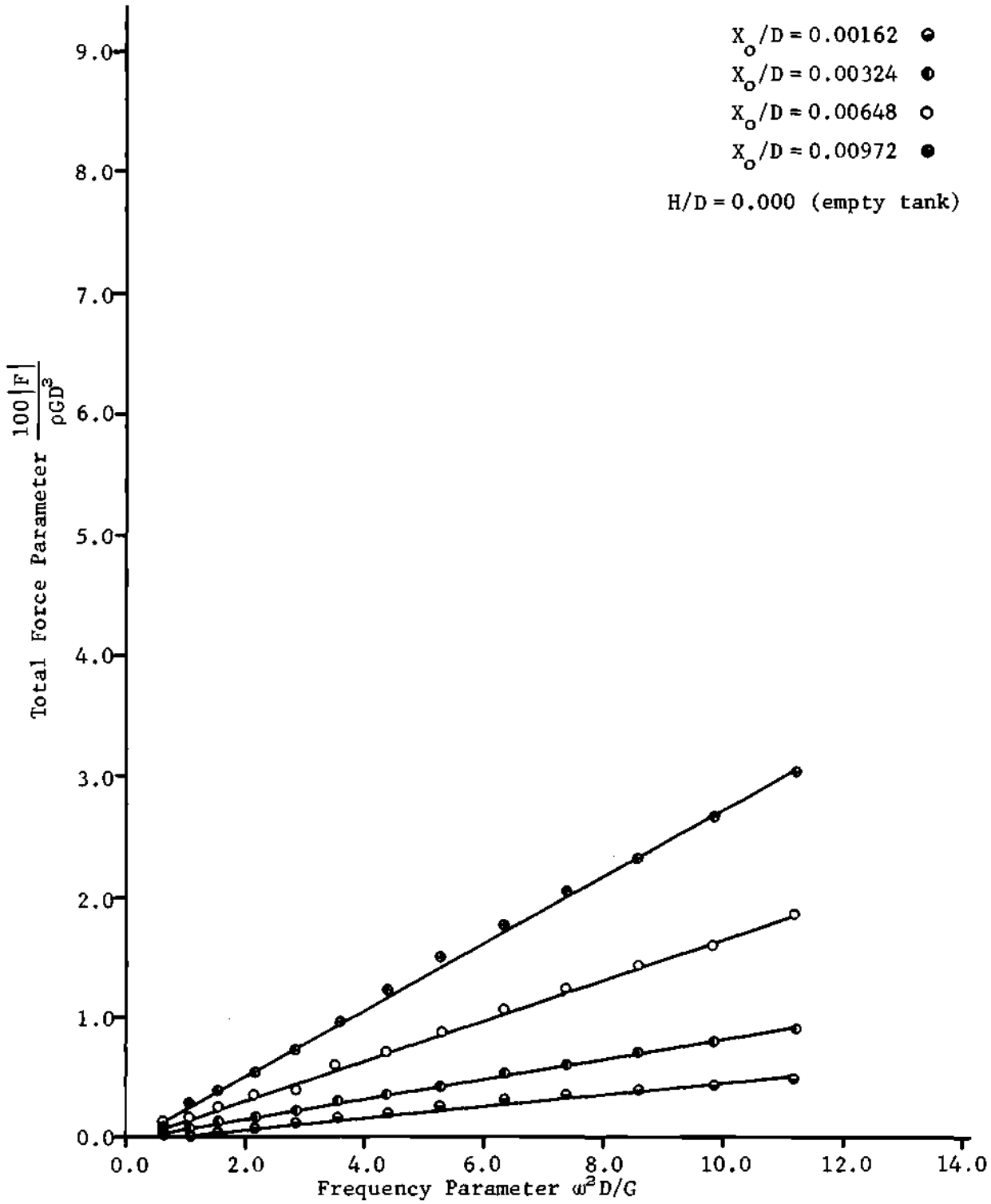

Figure 64. Force-Frequency Response (H/D = 0)

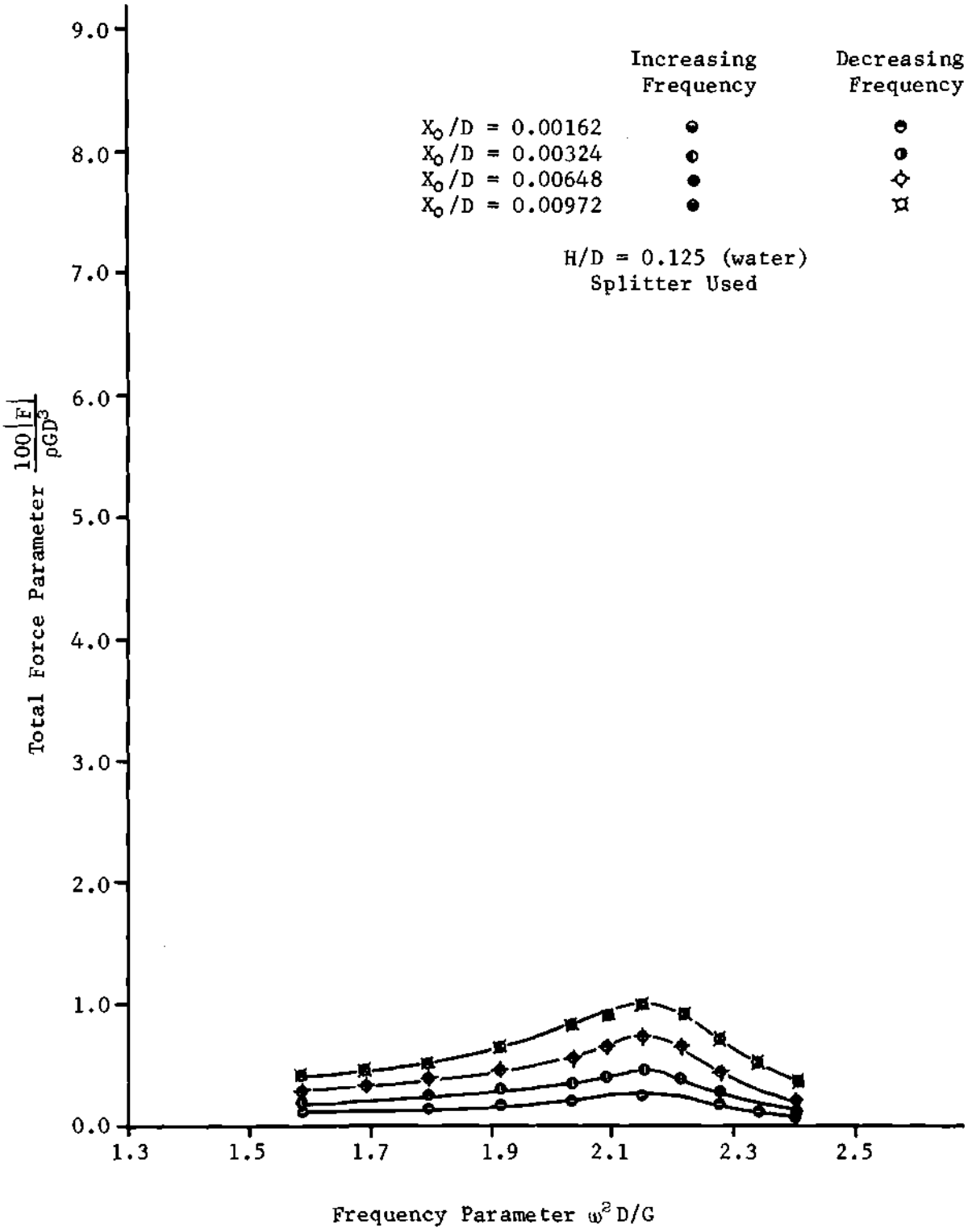

Figure 65. Force-Frequency Response (H/D = 1/8)

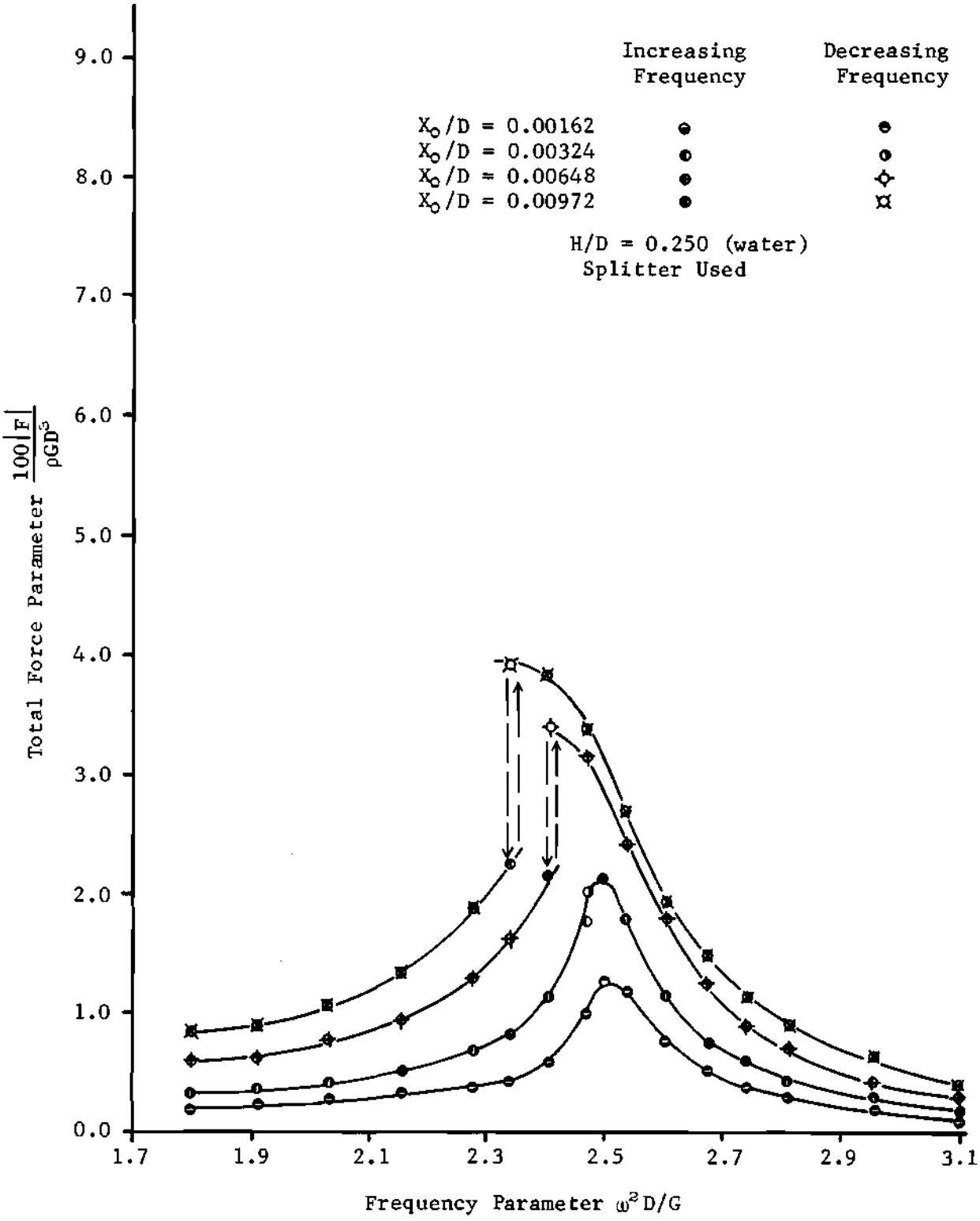

Figure 66. Force-Frequency Response (H/D = 1/4)

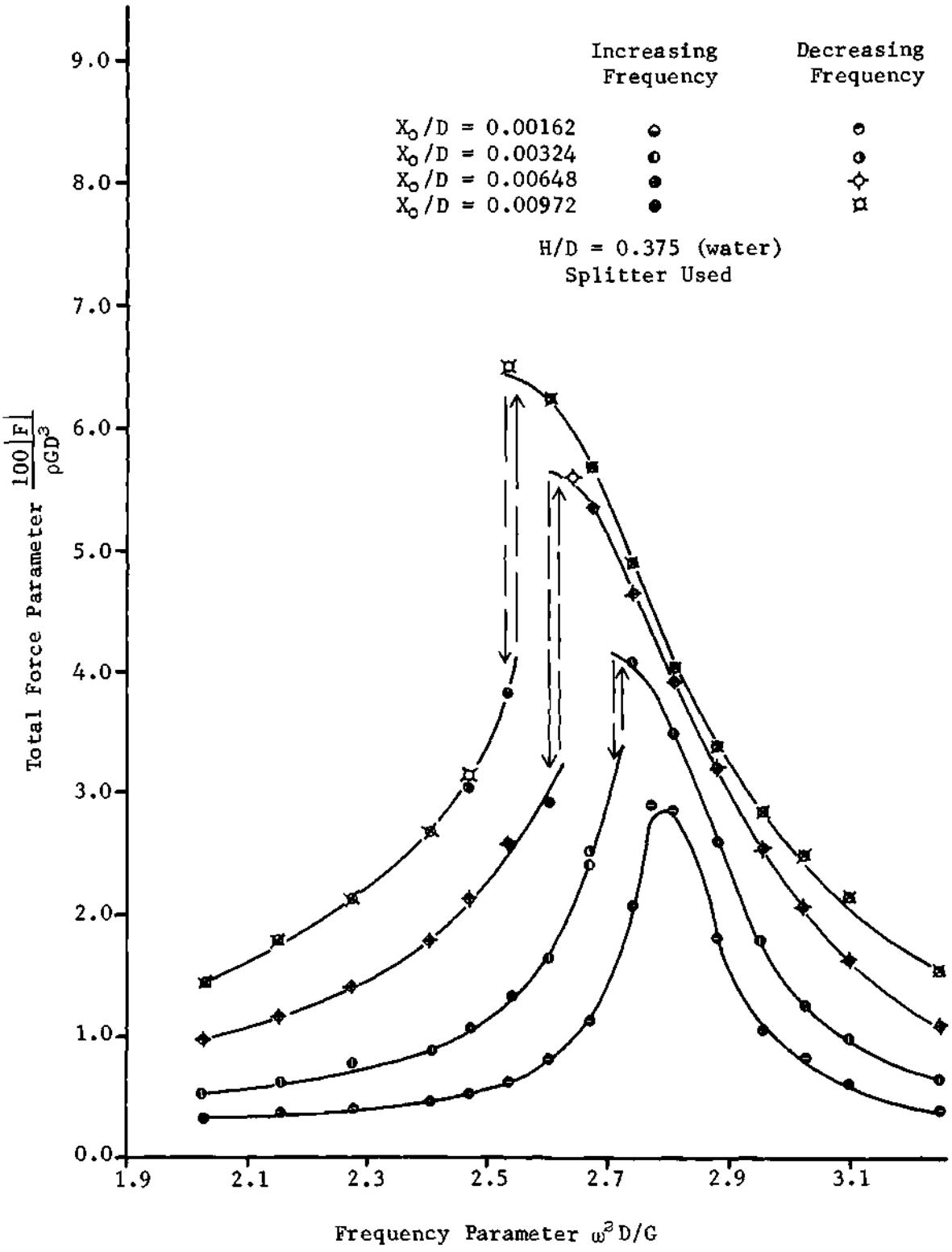

Figure 67. Force-Frequency Response (H/D = 3/8)

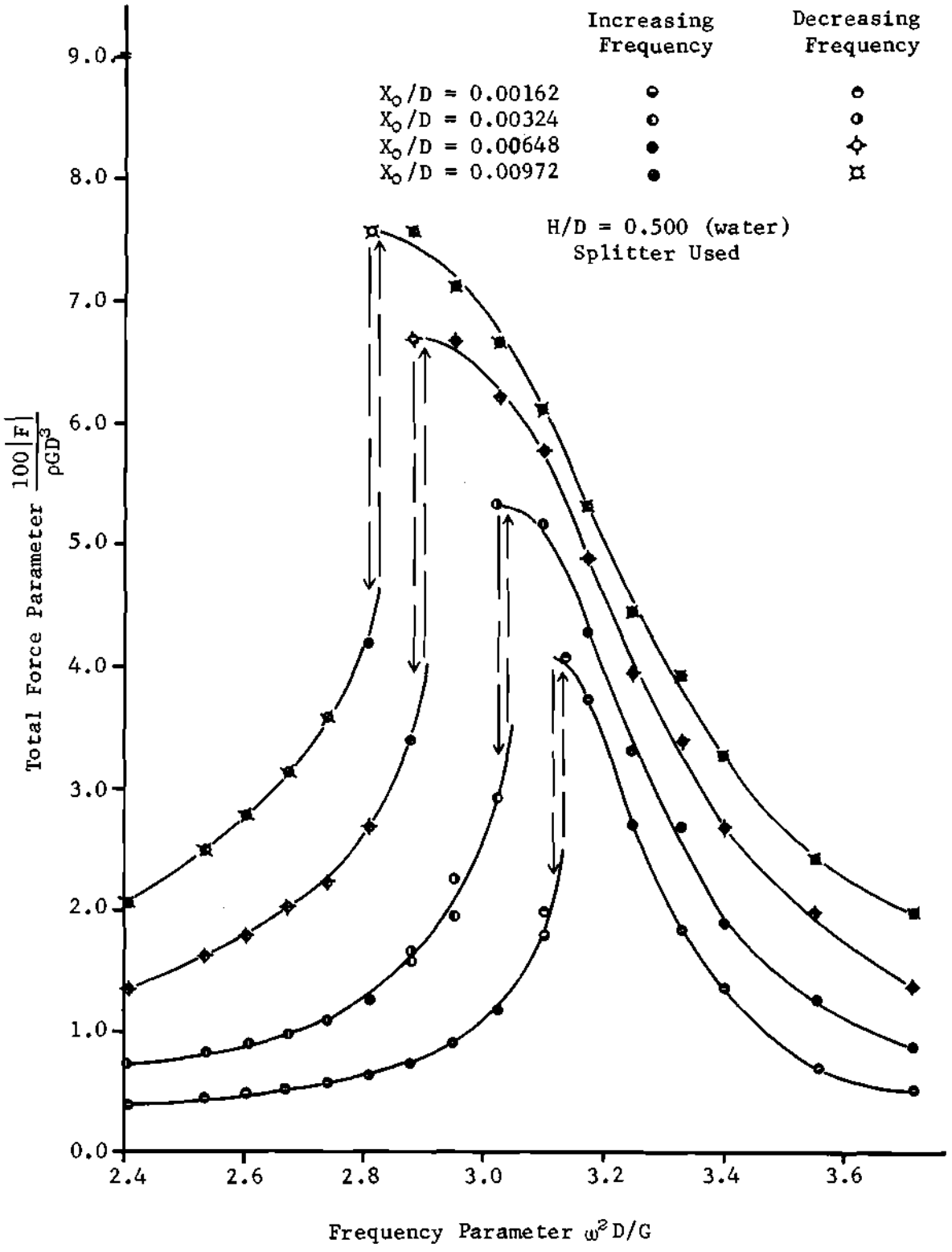

Figure 68. Force-Frequency Response (H/D = 1/2)

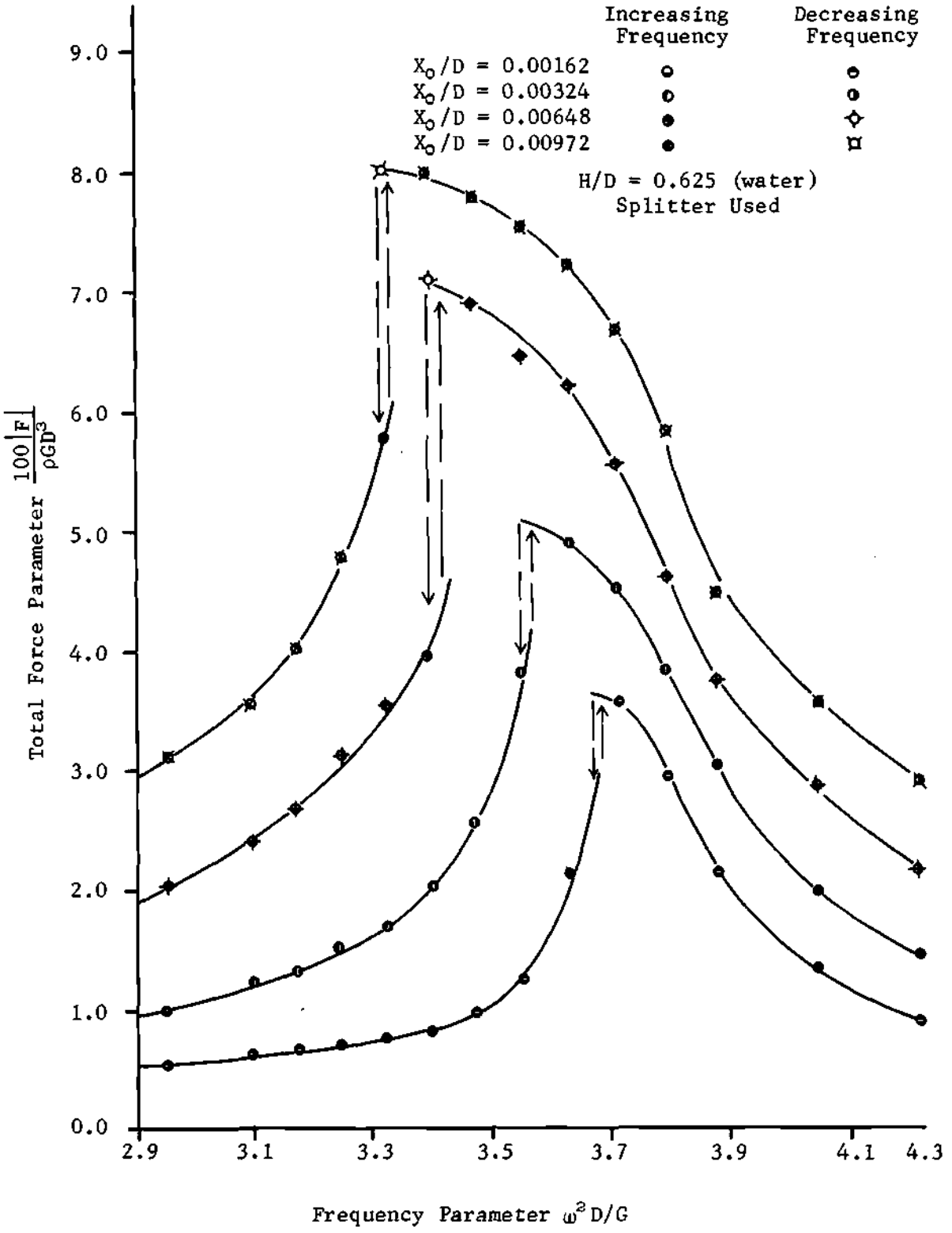

Figure 69. Force-Frequency Response (H/D = 5/8)

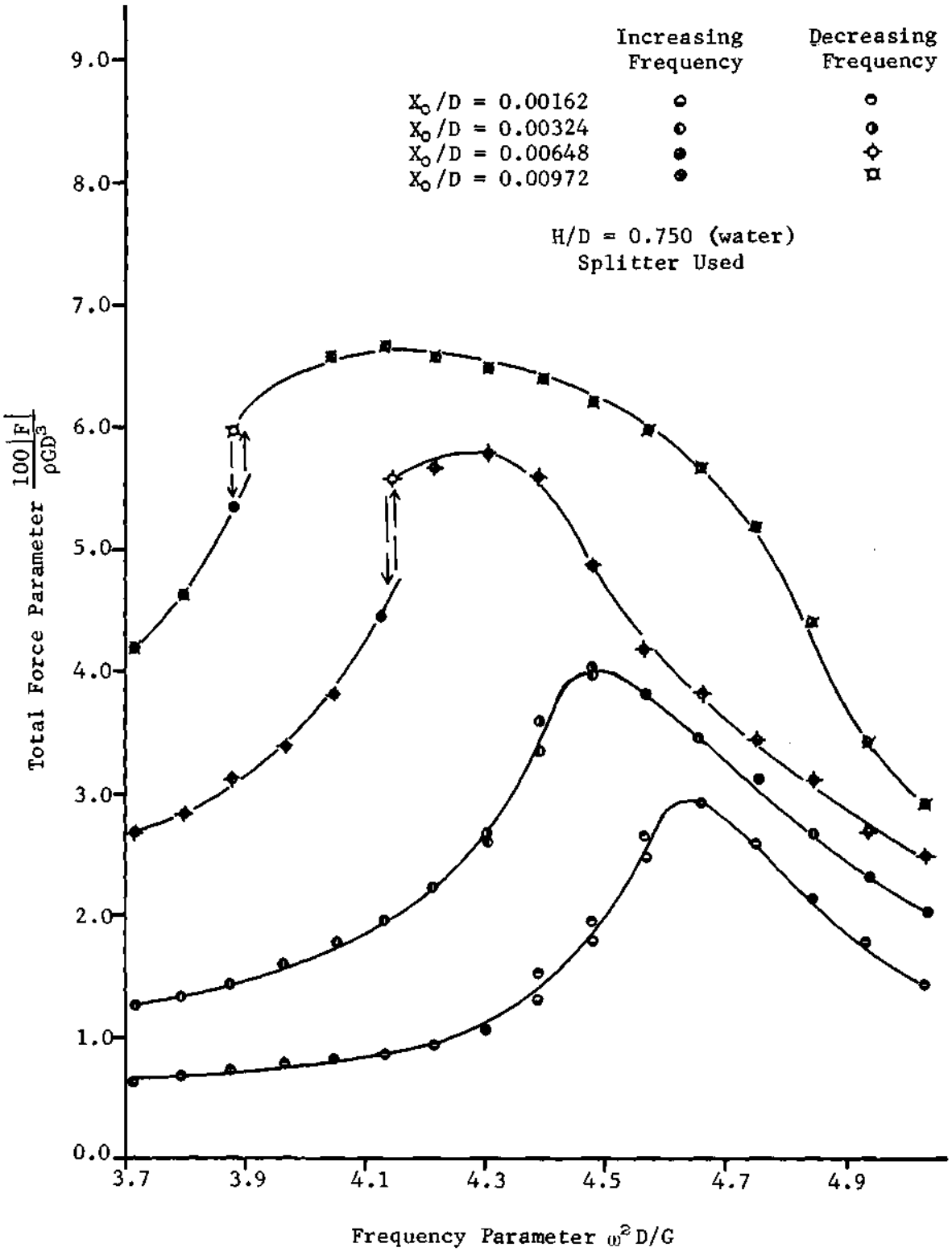

Figure 70. Force-Frequency Response (H/D = 3/4)

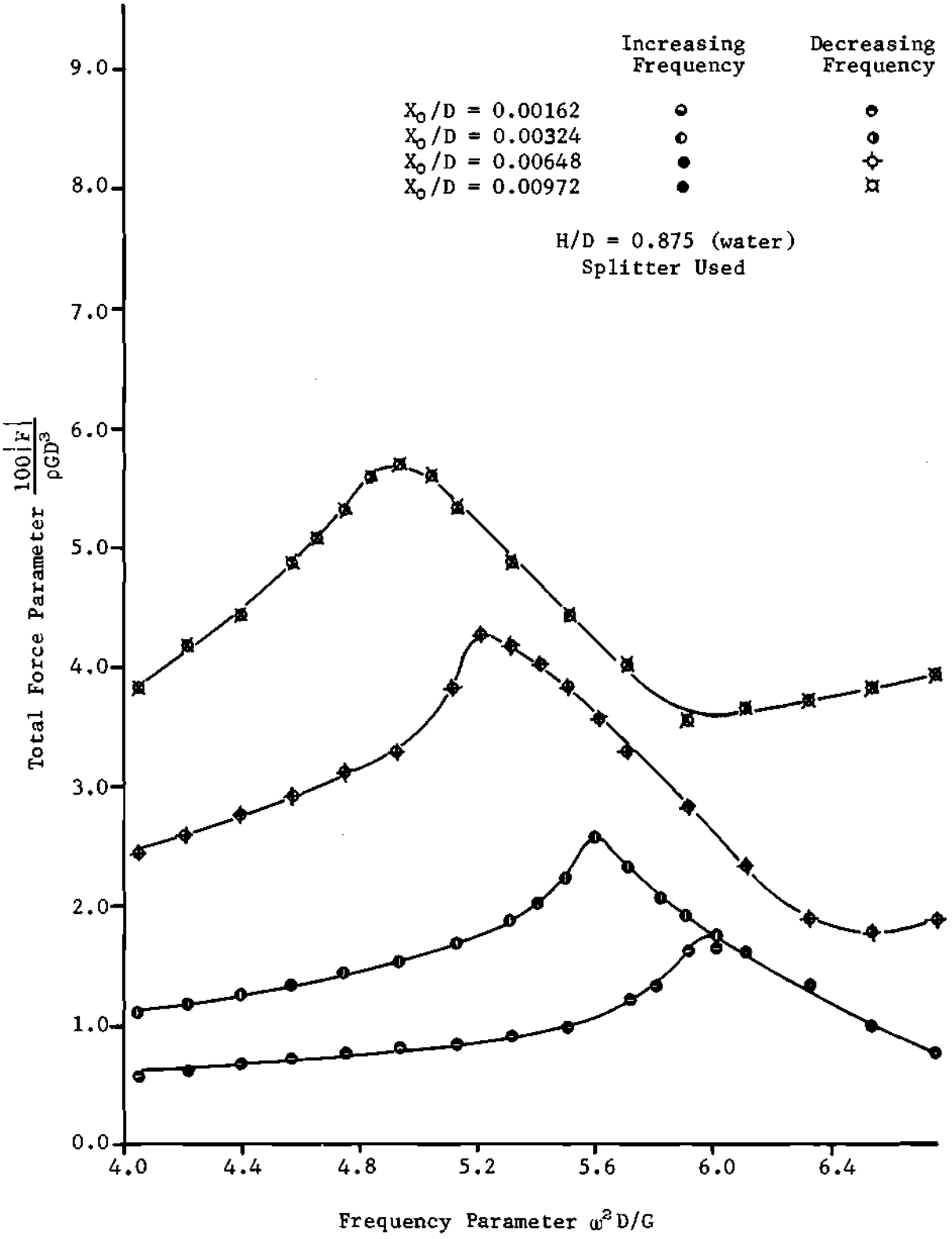

Figure 71. Force-Frequency Response (H/D = 7/8)

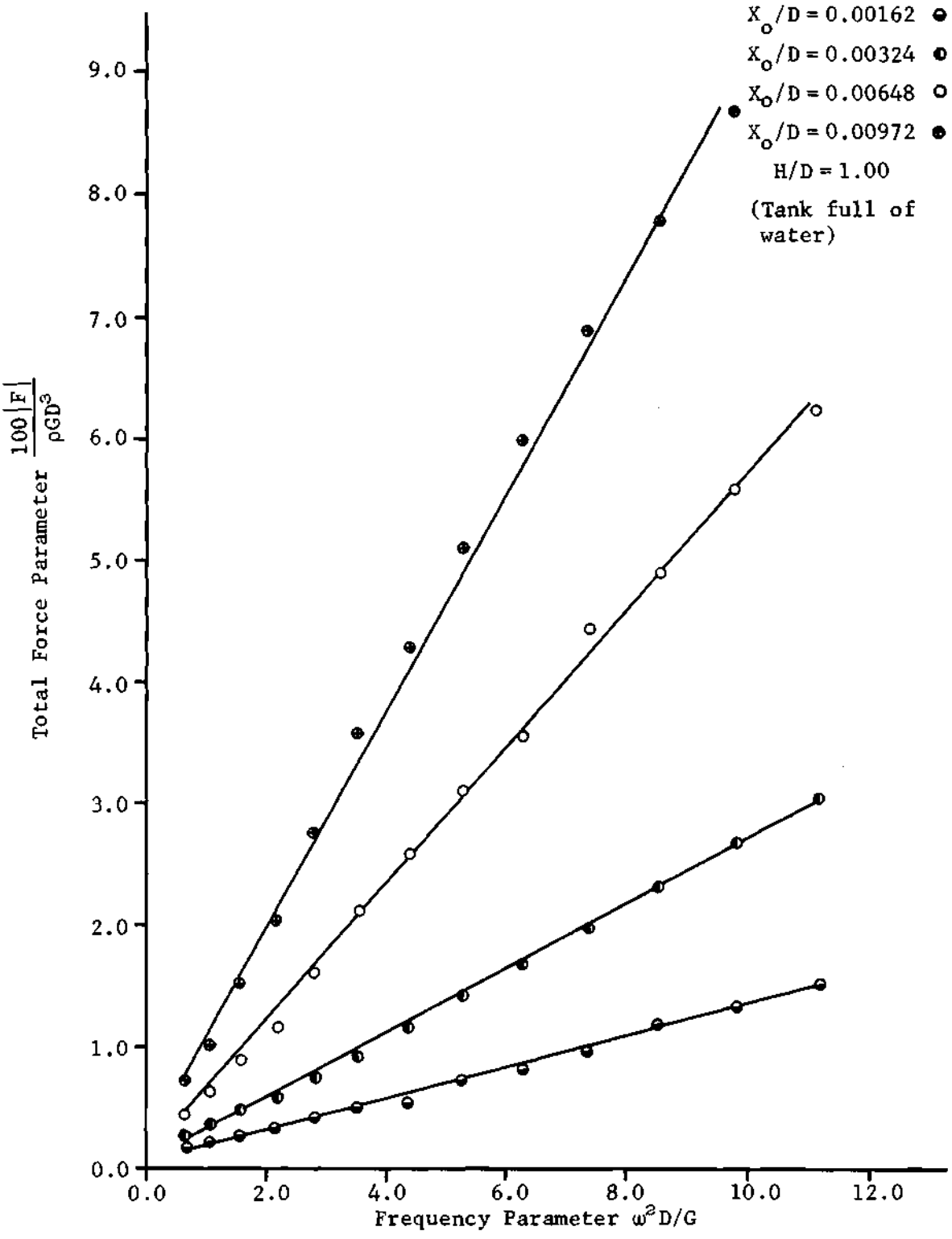

Figure 72. Force Frequency Response (H/D = 1)

APPENDIX D

PROGRAM AND OUTPUT ROOTS OF THE CHARACTERISTIC EQUATION OF THE LINEAR SYSTEM

1. Main Program.

2. Sample Output Roots.

Card numbers 24 and 25 were frequently replaced to make calculation for different combination and variation of parameters possible.

MAIN PROGRAM

```
 1*    C      FLUID SLOSH DAMPING
 2*    C      ROOTS OF CHARACTERISTIC EQUATION ,TWO DEGREE FREEDOM SYSTEM ,
 3*    C      LINEAR FREE MOTION.
 4*           REAL MUM
 5*           DIMENSION A(5),X(4)
 6*           COMPLEX A,X
 7*           READ (5,100) N,EPS,KMAX
 8*           READ (5,103) RHOM,RHOP,MUM,OMEGA
 9*           WRITE (6,101)
10*           WRITE (6,102) N,EPS,KMAX
11*         1 WRITE (6,108) RHOM,RHOP,MUM,OMEGA
12*           NP1=N+1
13*           A(1)=(OMEGA**2)
14*           A(2)=2*(RHOM*OMEGA**2+RHOP*OMEGA)
15*           A(3)=(OMEGA**2+4*RHOM*RHOP*OMEGA+1.)
16*           A(4)=2*(RHOM+RHOP*OMEGA)
17*           A(5)=(1.-MUM)
18*           WRITE(6,104) (I,A(I),I=1,NP1)
19*           CALL ROOTCP (A,N,EPS,KMAX,X,J,$2)
20*           WRITE (6,105)
21*           GO TO 3
22*         2 WRITE (6,106) J
23*         3 WRITE (6,107) (I,X(I),I=1,J)
24*           RHOP=RHOP+0.05
25*           IF (RHOP .LT. 1.0) GO TO 1
26*           STOP
27*     100 FORMAT (I4,F10.0,I4)
28*     101 FORMAT (//,20X,20HFLUID SLOSH DAMPING ,//)
29*     102 FORMAT (9H N    =    I4/7H EPS = 1PE16.7/8H KMAX=   I4 )
30*     103 FORMAT (4F10.0)
31*     104 FORMAT (//22H POLYNOM COEFFICIENTS.//1H 2X 2H I,20X 5H A(I)/
32*        1(1H I4,1P2E18.7))
33*     105 FORMAT (//42H SUCCESSFUL RETURN   ALL ROOTS CONVERGED .  )
```

```
34*      106 FORMAT (//77H ERROR RETURN   MAXIMUM NUMBER OF ITERATIONS EXCEEDED
35*         1DURING THE SOLUTION FOR I4,9H TH ROOT.)
36*      107 FORMAT (//14H OUTPUT ROOTS.//1H 2X 2H I,20X 5H X(I)/(1H I4,1P2E18.
37*         17))
38*      108 FORMAT (//8H RHOM = 1PE16.7/8H RHOP = 1PE16.7/8H MUM  = 1PE16.7/
39*         18H OMEGA=  1PE16.7 )
40*           END
```

SAMPLE OUTPUT

FLUID SLOSH DAMPING

```
N    =       4
EPS  =     9.9999999-04
KMAX=     50


RHOM =      0.0000000
RHOP =      1.0000000-01
MUM  =      1.0000000-01
OMEGA=      9.5000000-01
```

POLYNOM COEFFICIENTS.

I		A(I)
1	9.0249999-01	0.0000000
2	1.9000000-01	0.0000000
3	1.9025000+00	0.0000000
4	1.9000000-01	0.0000000
5	9.0000001-01	0.0000000

SUCCESSFUL RETURN ALL ROOTS CONVERGED .

OUTPUT ROOTS.

I		X(I)
1	-4.4302475-02	-8.5367075-01
2	-4.4302001-02	8.5367072-01
3	-6.1253143-02	-1.1698572+00
4	-6.1253489-02	1.1698572+00

```
RHOM =      0.0000000
RHOP =      1.5000000-01
MUM  =      1.0000000-01
OMEGA=      9.5000000-01

POLYNOM COEFFICIENTS.

   I                      A(I)
   1       9.0249999-01       0.0000000
   2       2.8499999-01       0.0000000
   3       1.9025000+00       0.0000000
   4       2.8499999-01       0.0000000
   5       9.0000001-01       0.0000000

SUCCESSFUL RETURN   ALL ROOTS CONVERGED .

OUTPUT ROOTS.

   I                      X(I)
   1      -6.7280338-02      -8.6168499-01
   2      -6.7280333-02       8.6168501-01
   3      -9.1052998-02       1.1550179+00
   4      -9.1052992-02      -1.1550179+00
```

Other roots.....

APPENDIX E

SAMPLE DESIGN CALCULATION

The effectiveness of fluid slosh dampers on the response of the vibratory systems was studied in parametric form. For the design of a more efficient slosh damper, certain critical values of the parameters were obtained.

The parameters used contain many physical constants of the damper and of the main system. Since many combination of physical constants yield to a single value of a particular parameter, the designer will find a wide range of selection of each individual physical constant.

In practice one should design fluid slosh dampers for the maximum damping of the response of the main system. But in the course of experimental analysis it was found easier to obtain a fluid slosh damper and design a vibratory system for which the damper is most suitable. Sometimes the physical constants of both systems (main system and auxiliary system) were altered to obtain the desired design parameters.

Suppose there is a mass-spring-dashpot model of a vibratory system that exhibits the following properties:

$$\zeta_m = 0$$

$$M_m = 4 \times 10^{-3} \ \frac{\#\text{-sec}^2}{\text{in}}$$

$$K_m = 1.768\#/\text{in.}$$

The objective is to design a fluid slosh damper which provides maximum damping.

1. As explained earlier smaller mass ratios are prefered because of the weight penalty. Therefore, a mass ratio of 0.1 is selected for this analysis.

2. It has been proven that for maximum damping the frequency ratio must equal the critical tuning frequency ($\Omega = \Omega_p$). Therefore, for the mass ratio ($\mu = 0.1$) selected, the frequency ratio must be $\Omega = \Omega_p = 0.95$. This value is obtained from Figure 20.

3. In the theoretical analysis of the free vibration of the coupled system, the critical value of viscous damping for $\Omega = 0.95$ and $\mu = 0.1$ is shown to be $\zeta_{pc} = 0.300$. This value is obtained from Figure 25.

It should be mentioned that the design parameters obtained lead the designer to the construction of an efficient fluid slosh damper, provided that it should be used in the linear range ($\epsilon << \epsilon_c$).

From the information obtained above, one can write

$$\mu = M_p/M = 0.1 \quad \text{or} \quad M_p = 0.1M, \tag{141}$$

$$\Omega = \omega_p/\omega_m = 0.95 \quad \text{or} \quad \omega_p = 0.95\omega_m, \quad \text{and} \tag{142}$$

$$\zeta_p = \zeta_{pc} = 0.30. \tag{143}$$

The above three equations determine the physical constants of a dampled planar pendulum which provides maximum damping for the main system, provided that $M = M_m$. But in design of a spherical container partially

filled with fluid the problem becomes more complicated. In such a case, the additional stationary mass of the fluid (M_o) and the mass of the container (M_t) will be included in M, and also ζ_p will be a function of D, H/D, and υ. It should be noticed that because of the new value of M, the magnitude of ω_m will also be altered.

In such respect the designer has the choice of selecting some reasonable values of some of the physical constants and determine the rest from the equations obtained above. From the previous experimental analysis it was found more convenient to arbitrarily select a partially filled container (D and H/D) and determine the viscousity of the fluid such as to satisfy equations 141, 142, and 143.

For this calculation the following arbitrary values are selected:

$$D = 3.862 \text{ ins.}, \quad H/D = 0.500$$

Letting $M_m = M_s + M_w$ and rewriting equations 141, 142, and 143 in terms of the physical constants of fluid slosh dampers one obtains

$$M_p = 0.1(M_m + M_t + M_o + M_p), \tag{144}$$

$$G/L_p = (0.95)^2 \left(\frac{K_m}{M_m + M_t + M_o + M_p}\right), \text{ and} \tag{145}$$

$$\zeta_p = \zeta_{pc} = 0.30 = f(D,H/D,\nu). \tag{146}$$

Substituting equation 144 in equation 145 one can write

$$G/L_p = (0.95)^2 \left(\frac{K_m}{10M_p}\right), \tag{147}$$

$$0.30 = f(D, H/D, \nu), \tag{148}$$

where equation 148 can be obtained from equations 138 and 140 of the text. For the H/D and D selected the value of L_p can be obtained from Figure 55.

Solving equations 147 and 148 yields

$$M_p = 5.18 \times 10^{-4} \frac{\#\text{-sec}^2}{\text{in}}$$

$$\nu = 113.8 \times 10^{-4} \text{ ft}^2/\text{sec}.$$

Knowing M_p and H/D one can obtain M_F from Figure 54 as $M_F = 1.95 \times 10^{-3} \frac{\#\text{-sec}^2}{\text{in}}$ and the value of M_o can be obtained from Figure 56 as $M_o = 3.9 \times 10^{-4} \frac{\#\text{-sec}^2}{\text{in}}$. The value of an allowable tank mass can be obtained from equation 144 as $M_t = 2.72 \times 10^{-4} \frac{\#\text{-sec}^2}{\text{in}}$.

The viscosity of the fluid obtained is in the neighborhood of pure glycerin at room temperature, and its density can be found from

$$M_F = \frac{\pi}{6} D^3 \rho \rightarrow \rho = 0.112 \frac{\text{slug}}{\text{ft}^3} .$$

According to the above calculations all the physical constants of the slosh damper and its pendulum model are known. It should be emphasized that the designer has the choice of predetermining any other parameters than those of the present calculation. The results of similar calculations sometimes yield unreasonable values for physical constants, in such cases the designer may have to adjust some other constant in order to obtain reasonable values. It should be mentioned also that fluid slosh dampers are best suited for low frequency systems.

APPENDIX F

PROGRAM AND SAMPLE OUTPUT OF NONLINEAR FLUID MOTION

1. Main Program.
2. Subroutine to reset the initial conditions.
3. RKDE subroutine.
4. Sample output solution.

Cards 26 and 27 were frequently replaced by other statements to make variation in other parameters possible.

MAIN PROGRAM

```
      DIMENSION Y(5),W(5),Q(5)
      COMMON EPS, MUM, OMEGA, RHOP, RHOM, SEE
      EXTERNAL DY
      REAL MUM
      READ(5,100)(Y(I),I=1,5)
      READ(5,150)DELT,N
C     Y(1)=OMEGAM*T,Y(2)=X/XO,Y(3)=XDOT/(XO*OMEGAM),Y(4)=THETA,
C     Y(5)=THETADOT/OMEGAM
C     DELT=STEP SIZE, N=TOTAL NUMBER OF STEPS, MUM=MASS RATIO
C     EPS=XO/LP, OMEGA=FREQUENCY RATIO, RHOP=DAMPING FACTOR OF FLUID
C     RHOM=DAMPING FACTOR OF MAIN SYSTEM,SEE=CUBIC SPRING COEF.
      READ(5,200)EPS, MUM, OMEGA, RHOP, RHOM, SEE
1000  WRITE(6,300)
      WRITE(6,400)EPS, MUM, OMEGA, RHOP, RHOM, SEE
      CALL RESET(Y)
      WRITE(6,500)Y(1), Y(2), Y(3), Y(4), Y(5)
      WRITE(6,600)DELT, N
      H=DELT
      Z=H
      J=0
10    CALL RKDE (DY,Y,Z,H,W,Q,5)
      WRITE(6,700)Y
      Z=Z+H
      J=J+1
      IF(J-N)10,10,30
30    EPS=EPS+0.064
      IF(EPS .LT. 0.193) GO TO 1000
      STOP
100   FORMAT(5F10.5)
150   FORMAT(F10.5,I5)
200   FORMAT(6F10.5)
300   FORMAT(20X,31HSOLUTION OF FLUID SLOSH DAMPERS,//)
```

```
      400  FORMAT(10X,4HEPS=,F10.5,5X,4HMUM=,F10.5,5X,6HOMEGA=,F10.5,
     15X,5HRHOP=,F10.5,//,10X,5HRHOM=,F10.5,5X,4HSEE=,F10.5,//)
      500  FORMAT(10X,18HINITIAL CONDITIONS,//,8X,9HOMEGAM*T=,F6.3,
     15X,5HX/XO=,F6.3,5X,17HXDOT/(XO*OMEGAM)=,F6.3,5X,6HTHETA=,F6.3,//,
     18X,16HTHETADOT/OMEGAM=,F6.3,//)
      600  FORMAT(18X,15HDELT(OMEGAM*T)=,F10.5,5X,27HTOTAL NUMBER OF INCREMEN
     1TS=,I5,//,10X,9HOMEGAM*T,9X,4HX/XO,9X,16HXDOT/(XO*OMEGAM),6X,
     15HTHETA,6X,15HTHETADOT/OMEGAM)
      700  FORMAT(5(7X,F10.6))
           END
```

Subroutine #1

```
           SUBROUTINE RESET(X)
           DIMENSION X(5)
           X(1)=0.0
           X(2)=1.0
           X(3)=0.0
           X(4)=0.0
           X(5)=0.0
           RETURN
           END
```

Subroutine #2

```
      REAL FUNCTION DY(Y,I)
      REAL MUM
      COMMON EPS, MUM, OMEGA, RHOP, RHOM, SEE
      DIMENSION Y(1)
      GO TO (10,20,30,40),I
10    DY=Y(3)
      GO TO 50
20    DY=(-(MUM/EPS)*(Y(5)*Y(5)*SIN(Y(4))+2*RHOP*OMEGA*Y(5)*
     1COS(Y(4))+OMEGA*OMEGA*SIN(Y(4))*COS(Y(4))+OMEGA*OMEGA*
     1SEE*Y(4)**3.)+2.*RHOM*Y(3)+Y(2))/(MUM*COS(Y(4))*COS(Y(4))-1.)
      GO TO 50
30    DY=Y(5)
      GO TO 50
40    DY=(-2*RHOM*EPS*Y(3)*COS(Y(4))-EPS*Y(2)*COS(Y(4))+MUM*
     1Y(5)*Y(5)*SIN(Y(4))*COS(Y(4))+2.*RHOP*OMEGA*Y(5)+OMEGA*OMEGA*
     1SIN(Y(4))+OMEGA*OMEGA*SEE*Y(4)**3.)/(MUM*COS(Y(4))*COS(Y(4))-1.)
50    RETURN
      END
```

SAMPLE OUTPUT

SOLUTION OF FLUID SLOSH DAMPERS

EPS= .12800 MUM= .10000 OMEGA= .95000 RHOP= .10950

RHOM= .00000 SEE= .00000

INITIAL CONDITIONS

OMEGAM*T= .000 X/XO= 1.000 XDOT/(XO*OMEGAM)= .000 THETA= .000

THETADOT/OMEGAM= .000

DELT(OMEGAM*T)= .20000 TOTAL NUMBER OF INCREMENTS= 400

OMEGAM*T	X/XO	XDOT/(XO*OMEGAM)	THETA	THETADOT/OMEGAM
.200000	.977901	-.219929	.002781	.027403
.400000	.912799	-.428341	.010725	.051279
.600000	.807992	-.615422	.022927	.069701
.800000	.668636	-.772526	.038138	.081160
1.000000	.501459	-.892613	.054857	.084657
1.200000	.314411	-.970574	.071439	.079762
1.400000	.116247	-1.003457	.086210	.066633
1.600000	-.083907	-.990547	.097588	.045994
1.800000	-.277006	-.933325	.104186	.019076
2.000000	-.454508	-.835331	.104907	-.012479
2.200000	-.608768	-.701941	.099015	-.046711
2.400000	-.733379	-.540096	.086187	-.081463
2.600000	-.823449	-.357969	.066545	-.114488
2.800000	-.875812	-.164570	.040655	-.143577
3.000000	-.889151	.030711	.009514	-.166681

3.200000	-.864022	.218619	-.025500	-.182050
3.400000	-.802773	.390554	-.062699	-.188358
3.600000	-.709369	.539055	-.100183	-.184810
3.800000	-.589120	.658162	-.135950	-.171208
4.000000	-.448356	.743634	-.168020	-.147955
4.200000	-.294082	.793007	-.194550	-.116016
4.400000	-.133619	.805546	-.213940	-.076830
4.600000	.025730	.782126	-.224917	-.032202
4.800000	.176984	.725111	-.226595	.015803
5.000000	.313776	.638241	-.218519	.064950
5.200000	.430616	.526515	-.200692	.112925
5.400000	.523127	.396035	-.173582	.157404
5.600000	.588242	.253774	-.138114	.196142
5.800000	.624349	.107213	-.095647	.227075
6.000000	.631344	-.036121	-.047924	.248452
6.200000	.610589	-.169193	.003006	.258967
6.399999	.564759	-.285968	.054887	.257886
6.600000	.497605	-.381792	.105378	.245121
6.799999	.413654	-.453565	.152191	.221243
7.000000	.317895	-.499718	.193209	.187414
7.199999	.215496	-.520029	.226601	.145279
7.399999	.111552	-.515396	.250898	.096823
7.599999	.010885	-.487629	.265054	.044241

.
.
.
.
.

Continues.....

BIBLIOGRAPHY

LITERATURE CITED

1. H. N. Abramson, "The Dynamic Behavior of Liquids in Moving Containers," NASA SP-106.

2. B. Budiansky, "Sloshing of Liquids in Circular Canals and Spherical Tanks," J. Aerospace Sci., Vol. 27, No. 3, March 1960, pp. 161-173.

3. J. L. McCarty and D. G. Stephens, "Investigation of the Natural Frequencies of Fluids in Spherical and Cylindrical Tanks," NASA TN D-252, Langley Research Center, Langley Field, Va., May 1960.

4. H. W. Leonard and W. C. Walton, Jr., "An Investigation of the Natural Frequencies and Mode Shapes of Liquids in Oblate Spheroidal Tanks," NASA TN D-904, Langley Research Center, Langley Field, Virginia, 1961.

5. A. J. Stofan and A. L. Armstead, "Analytical an Experimental Investigation of Forces and Frequencies Resulting from Liquid Sloshing in a Spherical Tank," NASA TN D-1281, Lewis Research Center, Cleveland, Ohio, July 1962.

6. D. G. Stephens, H. W. Leonard and M. A. Silveira, "An Experimental Investigation of the Damping of Liquid Oscillations in an Oblate Spheroidal Tank With and Without Baffles," NASA TN D-808, Langley Research Center, Langley Field, Virginia, 1963.

7. I. E. Sumner and A. J. Stofan, "An Experimental Investigation of the Viscous Damping of Liquid Sloshing in Spherical Tanks," NASA TN D-1991, Lewis Research Center, Cleveland, Ohio, December 1963.

8. I. E. Sumner, A. J. Stofan and D. J. Sharmo, "Experimental Sloshing Characteristics and a Mechanical Analogy of Liquid Sloshing in a Scale-Model Centaur Liquid Oxygen Tank," NASA TM X-999, Lewis Research Center, Cleveland, Ohio, August 1964.

9. I. E. Sumner, "Experimentally Determined Pendulum Analogy of the Liquid Sloshing in Spherical and Oblate-Spheroidal Tanks," NASA TN D-2737, Lewis Research Center, Cleveland, Ohio, April 1965.

10. H. N. Abramson, W. H. Chu and L. R. Garza, "Liquid Sloshing in Spherical Tanks," AIAA Journal, Vol. 1, No. 2, pp. 384-389.

11. H. N. Abramson, W. H. Chu and D. D. Kana, "Some Studies of Nonlinear Lateral Sloshing in Rigid Containers," J. Appl. Mech., December 1966.

12. P. Y. Chen, "On the Nonlinear Oscillation of Fluids in a Rigid Container with Application to Vibration Reduction," Ph.D. Thesis, Georgia Institute of Technology, June 1970.

13. R. R. Berlot, "Production of Rotation in a Confined Liquid Through Translation Motion of the Boundaries," Journal of Applied Mechanics, December 1959, pp. 513-516.

14. J. W. Miles, "Stability of Forced Oscillations of a Spherical Pendulum," Quart. Appl. Math., Vol. 20, No. 1, April 1962, pp. 21-32.

15. D. G. Stephens and H. W. Leonard, "The Coupled Dynamic Response of a Tank Partially Filled with a Liquid and Undergoing Free and Forced Planar Oscillations," NASA TN D-1945, Langley Research Center, Langley Station, Hampton, Virginia.

16. N. N. Moiseev and A. A. Petrov, "The Calculation of Free Oscillation of a Liquid in a Motionless Container," Advances in Applied Mechanics, Vol. 9, 1966, pp. 91-117.

17. H. F. Bauer, "Nonlinear Mechanical Model for the Description of Propellant Sloshing," AIAA Journal, Vol. 4, No. 9, Sept. 1966, pp. 1662-1668.

18. R. E. Hutton, "An Investigation of Resonant, Nonlinear Nonplanar Free Surface Oscillation of a Fluid," NASA TN D-1870, 1963.

19. J. J. Stocker, "Nonlinear Vibrations," Interscience Publishers, 1966.

20. R. M. Laurenson, "The Dynamic Characteristics of a Nonlinearly Damped System," Ph.D. Thesis, Georgia Institute of Technology, 1968.

21. H. H. Alvord, "The Mechanical Analysis Laboratory of the Department of Mechanical Engineering at the University of Michigan," Ann Arbor, Michigan, July, 1961, pp. 31-36.

22. G. N. Mikishev and N. YA. Dorozhkin, "An Experimental Investigation of Free Oscillation of a Liquid in Containers," (in Russian), Izv. Akad, Nauk SSSR, Otd. Tekh. Nauk, Mekh, i Mashinostr, No. 4, July/August 1961, pp. 48-83. Translated into English by D. Kana, Southwest Research Institute, June 30, 1963.

23. Handbook of Chemistry and Physics, 44th Edition, published by The Chemical Rubber Company, November 1963.

OTHER REFERENCES

01. R. L. Daugherty and J. B. Franzini, "Fluid Mechanics with Engineering Applications," McGraw-Hill Book Company, 1965.

02. J. P. Den Hartog, "Mechanical Vibration," McGraw-Hill Book Company, 1940.

03. S. T. Francis, I. E. Morse and R. T. Hinkle, "Mechanical Vibrations," Allyn and Bacon, Inc., 1966.

04. W. T. Thomson, "Vibration Theory and Applications," Prentice Hall, Inc., 1965.

05. S. Timoshenko, "Vibration Problems in Engineering," D. Van Norstrand Company, Inc., 1956.

06. M. L. James, G. M. Smith and J. C. Wolford, "Applied Numerical Methods for Digital Computation with FORTRAN," International Text Book Company, 1968.

07. C. A. Meyer and H. B. Saldin, "Model Tests of Two Types of Vibrations Dampers," Journal of Applied Mechanics, June 1942.

VITA

Bashir A. Sayar was born in Farah, Afghanistan on April 3, 1941. He is the son of Mr. and Mrs. Noor Mohamad. He was graduated from Habibia High School in 1959.

He entered the College of Engineering of Kabul University in 1959 and, while a senior in the college, was awarded an AID scholarship to pursue a graduate program at the Georgia Institute of Technology. Completing the requirements for a B.S. degree in the first two quarters of residence, he obtained his B.S. in Electro-Mechanical Engineering from Kabul University. Continuing his graduate program, he obtained an M.S. degree in the School of Mechanical Engineering at Georgia Tech in 1965. After returning to Afghanistan, he was appointed Assistant Dean of Engineering in Kabul University with a concurrent full-time teaching load. In the year 1967 he was awarded another AID scholarship to pursue a Ph.D. program in the School of Mechanical Engineering of the Georgia Institute of Technology.

While in the United States, Mr. Sayar married Shafica (his fiancée) by proxy, who joined him shortly after the marriage. They have a wonderful son, George Yama, who was conceived in the United States and was born in Kabul, Afghanistan.